Master Thesis

# Investigation of Velocity and Sensor Position Dependencies of Signals in Pipeline Inspection Tools using MFL Technique



**Written by:**
Ahmed El Menshawy

00935306

**Advisors:**
Univ.-Prof. Dipl.-Ing. Dr.mont. Herbert Hofstätter
Dipl.-Ing. Mikhail Pavlov
Dipl.-Ing. Felix Reining

Leoben,19/02/2018

# EIDESSTATTLICHE ERKLÄRUNG

Ich erkläre an Eides statt, dass ich die vorliegende Masterarbeit selbständig und ohne fremde Hilfe verfasst, andere als die angegebenen Quellen und Hilfsmittel nicht benutzt und die den benutzten Quellen wörtlich und inhaltlich entnommenen Stellen als solche erkenntlich gemacht habe.

# AFFIDAVIT

I hereby declare that the content of this work is my own composition and has not been submitted previously for any higher degree. All extracts have been distinguished using quoted references and all information sources have been acknowledged.

# Acknowledgement

I would like to express my thanks and gratitude to my Parents, brother and my sister for their love and the support they have provided me throughout the years, and I would like to dedicate this work to my late mother, whom I owe everything I have achieved in my life so far.

Special thanks go to my supervisor Dipl.-Ing. Mikhail Pavlov for his help, knowledge, time and for guiding me through this work.

I would also like to thank Dipl.-Ing. Felix Reining ,my supervisor at the company 3P-services, for all the support and knowledge he provided me with during my work at the company.

Last but not least I would like to thank the entire department of Petroleum and Geothermal Energy Recovery, led by Univ.-Prof. Dipl.-Ing. Dr.mont. Herbert Hofstätter for all the support they provided throughout my study years.

# Kurzfassung

Pipeline-Betreiber verwenden eine Vielzahl von Methoden, um Rohrleitungen zu ispizieren. Diese Methoden können zum Beispiel, Cathodic protection surveys, leak detection programs oder hydrostatic tests, sein.

Mit der Zunahme der weltweit eingesetzten Pipelines könnte es häufig zu korrosionsbedingten Leckagen kommen, was eventuell zur Verluste an Ressourcen und zur Umweltverschmutzung führen kann, deshalb sind zerstörungsfreie Prüfungsmethoden sehr wichtig um ein sicherer und optimaler Betrieb von Rohrleitungen zu gewehrleisten. Und das ist genau wo die MFL Technology zur Anwendung kommt. Es ist eine der beliebtesten Methoden der Pipeline-Inspektion. Es ist eine zerstörungsfreie Testtechnik, die magnetempfindliche Sensoren verwendet, um die magnetischen Streufelder zu detektieren, die durch die Anwesenheit von Materialverlusten entlang der Pipelinewände verursacht werden.

Die Positionierung sowie die Geschwindigkeit des Tools sind zwei sehr einflussreiche Parameter, wenn es um die Implementierung der MFL-Technik geht. Daher ist es das Ziel dieses Projekts, die Abhängigkeit dieser Technik von diesen beiden Parametern zu untersuchen, um das Einsetzen dieser Technology bei Pipeline Inspektionen zu optimieren.

# Abstract

Pipeline operators use a wide variety of methods to evaluate, inspect, and monitor the hundreds of thousands of miles of transmission pipelines now in operation worldwide. Such methods could be for instance Cathodic protection surveys, leak detection programs, excavations to look for pipe corrosion or protective coating failures, hydrostatic tests, and the use of in-line inspection tools that travel through the pipe.

With an increase of the number of pipelines being deployed around the world, corrosion leakage accidents happening frequently, causing a serious waste of resources and also considering the huge environmental impact of such incidents, a non-destructive testing technology is important to ensure the safe operation of the pipelines and energy delivery. And that is where the Magnetic flux leakage (MFL) technique comes into play. It is one of the most popular methods of pipeline inspection. It is a non-destructive testing technique which uses magnetic sensitive sensors to detect the magnetic leakage fields caused by the presence of material losses along the pipeline walls.

The positioning as well as the velocity of the tool are two very influential parameters when it comes to implementing the MFL-technique, which is why the aim of this project is to investigate the dependency of this technique on those two parameters in order to optimize the quality and efficiency of this inline inspection method.

# Table of Content

Page

# 1 Introduction

In order to minimize the risks of failure, pipelines have to be closely monitored and inspected on a regular basis that is why in-line inspection (ILI) plays a huge role in the oil and gas industry, which utilizes the use of pipe line inspection tools, commonly referred to as pigs, that can be inserted and propelled through a pipeline by the flowing medium. It has successfully been used and implemented in the industry for the detection of defects and anomalies along in-service oil and gas pipelines since the sixties.**Error! Reference source not found.**

One of the most commonly used ILI methods, is the magnetic flux leakage (MFL). With the help of magnetic components, the tool is able to induce magnetic flux within the pipe wall. The presence of any anomalies along the pipe will disturb the flow of the induced field causing it to leak, this change in the magnetic field can then detected by sensors. They are widely used for the detection of metal loss regions, and have been proved to be robust and successful in operating under harsh environments.[2]

The MFL signal can be used in order to derive information about the depth, length and width of an anomaly. The signal, however, does not only depend on the geometry of the anomaly itself, but also on other factors as well, most influential being[3]:

- Magnetization level
- Tool speed
- Sensor positioning

The magnetization should be high enough to deliver a magnetic flux that is strong enough to leak at metal-loss regions, uniform along the wall thickness of the pipe, so that the obtained signal can linearly related to the defect's length and depth, and consistent along the length of the pipe for the data gathered from a run to be comparable.[5]

In addition, sensor position between the magnet poles as well as the velocity of the tool has a big impact on the quality of the acquired MFL signal. Nowadays velocities up to 30 kilometres per hour can be used for an inspection run. These high velocities can compromise the ability to detect and characterize defects. Such effects need to be investigated in order to realise the full capability of the inspection system.[1]

The aim of this work is to provide a general understanding about the MFL technology, by illustrating the main working principle of it as well as explaining the main components of such an inspection tool and how they affect its performance, which shall be covered in chapter **Error! Reference source not found.**.

Then moving to the core point of the work, where a series of tests were conducted at the 3P-Services' laboratory and workshop in order to quantify the effects of magnetization, sensor positioning and velocity on the quality of the MFL signal. In chapter 4 the positioning dependency of the sensors alongside with the magnetization will be investigated, by performing several test runs using an MFL tool that will be run along different metal bars with different thicknesses. Those tests are done under very low speeds to avoid having any velocity effects on the eventually obtained signal. The acquired data will then be further evaluated and analysed.
The velocity dependency will be discussed in chapter 5, where the same above mentioned procedures will be performed but under different velocities ranging from very slow to very fast.

# 2 Main Working Principle of the MFL Technology

The basic principle of the MFL technology is that, a ferromagnetic material is magnetized close to saturation under an applied magnetic field. If there are no defects present in the material then the magnetic flux lines will pass through parallel to the surface of the material itself. However, if any defects were present along the material, then that local decrease of the thickness will cause the magnetic field to get distorted resulting in a magnetic flux leakage. That is due to the fact that the magnetic permeability of the defect site is much smaller than that of the ferromagnetic material itself leading to a higher magnetic resistance in the defected region. Eventually magnetic flux lines will bend, and a magnetic flux field will form around the defect area.[6]

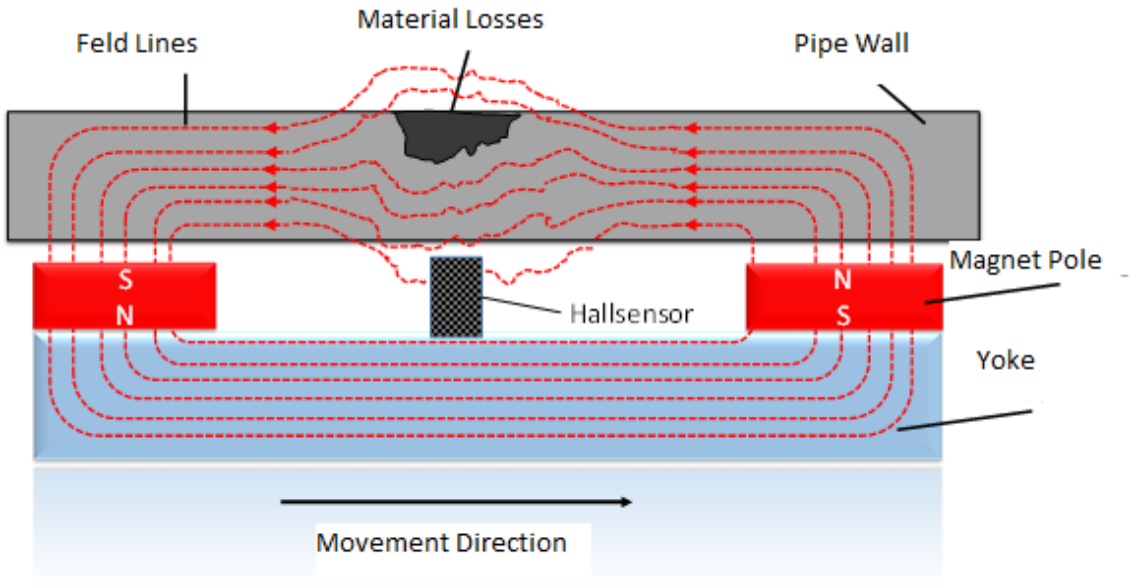


Figure 1: Change in Flux Leakage due to the presence of an anomaly.[3]

In order to measure the magnetic field at the pipe wall, a magnetic sensitive sensor is positioned between the two magnet poles. At the metal loss region, the sensor can detect the change in the magnetic flux field, which in that case would be a higher flux density compared to the one in the non-defected region. The measured leakage field depends on the geometry of the defect, as well as the magnetic property of the material. The measured leakage has to be analysed in order to get a clear idea about the defect.[4]

## 2.1 MFL Inspection Tool Components

In terms of structure, MFL tools can be generally classified into two types:

- **Segmented tools:** Several individual Segments are joined together with flexible connectors, allowing for data and power transfer and have a length of about 2 to 3 meters and are the most commonly used type.
- **Single-piece tools:** All the components are installed in one single package. They are usually longer than the segmented tools and can have a length of about 2 to 5 meters.

The length and the number of segments of a tool are limited by bends present in the pipeline.[4]

### 2.1.1 Drive System

A cup or a several set of cups at the front of the tool allow the movement through the pipeline due to the force exerted on them by the petroleum fluid. That differential pressure acting between the front and the back of the drive cups propels them, which in turn would pull the rest of the tool forward. That driving force has to overcome friction forces, as well as the magnetic drag that the tool exerts. The force needed is normally small and can be about 0.5 to 1 bar for a 24 in tool. These pressure differentials are smaller compared to the reduced in-line pressure of 25 to 50 bar during the inspection which is necessary to reduce the tools speed to the preferred range of 6 to 10 km/h.

The drive cups are normally mounted at the front of the tool. Additional cups can also be used on each segment of the tool to center it along the run. The driving force and the cup resistance affect how constant the tool velocity is. Velocity fluctuations can be encountered at low pressure intervals, bends, valves as well as when changes in wall thickness are present.[4]

### 2.1.2 Magnetizing and Sensor Systems

The magnetizing system can be located in the middle part of the tool. It helps magnetize the length of the pipe wall. Normally a set of magnets is used to provide a full coverage. These magnets can either be permanent or Electromagnets. Permanent magnets have a constant charge, and they require no power to operate. Electromagnets on the other hand, generate a magnetic field by passing a current through a coil of wire, which means a power source is required. The electromagnet has the advantage that it can be turned on/off by switching the current on/off. In addition to that, the power of the magnetic field can be increased by increasing the current. Permanent magnets are nonetheless, the most commonly used type as it is difficult to assure a consistent power supply for long distance inspection runs, plus permanent magnets comes in different strengths allowing for a wide range of choice for different wall thicknesses.[4]

Figure 2 below shows a typical 48 inch magnetizer segment of one of the tools utilized by 3P-Services for in-line inspection jobs. It consists of 28 magnet yokes to allow for an efficient magnetization of the pipeline walls. In between the two poles of each yoke, 12 hall sensors are installed to read the applied magnetic field as well as any flux leakage that could be caused due to the presence of any anomalies along the pipe wall.

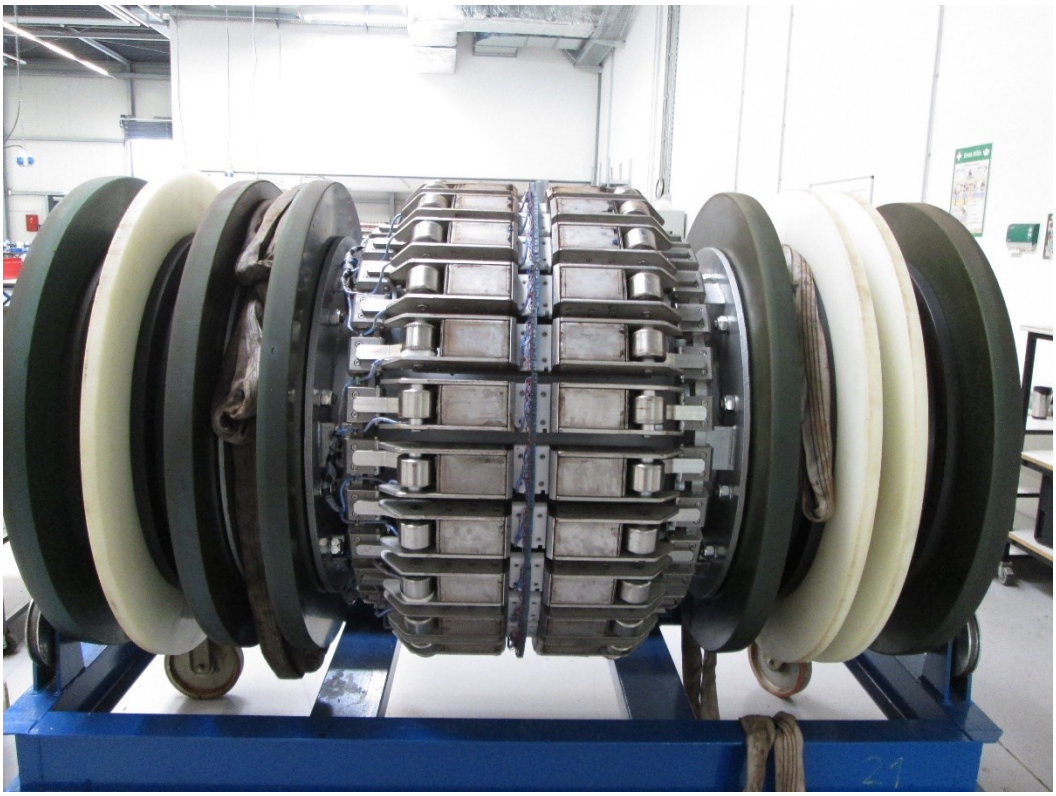

Figure 2: Magnetizing Part of the Tool.

Some companies implement permanent-magnet systems with pairs of magnets that are attached to backing bars and to metal brushes or magnet shoes that rub against the pipe wall. The brushes can help transfer the magnetic field effectively to the pipe body.

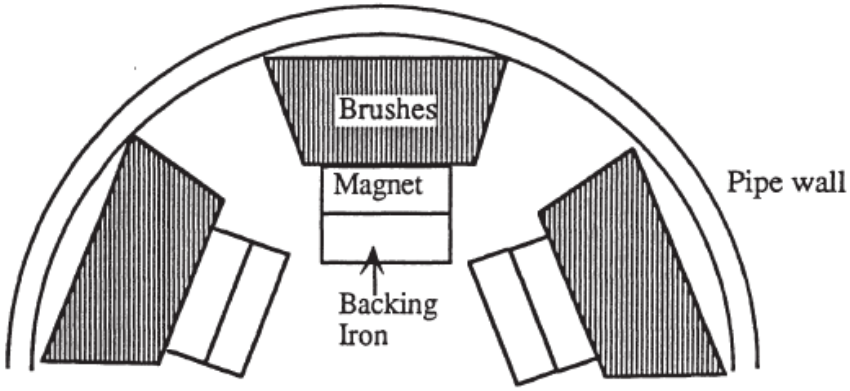


Figure 3: Cross sectional View of the Tool inside a Pipe [1]

The sensor system is installed between the magnet poles to measure the leakage in the magnetic field. The sensors convert the flux leakage into a signal that can be stored and analysed. The two types of sensors that are commonly used in the MFL tools are induction coils and Hall sensors.

### 2.1.3 Data Conditioning and Recording Systems

During Inspections, huge amounts of data are generated, and that amount depends on the number of sensors, number of samples per unit distance and distance traveled, which can be demonstrated by the following equation:

$$Data\ poimts = number\ of\ sensors * number\ of\ samples\ per\ unit\ distance * distance\ traveled$$

A pig with just 2 sensors with a sampling rate of 500 Hz having to travel 100 Km of pipeline recording 165 data points each meter, such configuration would collect about 35 million data for that run, that means that the tool shown in Figure 2 would obtain about 6 billion data points. That is why many tool designers use so called data conditioning systems to compress data and reduce storage. This type of data compression technique requires a threshold to be defined prior to the inspection.[4]

### 2.1.4 Power System

Power supply is needed in order to operate the data conditioning systems, data storage devices as well as some sensors, which means there is a limit of the kilometres that can be inspected in one run. Most tools operate with rechargeable batteries; the capacity of those batteries determines the length that can be inspected before having to be recharged again.

There are several types of batteries available, the most commonly used type are the nickel cadmium batteries. They have successfully been used for several years and are considered very reliable. That is due to the fact that they are rechargeable and have low operating costs, which make up for its lower power capacity.

Silver-zinc batteries are also another type that has been used by operators. They have bigger power capacity allowing for more data storage and longer inspection distances. These batteries are, however, not rechargeable and require safe disposal, which ultimately increases the operating costs.[4]

### 2.1.5 Other Essential Systems

- **Odometer:** To identify the location of indications, from the start of the inspection or from recognizable features such as pipeline connections, valves, road crossings and welds. Odometer systems vary in complexity. The simplest systems send a pulse to the data acquisition system every time the wheel makes one complete revolution.
- **Pressure Containment Systems:** Pressure vessels have to be provided in order to mount all the electronic and battery components in them, preventing any damage that could occur to those components from the line pressure, gas and moisture.
- **Vibration and shock Mounting Systems:** In order to isolate the electronic components and the battery from possible harmful shocks and vibrations.[4]

## 2.2 Running the Inspection Tool

In order to run an MFL inspection tool into a pipeline, special devices are required. These are the so called PIGs, which are installed at compressor stations and other accessible locations.

During an inspection, it is of huge importance to control the tool velocity through the pipeline, as it should be inspected later in this work, since it has impact on the accuracy of the data obtained.

After the tool is captured, the tool is inspected to check that all the components are still in a proper condition. Furthermore, some of the obtained data is analysed to make sure the tool operated properly during the run.[4]

### 2.2.1 Launching and retrieving an MFL Tool

The MFL is inserted into the pressurized pipeline via a ‘’PIG launcher’’. Through the utilization of valves, the launcher is isolated from the inline pressure while installing the tool. After the installation of the tool another set of valves is used to pressurize the launcher. Then gas pressure moves the tool from the launcher into the run pipe.

Running an MFL tool isn’t any different from running other inspection tool. As mentioned before the differential pressure on the front and back of the driving cups helps run the tool along the pipe. The velocity of the flowing gas is then reduced from the operating conditions to the desired velocity required for the tool.

Retrieving the tool is basically similar to launching it. By using a bypass flow system or valves, the tool can be stopped when it approaches the receiver. Valves allow gas pressure from the line to move the tool into the receiver. Again as in in the launching process, after the tool is in place the receiver is isolated from the line pressure and the pressure in the receiver is then released, then the tool is removed from pipeline.[4]

## 2.3 Utilization of the MFL Technology in Pipeline Inspection

When implementing the MFL technology into pipeline inspection, there are several parameters which should be accounted for that could severely impact the efficiency of the result in several areas. Each of all these areas has its own capabilities and limitations, when designing an MFL system those limits should be reached within the economical constrains.

### 2.3.1 Magnetization

As mentioned before, the flux leakage is produced by the interaction between the applied magnetic fields of the magnetization system with the anomalies at the pipe wall. In order to fulfil its purpose, that magnetic field has to be strong, uniform and consistent.

If an MFL tool is functioning at a low magnetized area, it is difficult to avoid the adverse effects of magnetic disturbance factors and the resultant measurement errors, simply

because magnetic disturbance factors occur in such areas. The relationship between the applied magnetic field and the flux density in a pipe is nonlinear. For low applied magnetic fields, a large change in in flux can be observed for small changes in the applied field and vice versa for higher magnetic field levels. That is why a reduction in material alone may not always lead to flux leakage.[4]

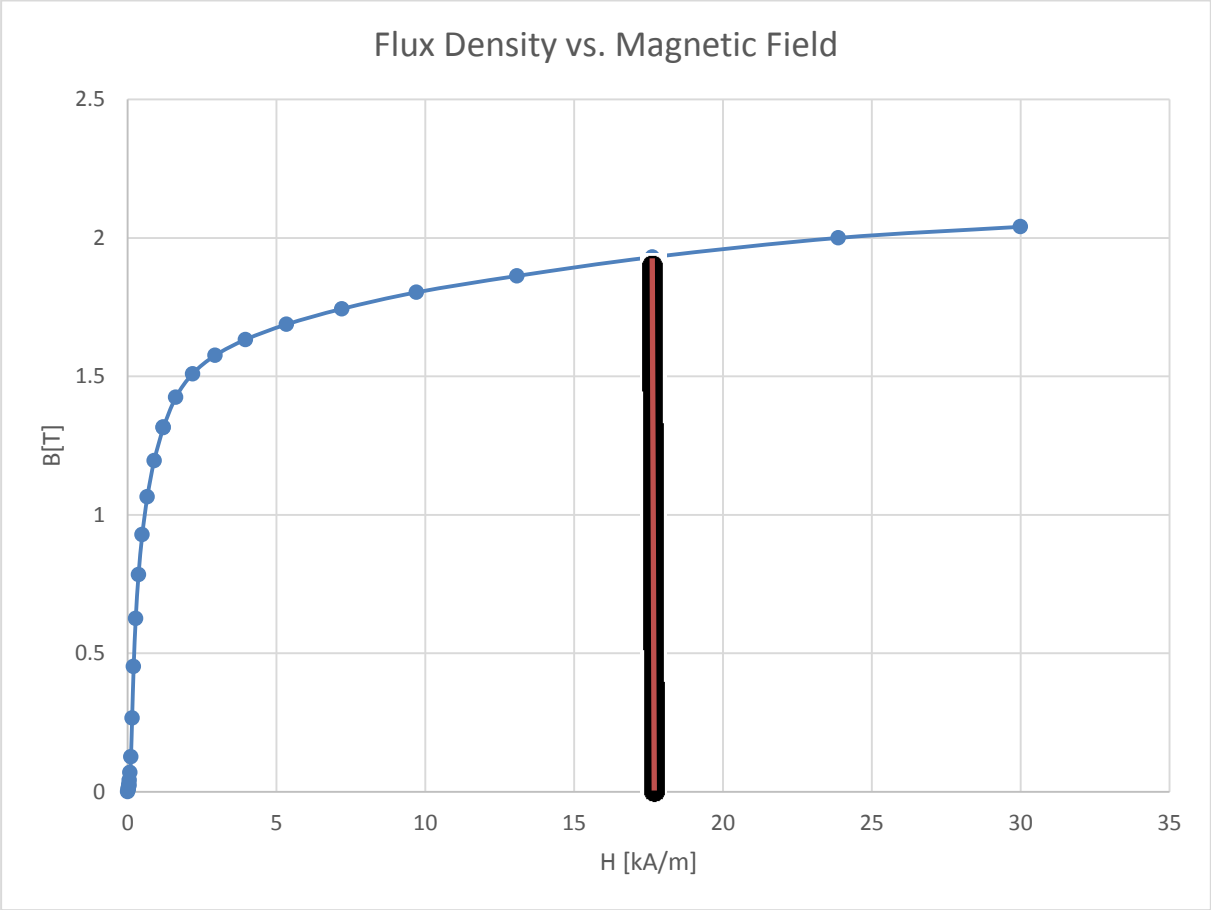


Figure 4: Flux Density vs. Magnetic Field.[3]

Another term that should be understood in relation with the matter in hand is the saturation, which can be defined as the point at which further magnetization level will not lead to any significant change in flux density. Looking now at Figure 4 above, which shows the B/H curve for a S235JR grade steel, it can be seen that the curve behaves almost linear at about 17,5 kA/m with only marginal increases in the Magnetic field after 20 kA/m. There will always be different interpretation as to where the saturation level of a B/H curve lies, that is why real defect data has to be considered in order to be able to determine inspection capabilities as well as an acceptable field level.[5]

How the magnetization level can affect the quality of an obtained MFL signal will be investigated more in depth in Chapter 4, as 4 different metal bars, where different anomalies were drilled, will be magnetized under 4 different magnetization levels.

### 2.3.2 Velocity

The velocity effects can have a dramatic influence on the results, as it does not only affect the applied magnetic field but also the flux leakage. In general, velocity effects can be detected at speeds exceeding a few kilometres per hour. These effects need to be quantified in order to have a complete understanding of the capability of the inspection system.[10]

The physical principle behind the velocity effect can be understood based on Lenz's law which states, that the direction of a current induced in a conductor by a changing magnetic field will be such, that it will create a magnetic field that opposes the change that produced it; during an MFL inspection it's no different. The moving tool will produce eddy currents in the pipe that oppose the originally applied magnetic field, which in turn will decrease the flux leakage levels and with it the efficiency of the detection and characterization of defects.[1]

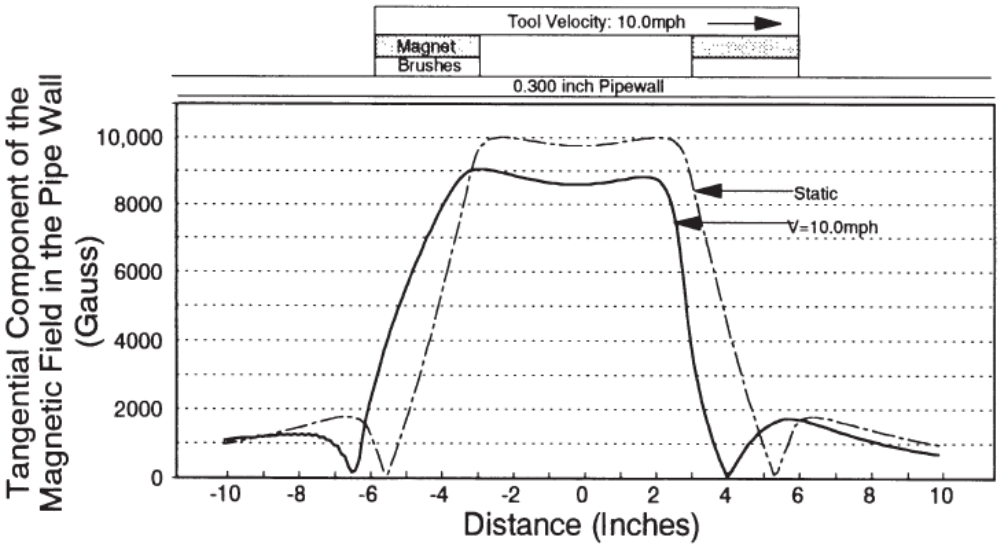


Figure 5: Velocity Effect on the magnetic field.[1]

Figure 5 shows the expected field levels due to velocity effects on a pipe with no defects. For the static case, the magnetic field stays more or less uniform, note that 1 Gauss = $10^{-4}$ Tesla. With the increase in speed it can be clearly seen that the strength of the magnetic field dropped significantly and its symmetry is lost, which would affect the detection and the characterization process.

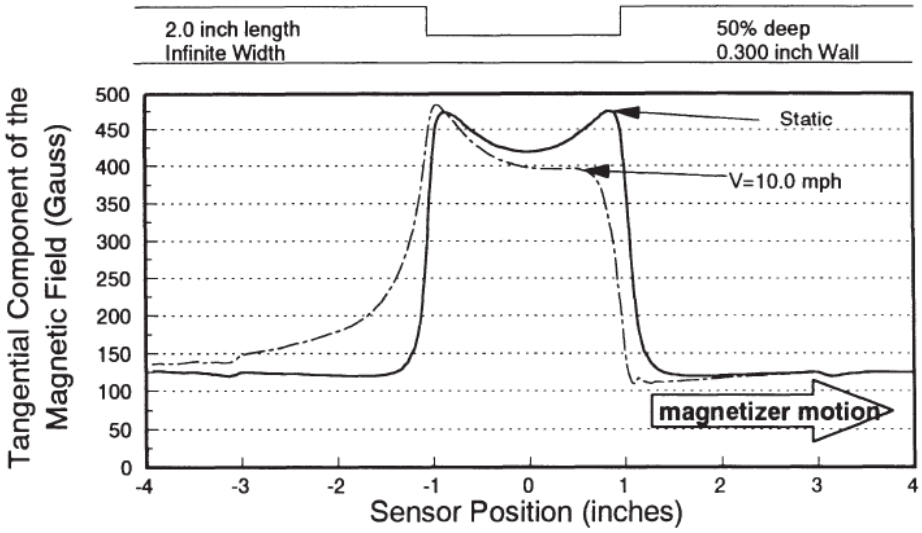


Figure 6: Velocity Effect at the Presence of a Defect.[1]

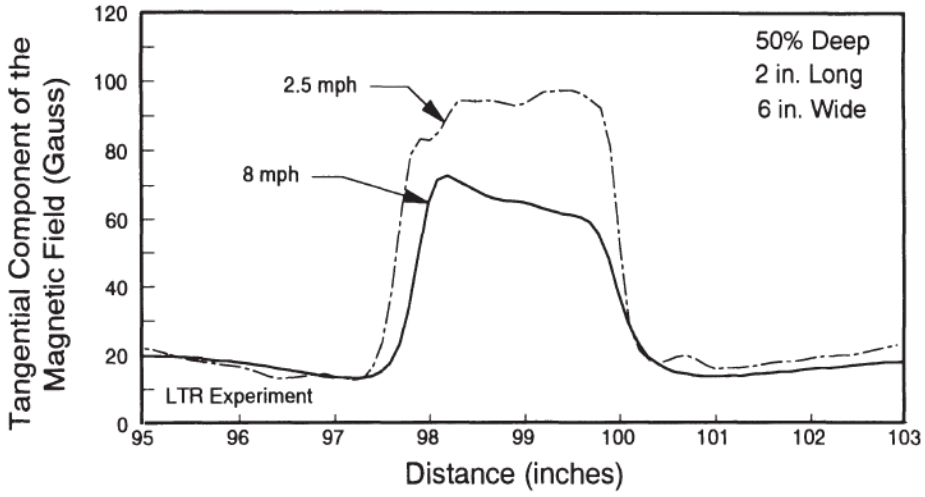


Figure 7: Velocity Effects at different Speeds.[1]

Figure 6 shows the expected behaviour of the leakage fields around a defected region when velocity is increased. Figure 7 shows the tangential field components at 2.5 and 8.0 miles per hour. From these two figures it can be concluded that:

- An increase in velocity causes a decrease in the flux leakage field, reducing the defect detection and characterization accuracy.
- Symmetry of the flux leakage field is lost as the signal tends to shift towards the trailing pole, making it difficult to interpret defect length as it is highly dependent on the length of the measured leakage field.

### 2.3.3 Sensors

As previously mentioned, sensors are utilized in the MFL tools in order to measure the flux leakage. The sensors work by transforming the leakage field into an electrical signal that can be stored and later on analysed. The sensors perform two main tasks, the first one is to provide enough data to allow the signal to be analysed properly in order to detect any present defects, and the second one is to make that provided data manageable.

The two most used types of sensors are either induction coils or Hall elements. While the coils measure the rate of change in the magnetic field, the Hall elements measure the actual magnetic field strength.

In the past, the induction coils have been mostly commonly used as they did not require a power source, since voltage can be generated in the coil as it passes through a changing magnetic field.[13]

Nowadays newer MFL tools use Hall sensor instead of the induction coils. On the contrary to coil sensors, Hall sensors can directly convert the magnetic field level to an output voltage.

Another very important parameter when it comes to sensors is the position of the sensor with respect to the magnet poles. For a slow moving or a static tool, sensor located exactly in the middle between the two poles will provide a symmetric signal for symmetric defected regions. The further the sensors are moved away from the poles the more the asymmetry in the signal.[4]

In the following chapter the dependency of the MFL signal on the positioning of the sensor relative to the two magnet poles of the tool will be investigated by performing several test runs involving a varying distance between the magnet poles and the sensors.

# 3 Tool Assembly and Test Set up

As explained earlier the aim of this project is to investigate the dependency of both the sensor positioning and velocity, in order to achieve that this work will be divided into two main sections each discussing each of those dependencies, which will be referred to as part A for the sensor dependency section and part B for the velocity section . In this chapter, the tool assembly as well as the tests' setup and procedures for both sections will be explained before going into the results later on in the following chapters.

## 3.1 Tool Assembly Part A

Figure 8 shows the tool that was used for the tests conducted in part A, which consisting of:

1) **The yoke:** Containing two magnet poles, with each pole housed on each side of the tool, and contains 4 pieces of magnets. In addition to that, two wheels at the front and the back to help push the tool along the metal bars.
2) **The Odometer:** At the front of the tool to record the distance.
3) **The Sensor carrier:** Which is a plate where 32 Hall sensors are installed in a row, which will help detect any changes occurring to the magnetic field due to the presence of the defects.
4) **Electronics:** Which serves as battery and a storage to collect the sensor as well as the odometer data

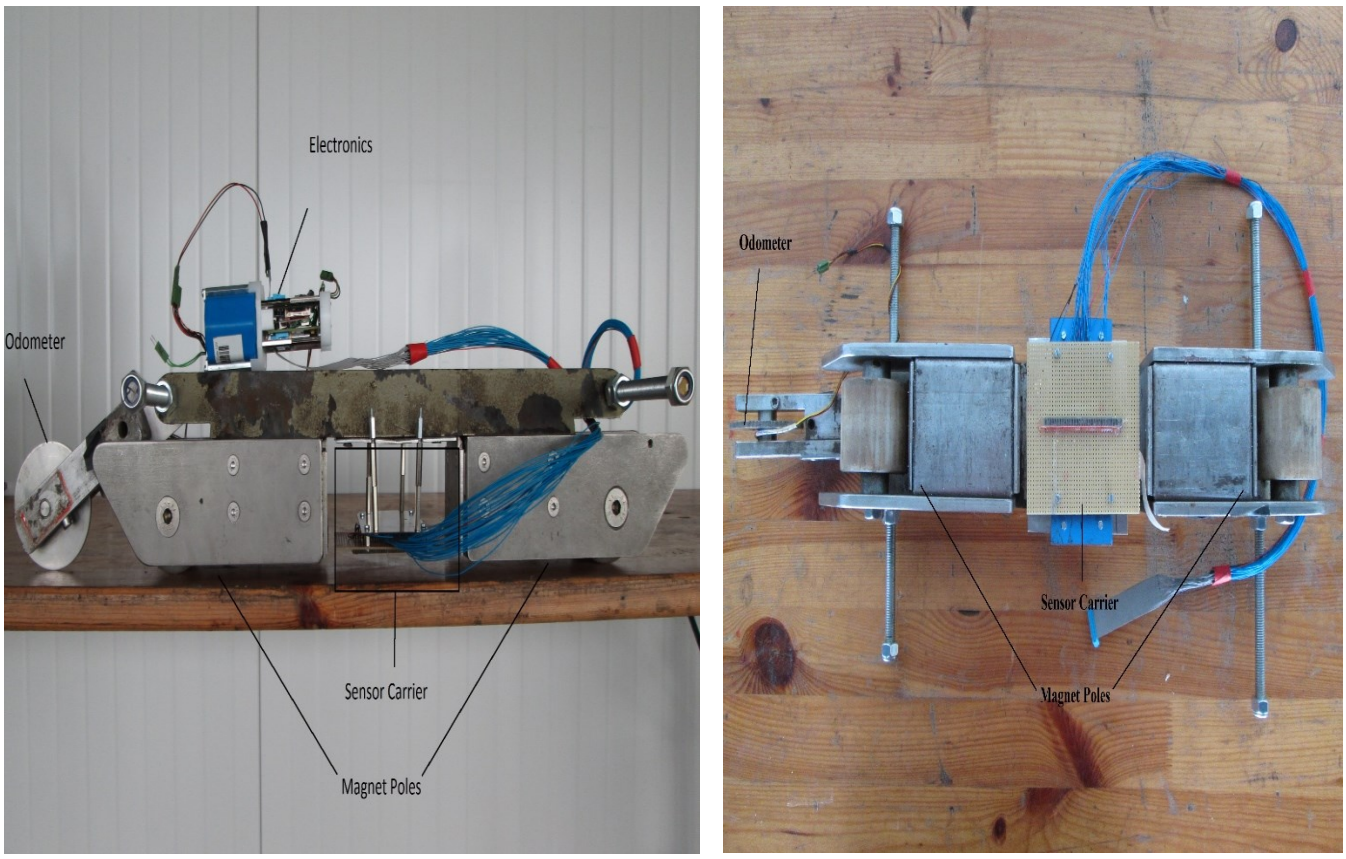


Figure 8: Sensor Carrier Side and Top View.

Figure 9 shows how the sensor were installed on the sensor carrier, they were also covered with a strong glue material in order to protect them from any damage.

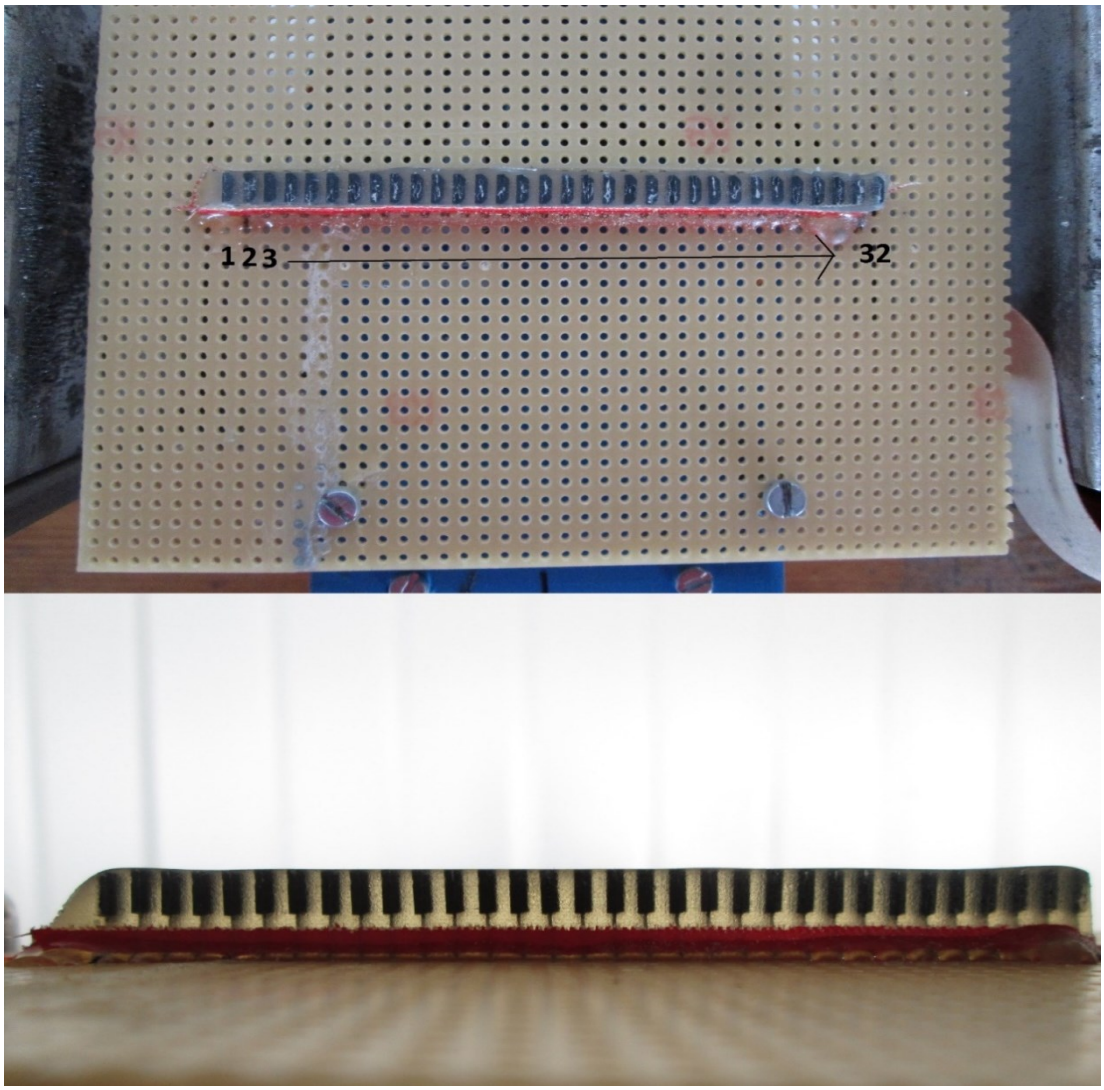


Figure 9: Sensor Carrier.

## 3.2 Test Setup Part A

The tool will then be run in an axial direction along four different metal bars, each of which having a different thickness, resulting in different magnetization level in each bar. Table 1 below shows the dimensions of each bar as well as the corresponding magnetization level. Each bar has 5 defects, 4 of which are circular with a diameter of 16mm and depths varying from 2mm to 8mm. The fifth defect is a 100mm x 16mm groove. The five defects are the same in all the metal bars. Having the same defects in all the bars will insure that the data obtained is consistent and comparable among each other. Table 2 below shows the dimensions of each defect. The sensors should then move centrally one after another along those defects. Since the velocity effects are not to be investigated in this part, running the tool along the bars will be performed simply by pushing it by hand at a low and constant speed.

Table 1: Magnetization Levels.

| Bar Dimension[mm] | Magnetization Level |
|---|---|
| 100x30 | 2,94 kA/m(very low) |
| 100x20 | 6,75 kA/m(low) |
| 100x12,5 | 14,20 kA/m(intermediate) |
| 100x8 | 21,02 kA/m(high) |

Table 2: The Dimensions of the five Defects.

| Defect 1 | Defect 2 | Defect 3 | Defect 4 | Defect 5 |
|---|---|---|---|---|
| Φ16<br>Depth:2[mm] | Φ16<br>Depth:4[mm] | Φ16<br>Depth:6[mm] | Φ16<br>Depth:8[mm] | 100 x 16<br>Depth:2[mm] |

After running the tool, the data collected from each of the four runs is then separately imported into the company's software ''PipeAnalysis'' to be further investigated, as it will be explained in the following chapters.

## 3.3 Tool Assembly Part B

For this part the sensor carrier was modified with another one where the sensors are spread further from one another with the outer sensors closer to the magnet poles, the number of sensors however, stayed 32. This shall allow for a better coverage of the whole area in between the two poles, allowing for a more accurate investigation of the sensor positioning dependency. Figure 10 below shows the assembly of the new sensor carrier.

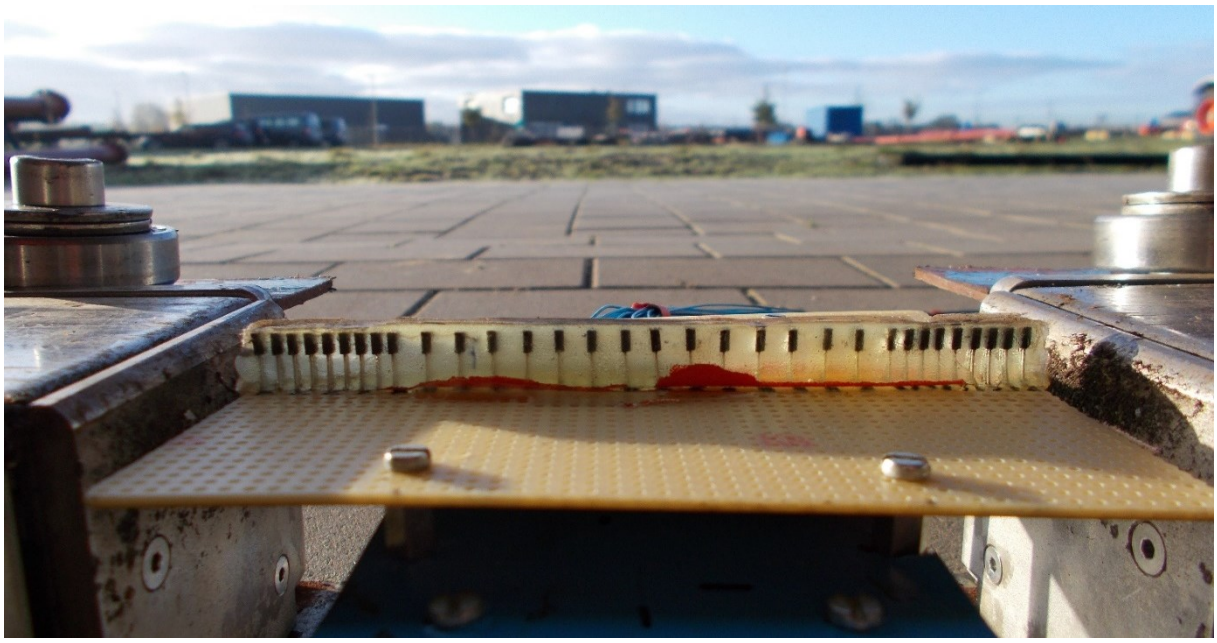

Figure 10: Sensor Carrier Part B

Furthermore, four ball-bearings were also mounted on each side of the tool in order to make sure that the tool will remain centralized over the metal bars throughout the pulling procedures as seen in Figure 11 below. Apart from that there were no more changes to the tool assembly.

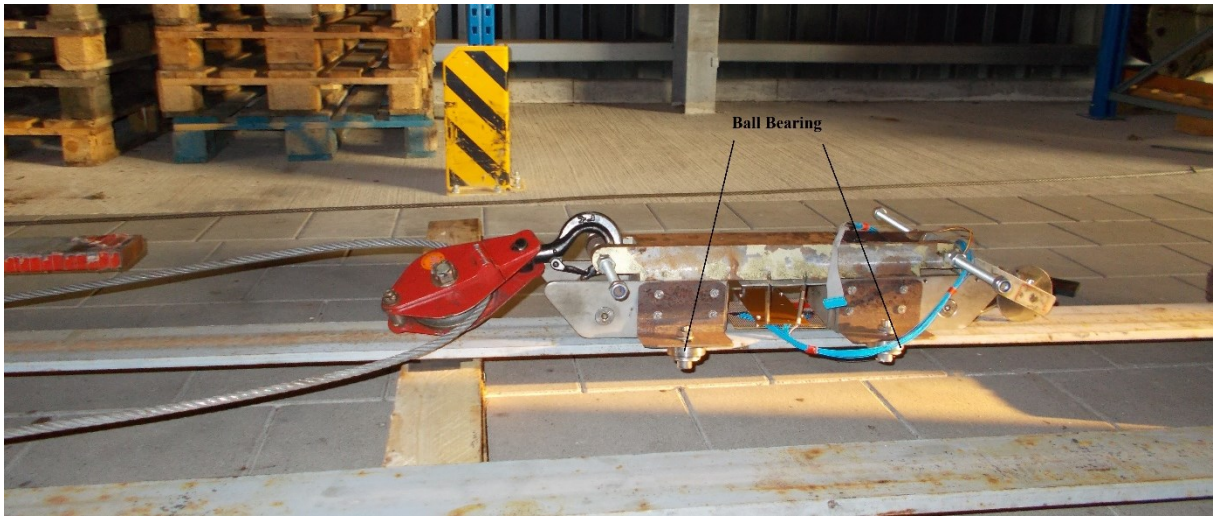


Figure 11: Ball Bearings.

## 3.4 Test Setup Part B

For this part, the bar 100mmx30mm will be left out for reasons that shall be explained later in the coming two chapters.

In order to fully understand the effect that the velocity can have on the obtained MFL signal, the tool was run under seven different velocities over each of the remaining three bars. Those velocities vary from very slow i.e. 0,1 m/s, to very high i.e. 4,5 m/s. Basically the

procedure is the same as it was in Chapter 0, the only difference is how the pulls were performed for velocities above 2 m/s. Table 3 below as well as Figure 12 and Figure 13, illustrate how the pulling was performed for each velocity.

Table 3: How the pulling was performed.

| Velocity[m/s] | How the pulling was performed |
|---|---|
| 0,1 | By Hand |
| 1 | By Hand |
| 1,5 | By Hand |
| 2 | Fork lift |
| 2,5 | Fork lift and a sheave |
| 3 | Fork lift and two sheaves |
| 4,5 | Wire winch and a sheave |


Figure 12: 3m/s pull test.

Figure 13: 4,5 m/s pull test.

Figure 12 shows how the 3 m/s velocity was reached by using a wire rope where one end is fixed(the right part of the wire on the picture), then going through one sheave hooked to the fork lift and another one to the tool, the loose end of the wire is then attached to the fork lift. For the 2,5 m/s same principle was applied with only one sheave hooked to the fork lift and the loose end of the wire attached to the tool.

In order to come up to the 4,5 m/s velocity a wire winch had to be utilized in addition to a sheave as seen in Figure 13 above. The first three velocities were simply performed by pulling the tool over the defect by hand and the 2 m/s were reached by pulling the tool directly with a wire rope by the fork lift.

In the following chapters, data obtained from the tests conducted in both part A and B will be illustrated and interpreted.

# 4 Sensor Positioning Dependency

As explained before, the positioning of the sensors relative to the magnet poles can have a significant effect on the quality of the results. In this chapter this dependency will be further investigated and analysed through a series of tests conducted at 3P-Services workshop as it was previously explained in chapter 3. After running the tool, the data collected from each of the four runs is then separately imported into the company's software ''PipeAnalysis'' to be further investigated, as it will be explained in the following segments of this chapter.

## 4.1 Very low Magnetization (2,94 kA/m)

As discussed in chapter 2, magnetization is an important factor when it comes to applying the MFL technology. As shown in Figure 14, 4 metal bars were used with the same width but different wall thicknesses; this will lead to a different magnetization level in each bar, from very low in the thickest bar to very strong in the thinnest one. Eventually the impact of the different magnetization levels will be seen in the quality of the data obtained from each bar.

First the thickest bar will be inspected, which is the 100mm x 30mm one.


Figure 14: The 100mm x 30 mm Bar.

In Figure 14, it can be seen how the defects were drilled into the bar as well as their dimensions. The defects 1 to 4 are normal circular defects, whereas defect 5 is a groove, which is a rectangular slot drilled across the complete width of the bar. The groove is then filled with a strong glue material to facilitate the movement of the yoke over it. The tool will then be run from the right hand side, starting with defect 1 all the way to defect 5. After the run is done the electronic piece, where the data has been stored, is then disconnected from the tool and taken for the data to be read and visualized via the software ''PipeAnalysis''. Figure 15 below shows how the data looks like when imported to the software.

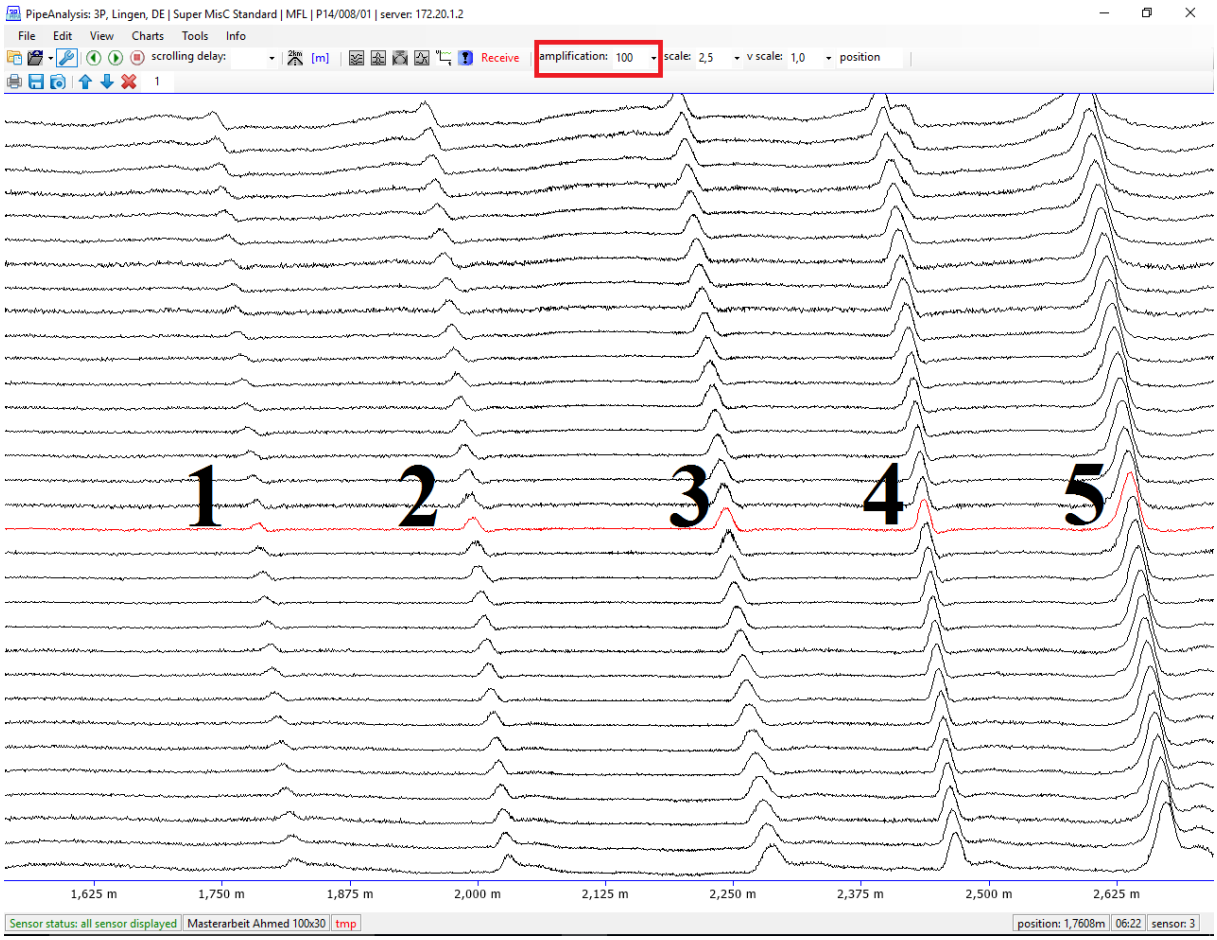


Figure 15: Corresponding signal for the first Bar.

The first remark to be noted in this case is that the signal had to be amplified to a magnitude of 100, in order for the defects to be identifiable the way they are in the picture. That can be related to the fact that the magnetization level in this bar is as low as 2,94kA/m when measured with a Gauss Meter, which shows the importance of magnetic saturation when it comes to implementing the MFL technology.

Figure 15 shows 32 lines lying on top of each other, each one represents the magnetic field lines read by each of the 32 sensors that were connected to the electronic device.

When the tool runs over parts where no anomalies are present the field lines stay parallel and no leakage occurs, hence the straight signal lines in Figure 15. Once the sensors run over a defect flux leakage occurs, causing the signal to peak at the defected region. Each peak represents a defect detected by one of the sensors, meaning for each defect there are 32 peaks on top of one another with a slight shift between each sensor reading for the same defect since the sensors are installed in a row as seen previously shown on Figure 9.

It can clearly be seen that as the defects get deeper and deeper, the signal peaks increase in amplitude, showing a bigger material loss in each case.

It can also be noticed that the groove, despite having a depth of only 2mm like the first defect, shows the highest amplitude. That is because the groove is drilled along the whole width of the bar, meaning there is not as much area of the bar around it when compared to the other defects. Magnetic flux always forms a closed loop, but the path of the loop depends on the resistance of the surrounding materials. It is concentrated around the path of least resistance. Air and vacuum have high resistance, while strong magnetized materials have low resistance. So coming back to the situation in hand, the normal circular defects have more metal area around them for some of the field lines to ‘’escape’’ through, whereas at the groove the field lines have no choice but to go through the air gab and eventually to leak, creating a higher amplitude despite the smaller depth.

Another factor that should be taken into consideration is the magnetization level of the bar. So in the case of the circular defects, not only do they have a bigger area around them, but also the magnetization level is too low.

In order to analyze the data more in depth, the amplitudes recorded for each defect by all the sensors have to be looked at.

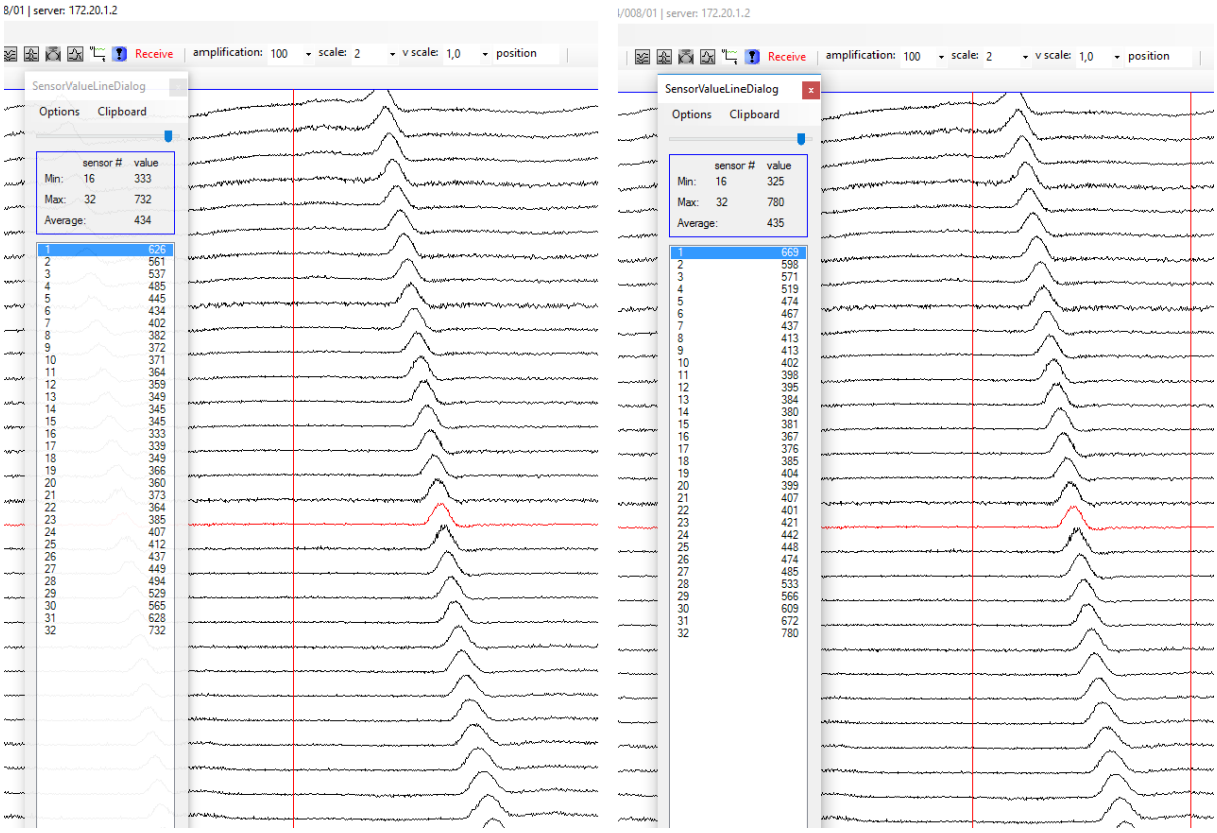


Figure 16: Obtaining the Amplitude.

With the help of the software the offset values for each effect can be determined, as seen on the left hand side of Figure 16. The offset represents the magnetic field at non-defected intervals, meaning areas where no flux leakage is present, and it is the basis for measuring the signal’s amplitude for a present defect. Then the maximum values for a highlighted interval can also be obtained for each sensor, which can be seen on the right of Figure 16.

The values are given in so called ‘’counts’’, which is a unitless and are proportional to the output voltage recorded by the sensors as a result of the presence of the changing magnetic field. By subtracting the offset values from the maximum values, the amplitude can be calculated. This is then performed for all other defects. The results are then illustrated by recording the amplitude against the corresponding sensor, with sensor 1 being the leading sensor as seen in the Figure 17 below. In this work the amplitude will be referred to as ‘’A’’, so for example the amplitude values of defect one will be described as ‘’A1’’ and so on for the other defects.

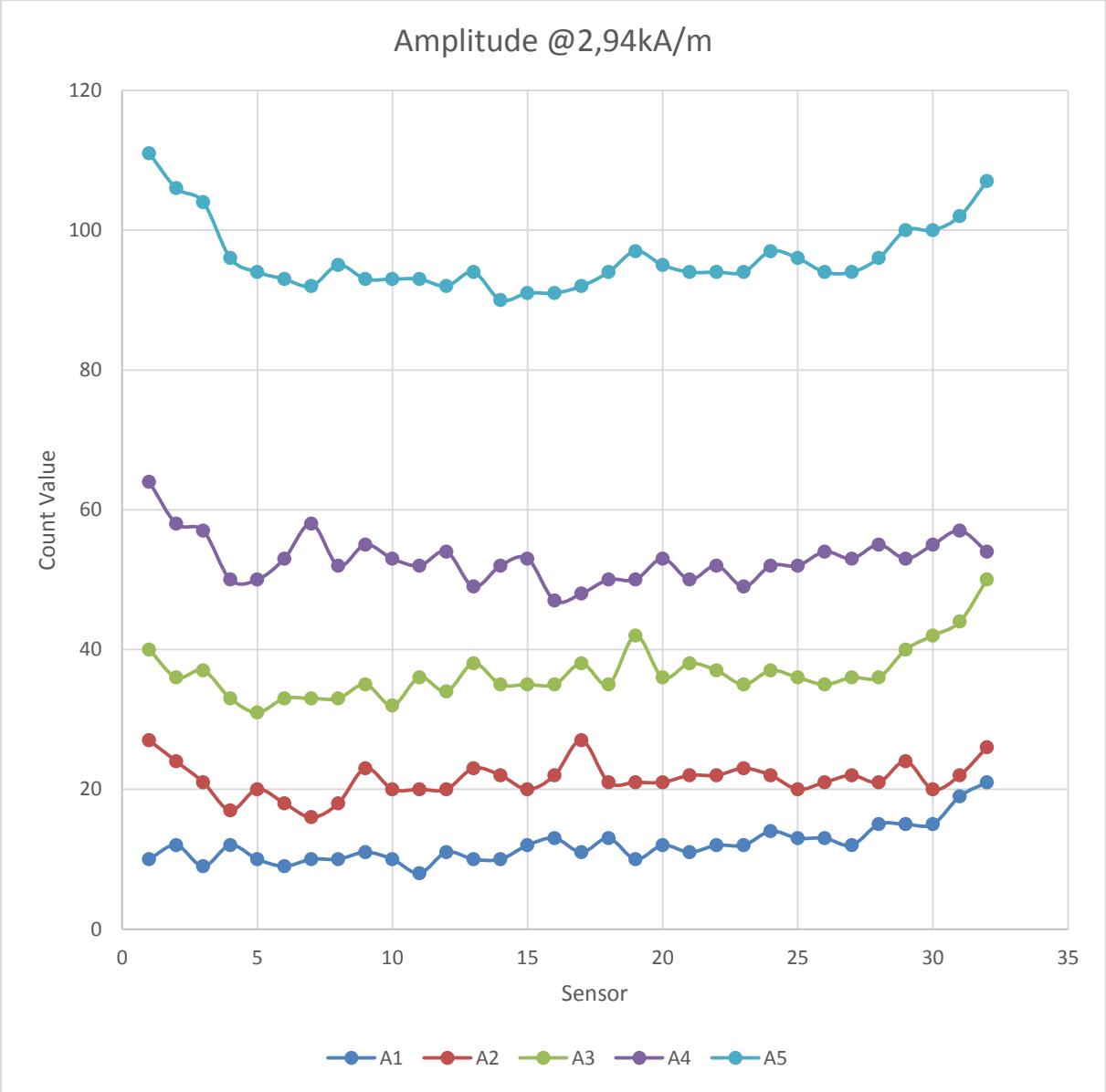


Figure 17: Amplitude @2,94kA/m.

The first thing that can be noticed is the strong fluctuations in each line. That is due to the fact that since the magnetization level is really low, just a small change in the offset or the maximum values can already make a big impact on the behaviour of the lines. At the smaller defects, especially 1 and 2, it is hard to notice any change in the amplitude, the values are

almost constant. As defects get deeper, a general trend can be observed with the sensors lying closer to the poles showing higher amplitude than the ones close to the centre. That trend is clearer at the groove, the sensors closer to the magnet poles show higher amplitude. But nonetheless, as mentioned before the low magnetization levels have a huge impact on the obtained results, so one cannot make a distinctive judgement based on these data alone.

Another thing that can be noticed is the big gap between the groove and the other defects. The reason is the same as why higher peaks were obtained for the groove despite the smaller depth, which was explained earlier.

In addition to the amplitude, the width of a defect can have a huge contribution to anomalies detection. In order to investigate how the width is affected with changing sensor positioning as well as different magnetization levels, the ‘’Full Width at Half Maximum’’ (FWHM) was measured for each defect for each sensor signal.

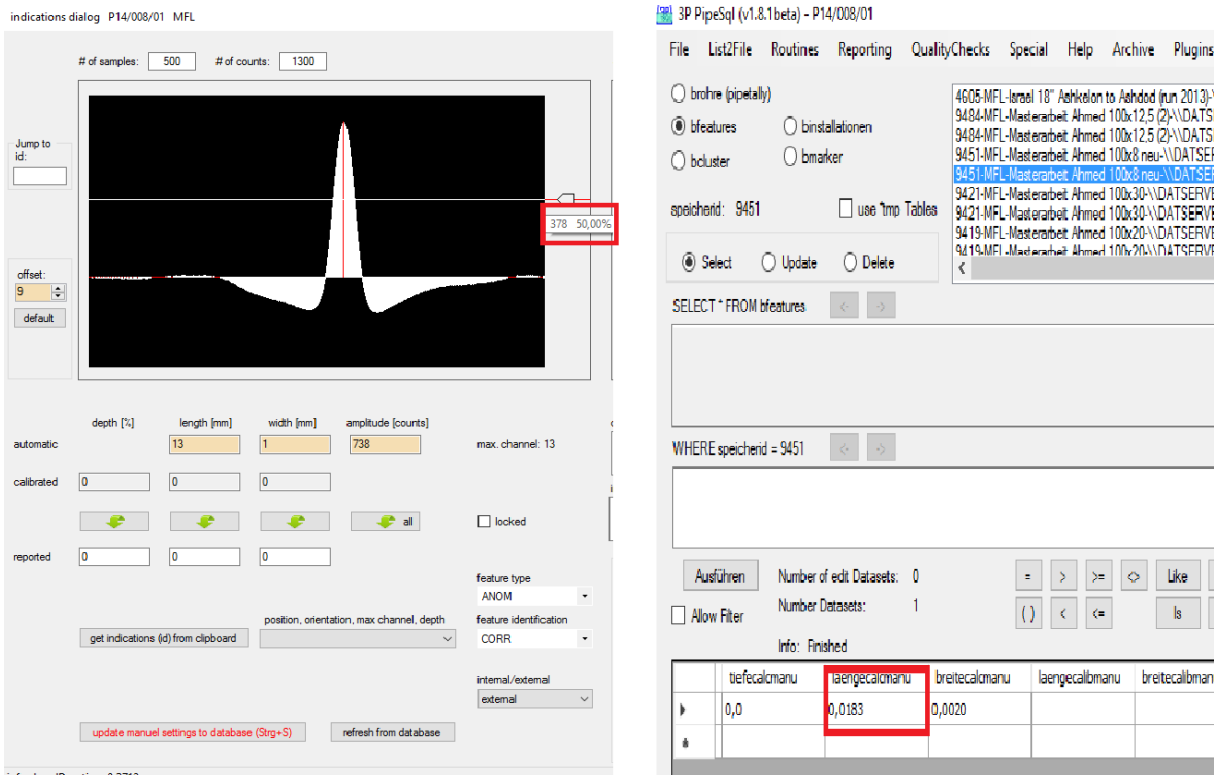


Figure 18: Obtaining the FWHM.

By accessing each defect via the software, any assigned length can be obtained as seen in Figure 18, in this case it is assigned at the middle of the amplitude in order to get the FWHM. All the assigned lengths are then stored in the company’s data base and can be recovered from there.

Like the amplitude, the same graph is generated again, but this time for the width.

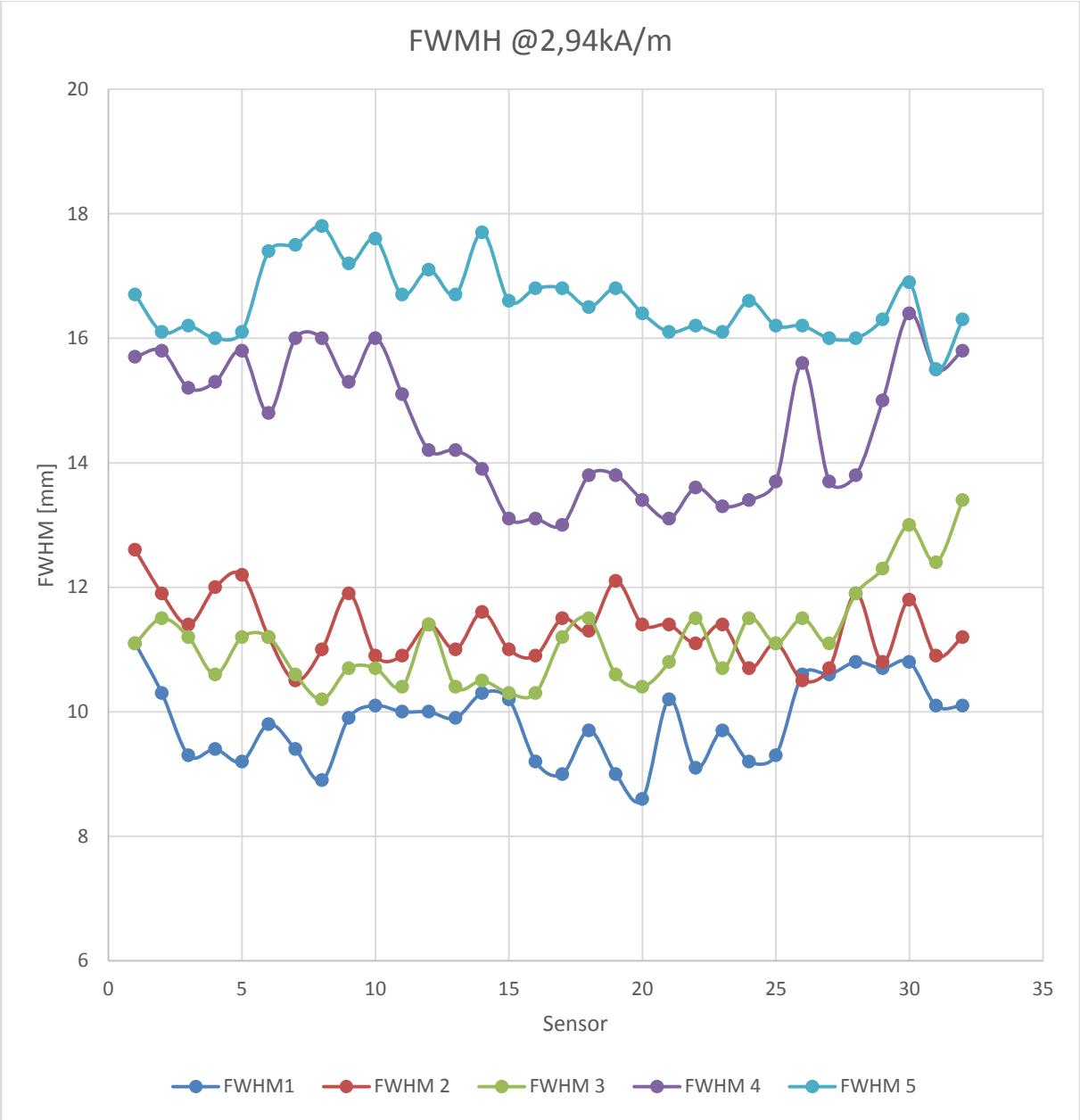


Figure 19: FWHM for the first Bar.

As was the case for the amplitude, fluctuations are once again present at each defect due to the strong sensitivity of the offset, caused by the low magnetization level, which is why further investigation is required in order to precisely characterize the behaviour of the signal.

## 4.2 Low Magnetization (6,75kA/m)

For the next Bar a thinner wall thickness was chosen (20mm) in order to achieve stronger magnetization with the same magnet, in this case it was 6,75 kA/m.

The bar, like all the other ones, contains again 5 defects with the same dimensions as the 100mm x 30mm bar, with one being a groove. Figure 20 below shows the order in which the defects were drilled.

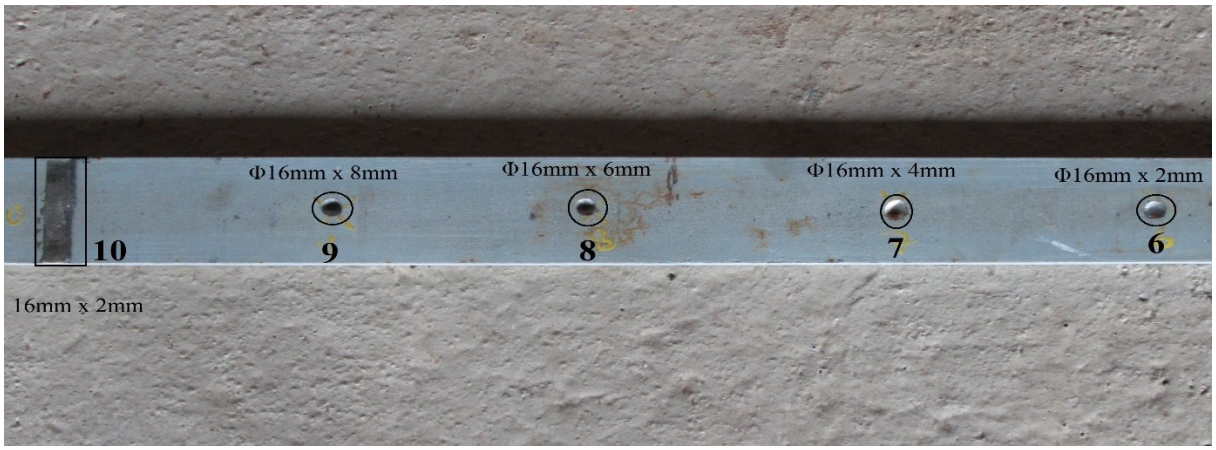


Figure 20: The 100mm x 20mm Bar.

Same as before the tool was run and the data was imported to the software.

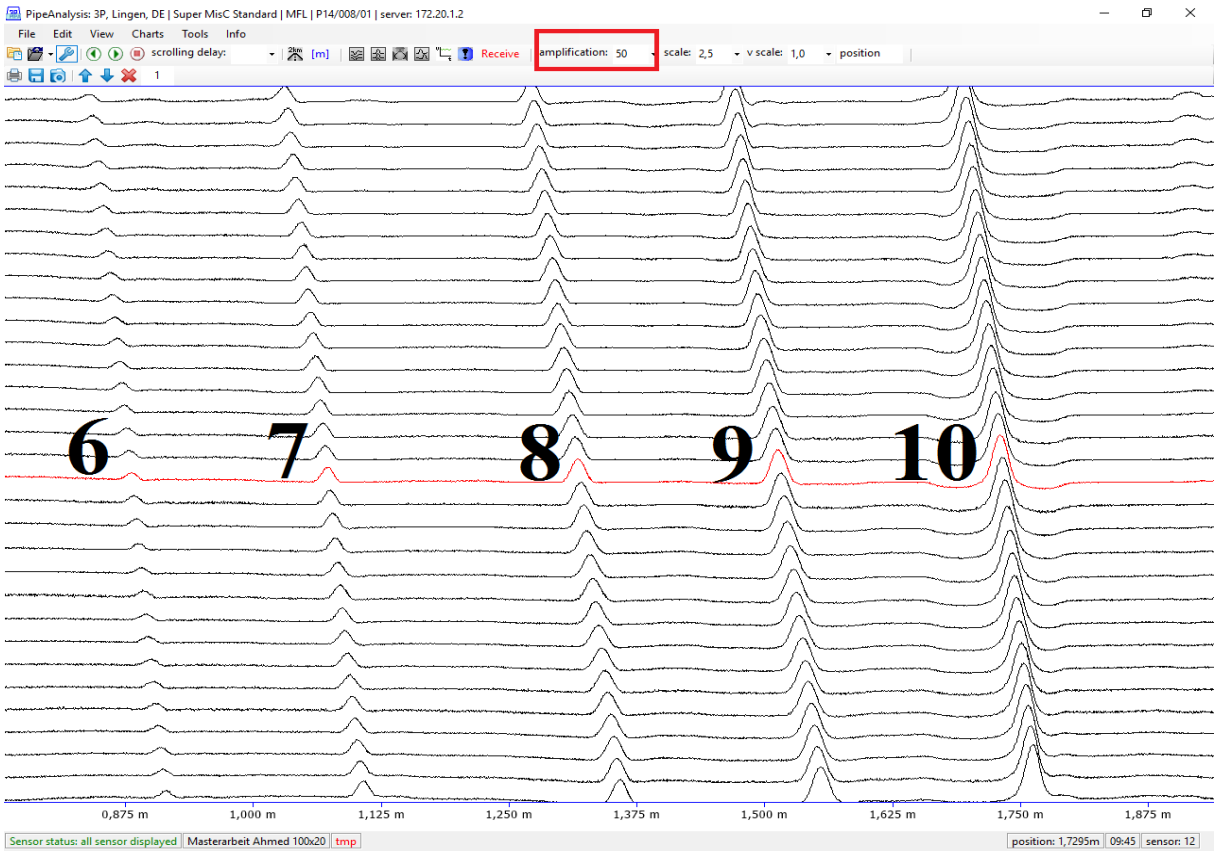


Figure 21: Corresponding signal for the second Bar.

Compared to the previous bar higher peaks can already be recognized for all the defects, in spite of an amplification that is only half as much and at a magnetization level that is still lower compared to the previous case, especially when it comes to the shallower defects.

To analyse the data more closely, the amplitude and the FWHM curves were generated again.

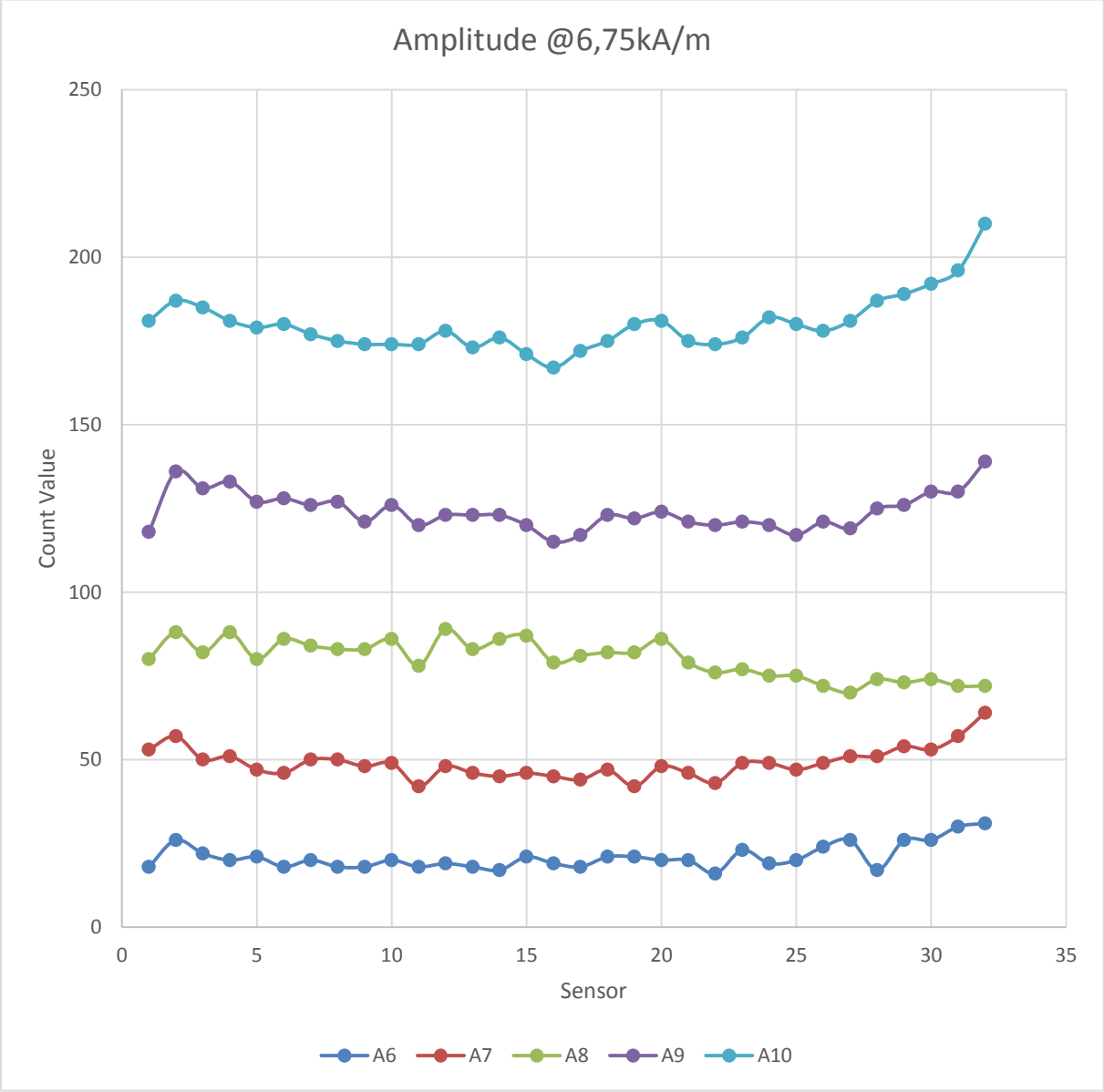


Figure 22: Amplitude @6,75kA/m.

Compared to the previous bar, it can be seen that the data is smoother and more consistent. What remains the same is the behaviour of the first four defects (6, 7, 8 and 9), they all show relatively constant values. When it comes to the groove, the curvature can again be noticed, with an increase in values from the middle up to the sides, but this time it is more gradual, and not as steep as before. That is of course due to the fact that the magnetization level is higher, leading to higher count values for the amplitude when compared to the

100mmx30mm bar. So the behaviour of the curves won't be as sensitive to a change in the offset as before.

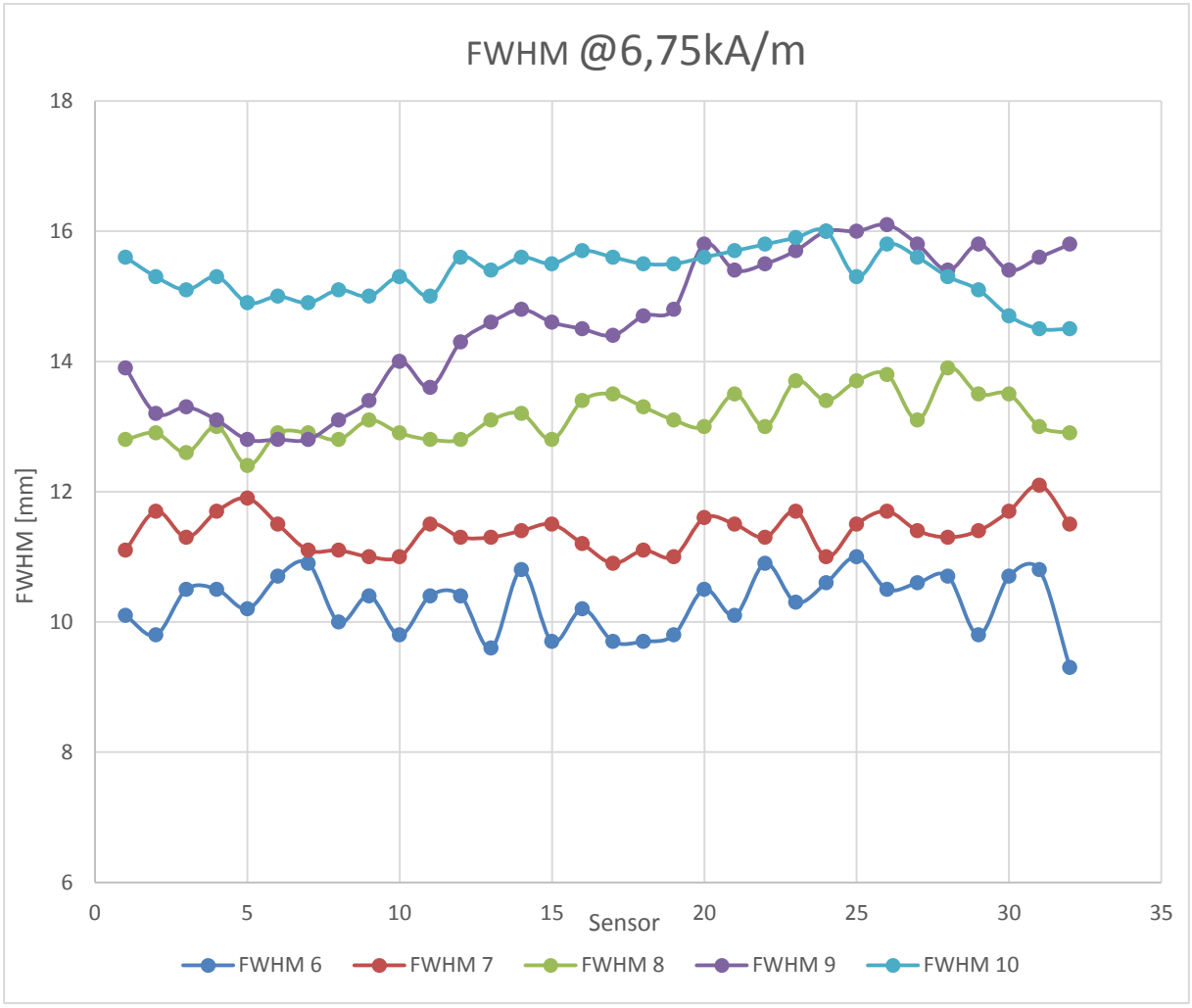


Figure 23: FWHM @6,75kA/m.

Even though some fluctuation and irregularities are still present, the FWHM plot shows a much better trend this time.

It can be seen that the general trend is for the FWHM to stay constant and not increase when moving towards the sides, as was the case for the amplitude.

But yet again the magnetization levels are still too low to verify any distinct theories regarding the behaviour of the amplitude or the width. However, it can still be seen how a slight increase in the magnetization, affected the quality of the results and the data obtained from the two previous tests.

## 4.3 Intermediate Magnetization (14,20 kA/m)

So far the wall thicknesses that have been dealt with had low saturation magnitudes, in this case the thinner 12,5 mm bar will deliver a magnetization of 14,20kA/m.

Figure 24 below shows the defect present along the bar. Note that the order in which the first 4 defects were drilled is different than it was in the two previous cases, with the deepest defect at the beginning, but maintaining the same numbering order, starting with the shallowest defect as number 11 and ending with deepest defect then the groove as number 14 and 15 respectively.

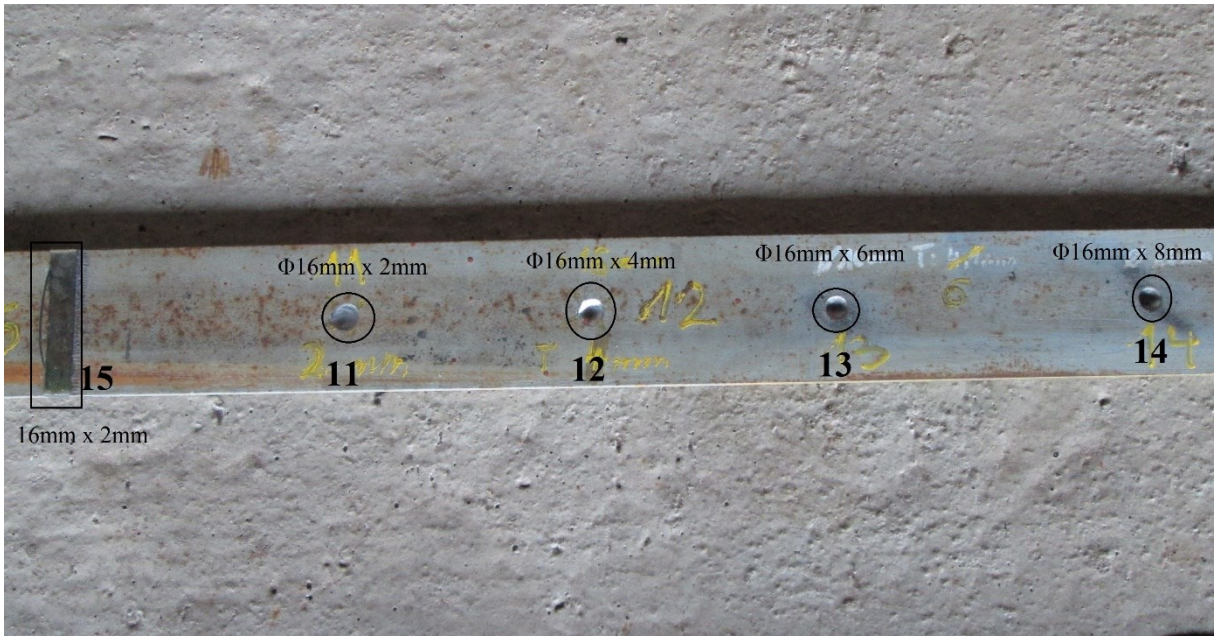


Figure 24: The 100mm x 12,5mm Bar.

The following signal is then generated after running the tool and importing the data into the software.

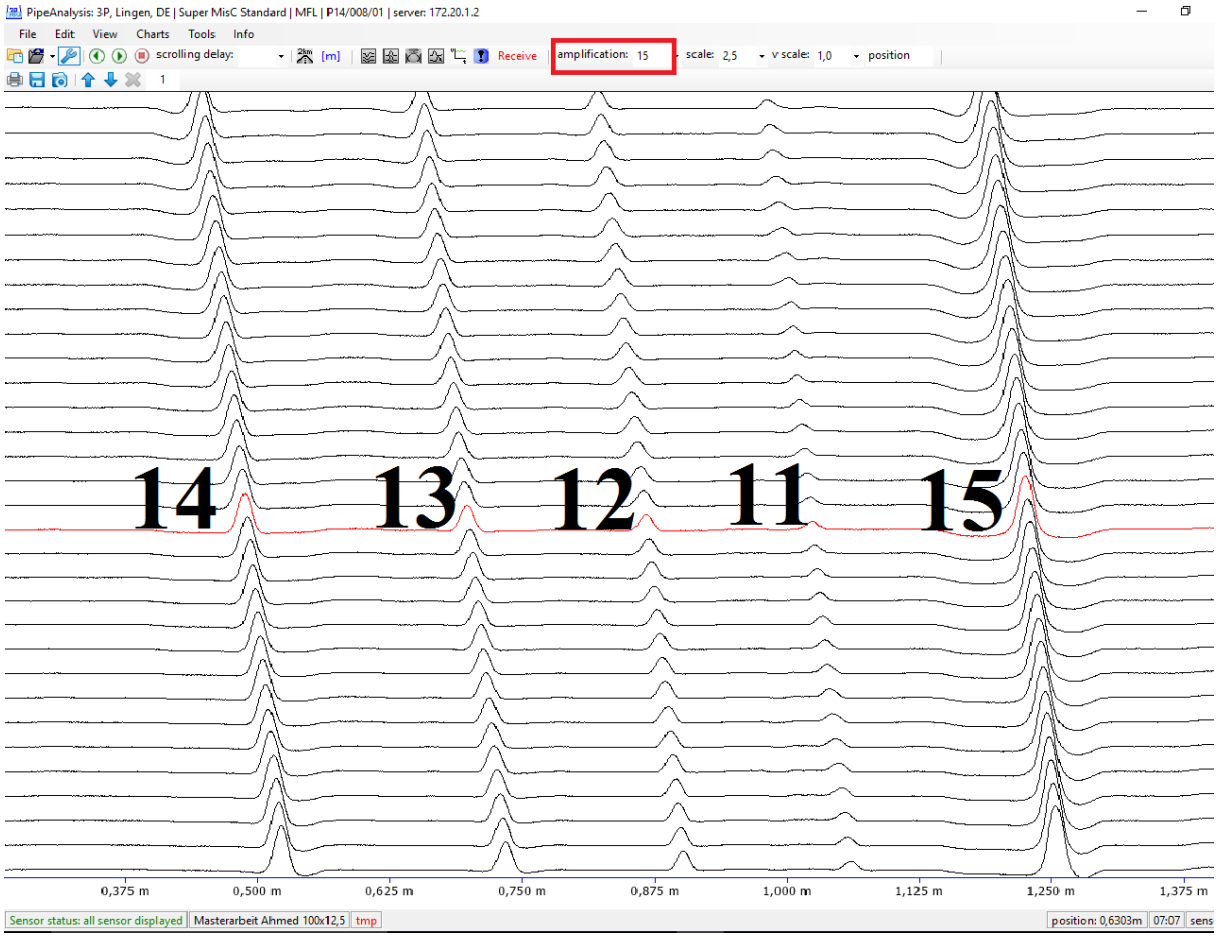


Figure 25: Corresponding signal for the third Bar.

Since the magnetization level is really high in this case. The signal had to be amplified only to a magnitude of 15 compared to 50 and 100 in the previous two bars.

To illustrate the difference a bit more Figure 26 below shows how the same signal would look like if it was amplified to 100 like the very first bar.

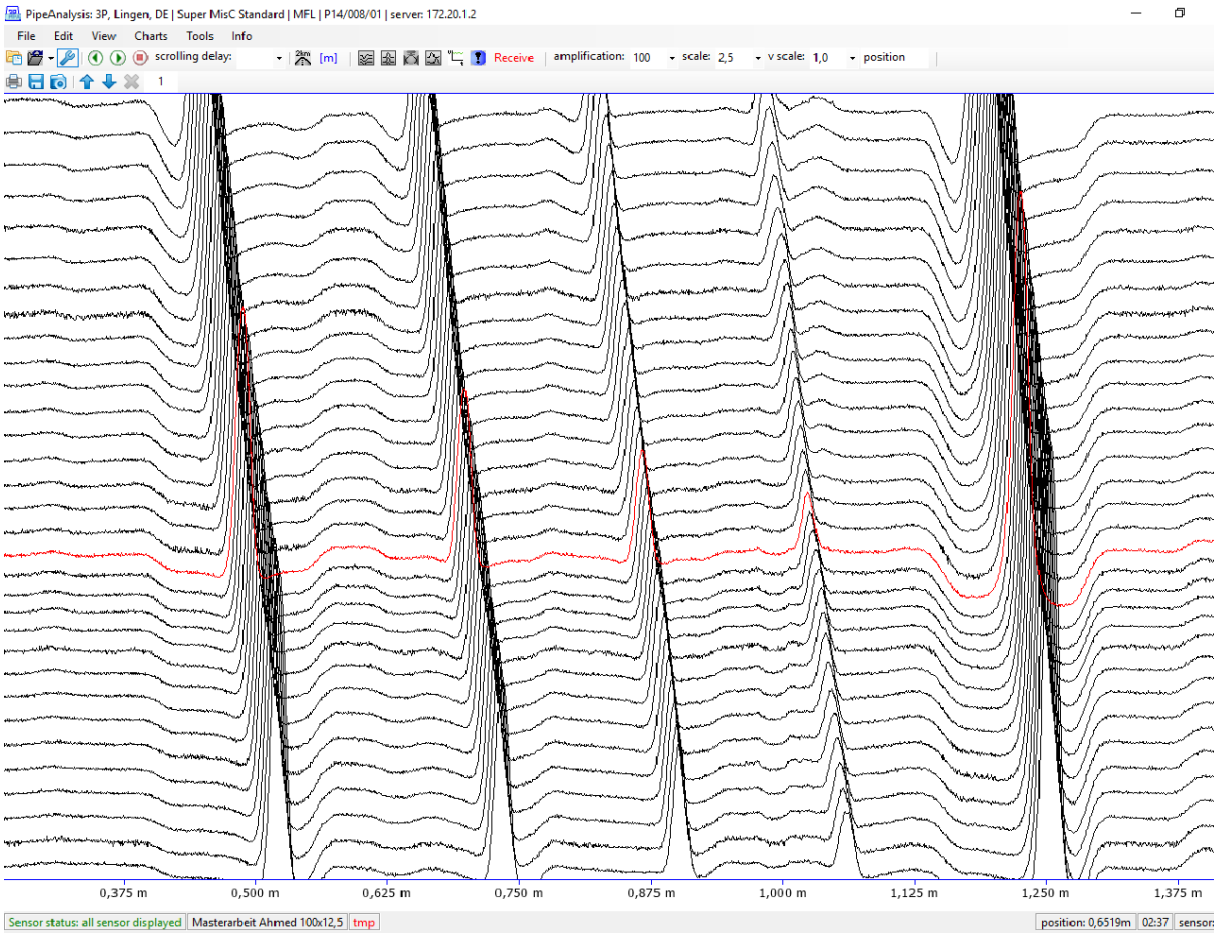


Figure 26: Amplified Signal.

It can be clearly seen how the magnetization level can strongly affect the strength of the obtained signal and with it the ability to detect any anomalies.

The difference between this bar and the previous two is strongly evident. With the increase in the magnetization level, bigger values for the amplitude were reached, and consequently the data are not as sensitive to small changes in the offset like before. As a result the curves show a smooth and less fluctuating form. Like the previous cases, the amplitude tends to increase as the sensors get closer to the magnet poles, giving that curveted form.

Important to notice is also the fact that, the smaller defects, especially 12 and 13, now show the same behaviour as well, which was not the case at low magnetization levels. Defect 1, however, did not behave accordingly and stayed rather constant for all the sensors.

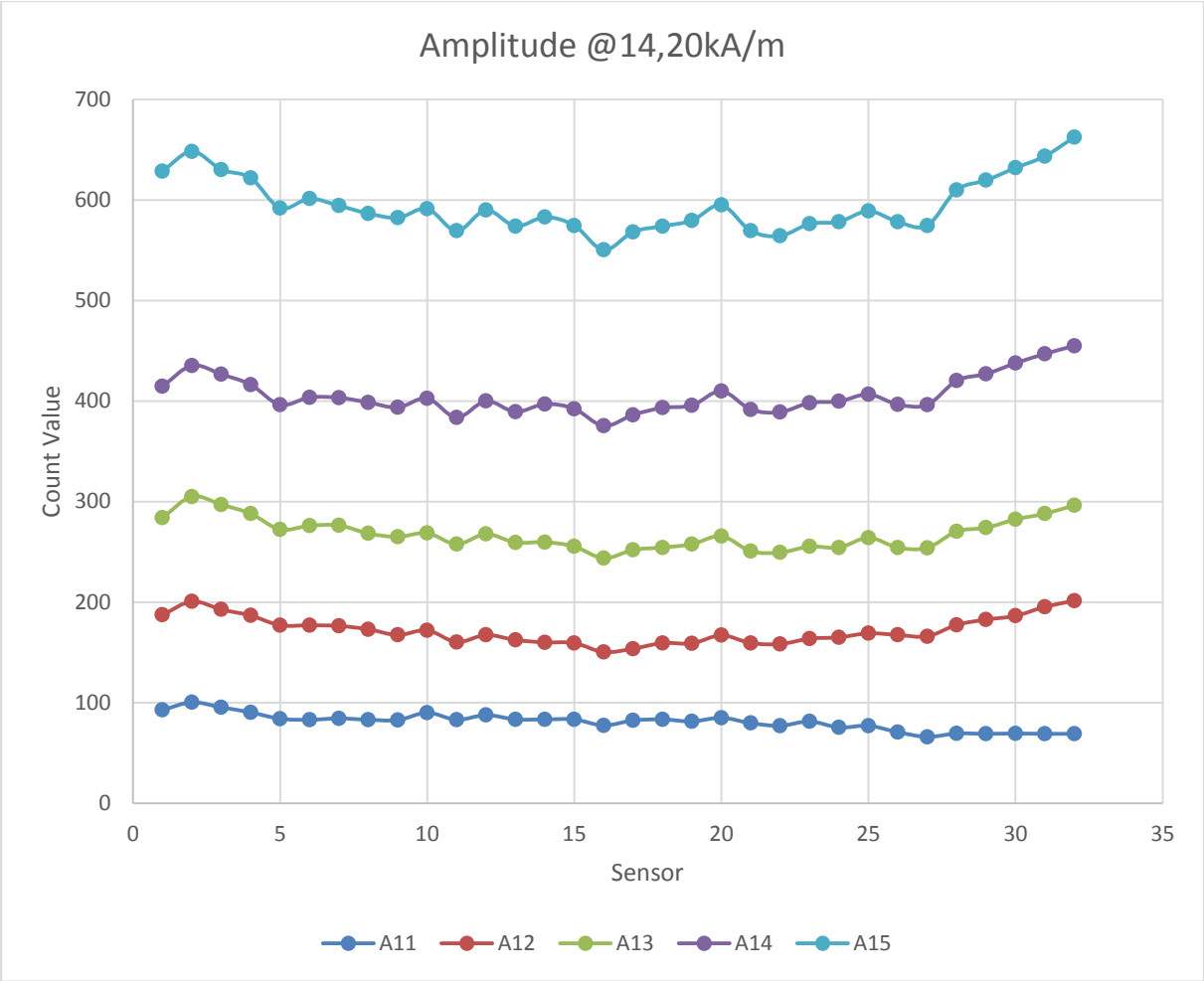


Figure 27: Amplitude @14,20kA/m.

To analyse the data furthermore, the FWHM curve was generated again, and can be seen in Figure 28 below.

Once again a big difference between the data collected from this run and the previous ones can be easily identified. Except for defect 11 all the other defects show an almost constant FWHM for all the sensors. The best consistency can be seen at defect 15, where the strongest flux leakage is expected. The reason why the FWHM values for the groove are close to 18 despite the actual length being only 16, is because the stronger the magnetization level the sooner the field would start leaking even before reaching the defect. Meaning the signal will deliver a slightly bigger. Figure 29 below shows the length of the groove provided by sensor 23. At the bottom left it can be seen that the signal reads an anomaly with a length of approximately 34mm, which explains the FWHM of about 18mm.

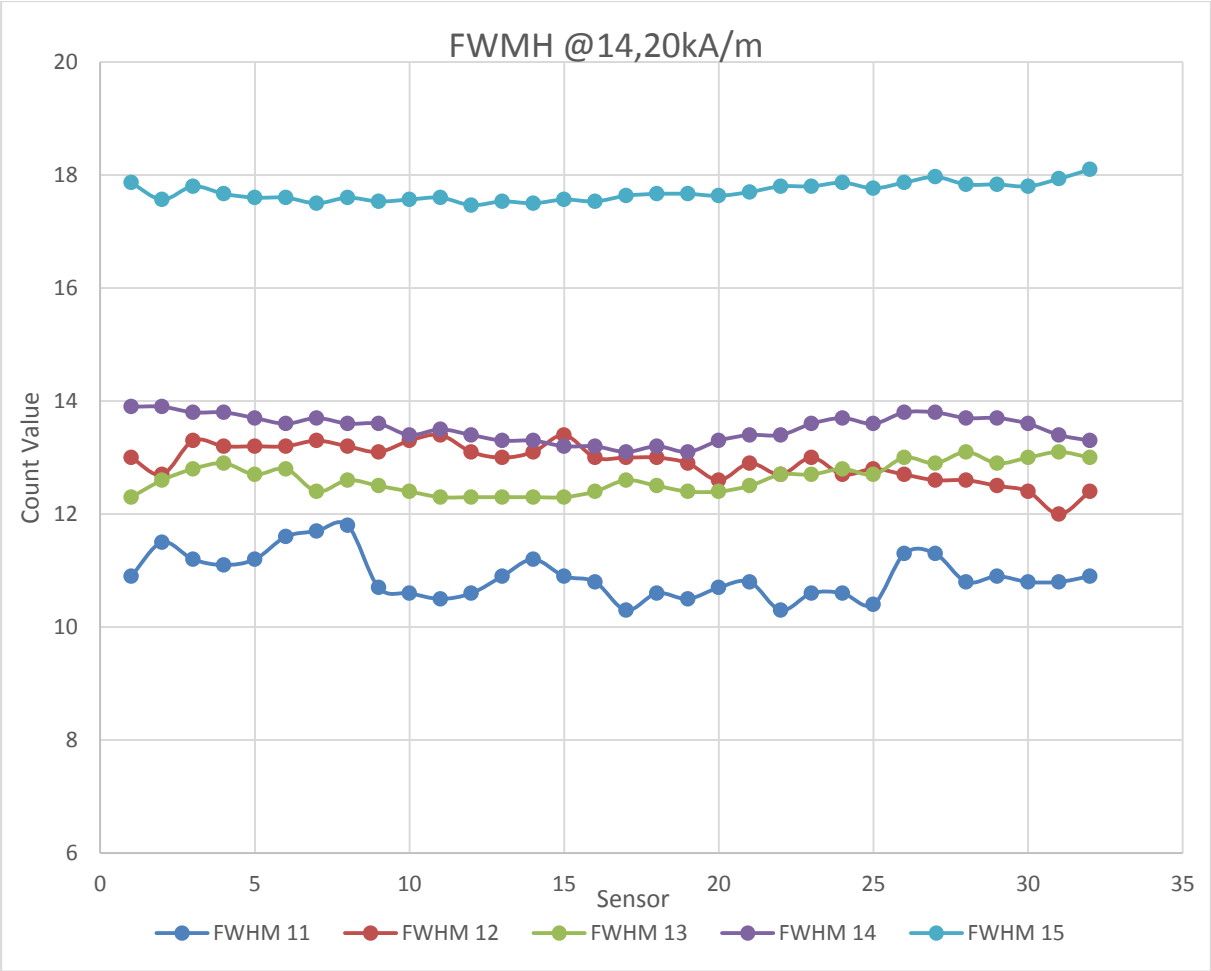


Figure 28: FWHM @14,20kA/m.

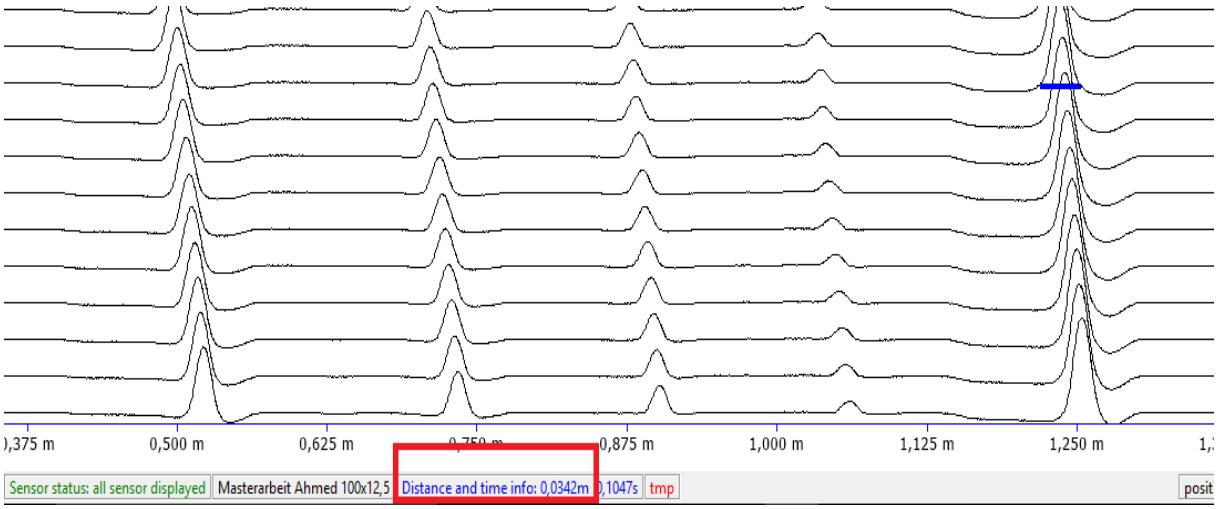


Figure 29: Obtaining the Length of a Defect.

## 4.4 High Magnetization (21,02kA/m)

Coming now to the thinnest bar, magnetization levels as high as 21,02 kA/m were recorded.

Figure 30 below shows how the defects were drilled into the bar. The three non-circled defects were already present in the bar, and are not part of the evaluation process. It should also be noted that the order in which the defects were drilled is not the same like the first two bars, but the numbering order stays the same, with the shallowest defect being 16, and the deepest as well as the groove being 19 and 20 respectively.

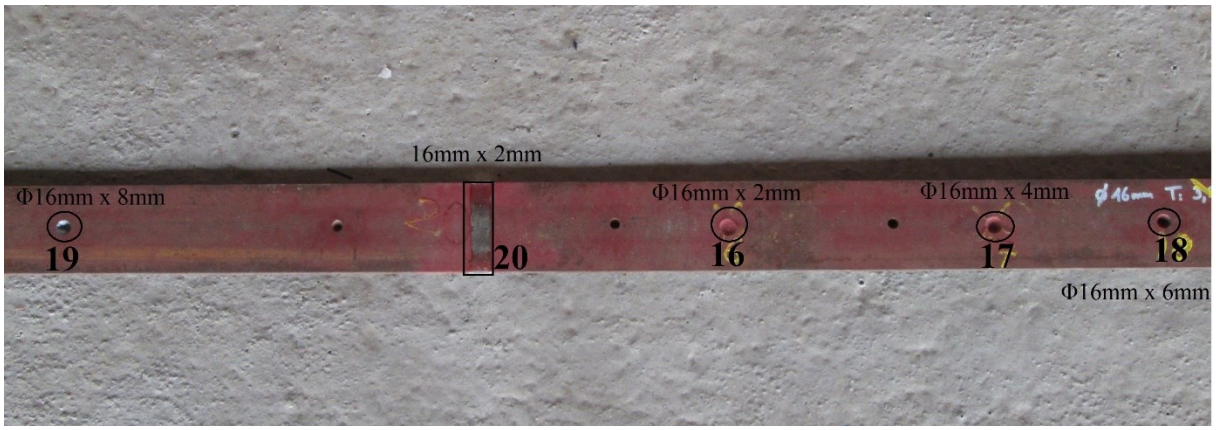


Figure 30: The 100mm x 8mm Bar.

The signal is then generated by the software after the test run is done and the data are acquired. The corresponding signal can be seen in Figure 31 below. The signals from the three defects that were mentioned before were shaded to avoid confusion. Only an amplification magnitude of 5 was required in order to view the data the way they are in Figure 31.

Same as before it can be seen how the signal peaks were affected by the geometries of the defects, with deeper defects resulting in stronger signals. In addition, the groove still delivers the highest peak despite having the smallest depth, for the reasons explained earlier in this chapter.

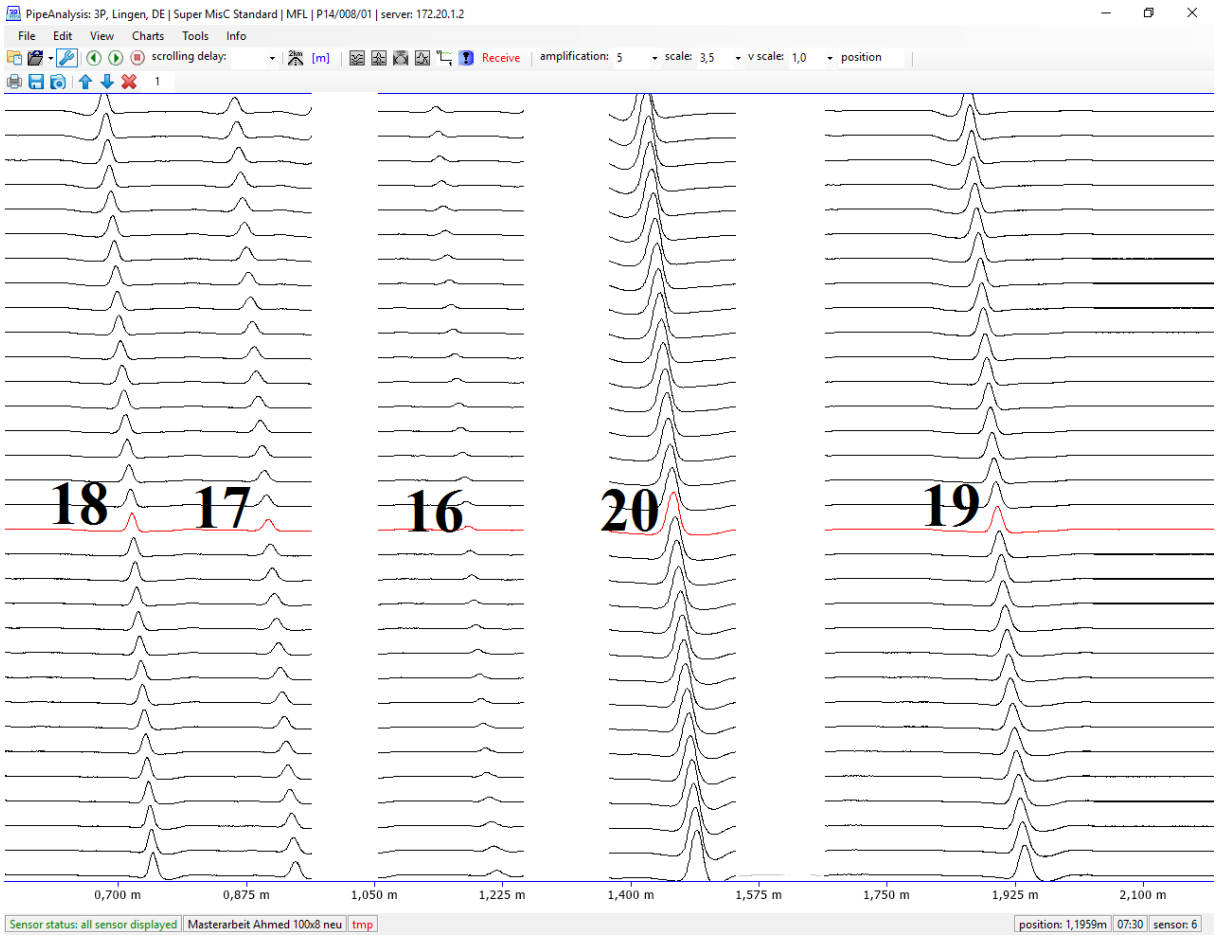


Figure 31: Corresponding signal for the fourth Bar.

Again both the amplitude and the FWHM curves were generated for this bar as well in order to investigate the acquired signal furthermore, the results can been seen in Figure 32 and Figure 33.

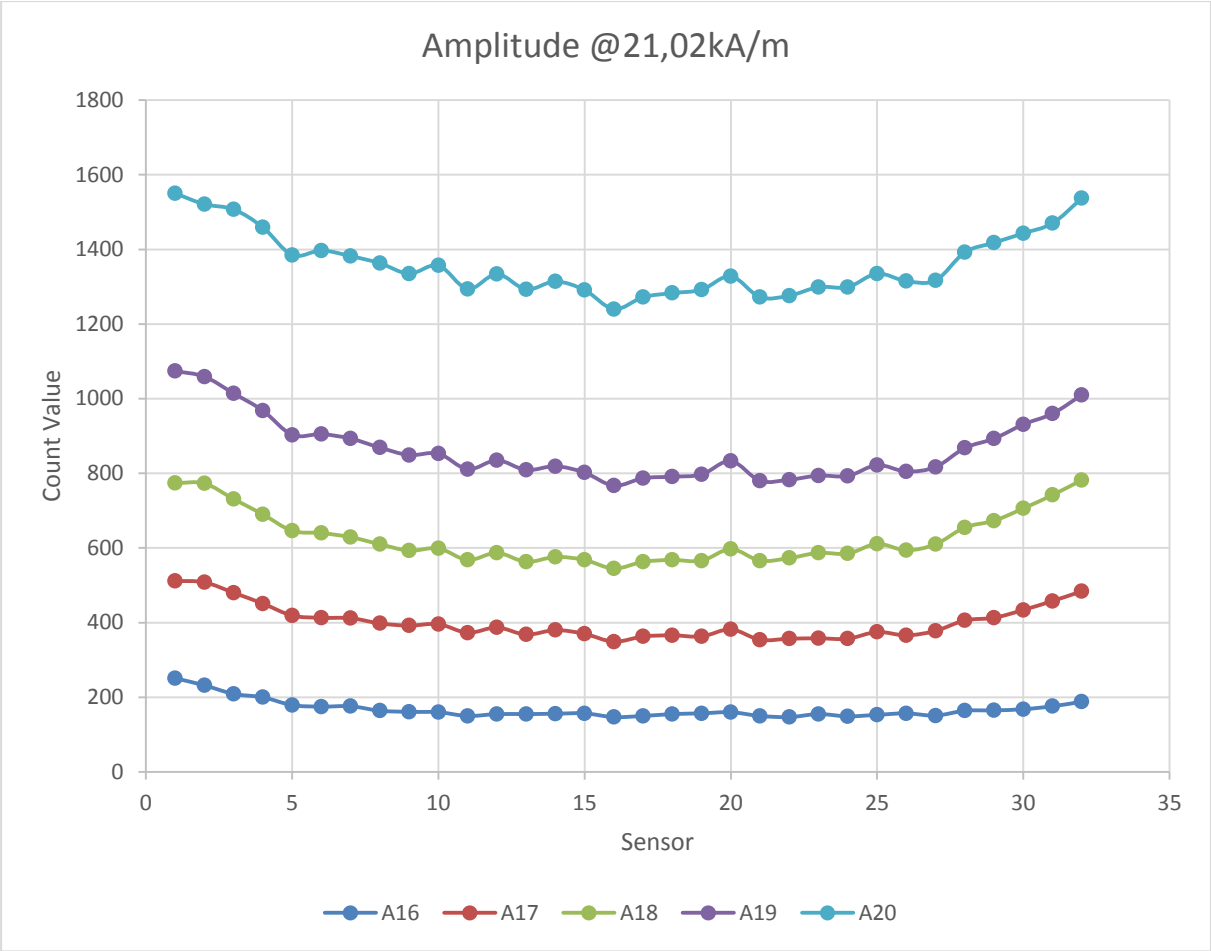


Figure 32: Amplitude @21,02kA/m.

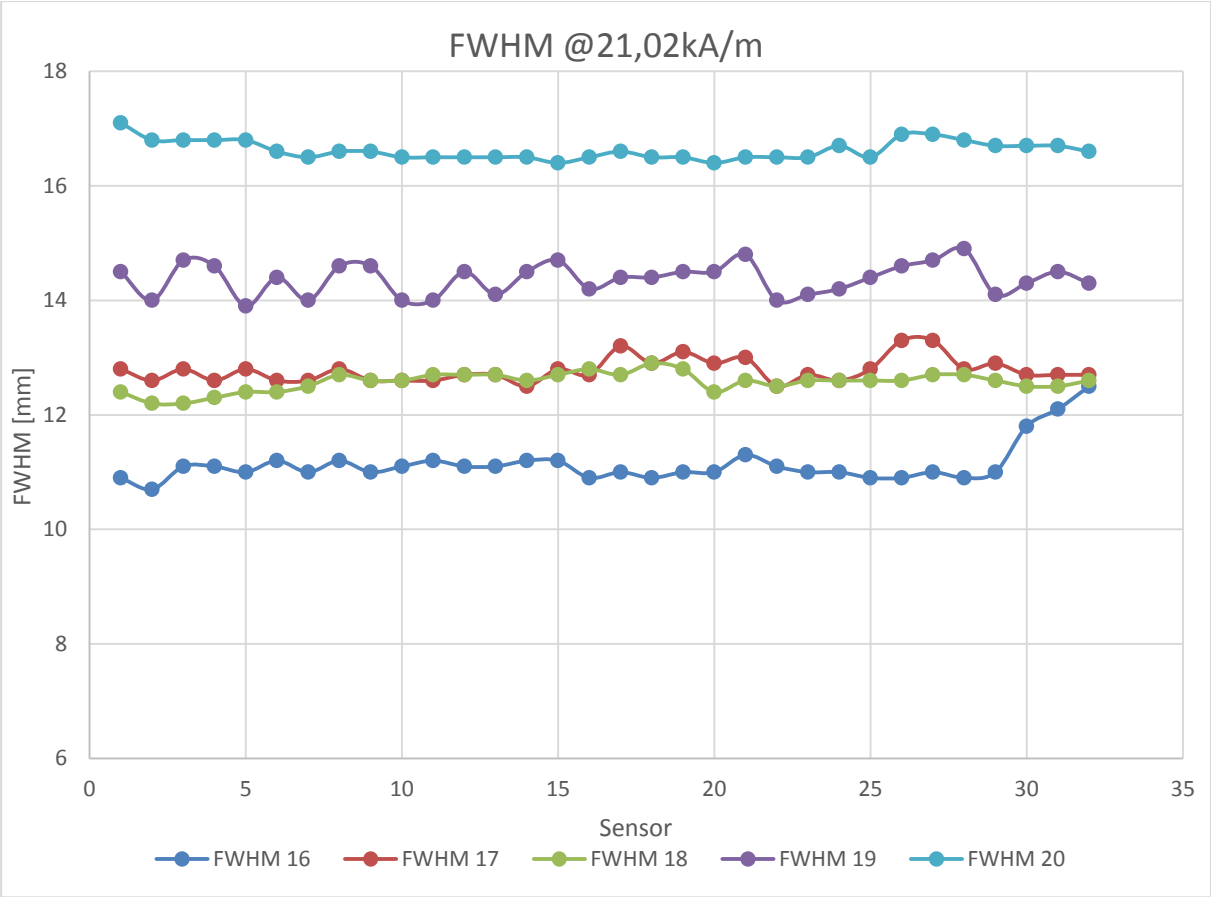


Figure 33: FWHM @21,02kA/m.

Comparing the amplitude results with the ones from the previous runs, it can be clearly seen how much better the resolution of the data has become, even when compared to the third bar which had a magnetization of 14,20kA/m. There are almost no fluctuations in the data sets, and the behaviour is rather smooth and gradual with no steep increases as before.

Another important remark, is the fact that the smaller defects, especially the first one (defect 16), now have that curvature towards both ends of the sensor array, that trend gets clearer as the defects get deeper or at the groove where the highest flux leakage occurred. The high magnetization levels also resulted in higher count values for all the defects, which when compared to the 100mm x 12,5mm bar, are almost twice as much for each defect respectively.

The FWHM curve for the previous bar showed high resolution for all the data sets, except for defect 11, which is the shallowest one. This is the case no more, the defect behaves exactly like the other ones and remains almost constant for all the sensors.[1]

## 4.5 Result Interpretation

So far the gathered data were presented, and recognizable trends within one bar and from one bar to another were illustrated. What was known and expected before the tests were two features. The first one is that deeper defects would result in higher amplitudes, that's simply because, when it comes to geometry dependency, the leakage field is mostly affected by parameters that define the volume of a defect. The second one would be that increasing magnetization leads to higher amplitudes as the bars get thinner. That can be related to the fact that, higher magnetization leads to higher saturation with a metal bar. In other words, there are more field lines that could potentially leak at a defected region when compared to a situation with weaker magnetization.

With that being established, now it is time to look at what was newly identified, which two more features:

1) Sensors lying closer to the magnet poles read higher amplitude than the one suited at the middle of the yoke.
2) The FWHM stayed constant for all the defects along all the bars for each sensor.

The amplitude vs. Sensor plots showed that the more the sensors are closer to the magnet poles, the higher the amplitude values they read, resulting in that curvetted behaviour. That of course is because the magnetic field is strongest at the poles, and as illustrated before, stronger magnetic field results in stronger flux leakage. As a result, sensors situated right in the middle of the yoke read the lowest amplitude values, since the leakage field at that point are lower compared to the sensors lying further to the sides.

Contrary to the amplitude, the FWHM didn't behave the same way. The FWHM stayed almost constant for each defect, even when looking at the same defect in two different bars. It can be seen that it always comes down to almost the same values again.

**Error! Reference source not found.** below shows the average FWHM calculated for each defect in each bar as well as the volume of each defect.

Table 4: Average FWHM.

| Volume[mm$^3$] | FWHM 100x30 [mm] | FWHM 100x20 [mm] | FWHM 100x12,5 [mm] | FWHM 100x8 [mm] |
|---|---|---|---|---|
| 804,25 | 9,83 | 10,28 | 10,90 | 11,14 |
| 1608,50 | 11,32 | 11,38 | 12,92 | 12,78 |
| 2412,74 | 11,16 | 13,13 | 12,63 | 12,58 |
| 3216,99 | 14,58 | 14,59 | 13,52 | 14,38 |
| 3400,00 | 16,60 | 15,33 | 17,70 | 16,63 |

To illustrate the data a bit more, Figure 34 was generated by plotting the average FWHM of each defect against the volume, so that every line in the plot represents one bar with its 5 defects and their calculated average FWHM.

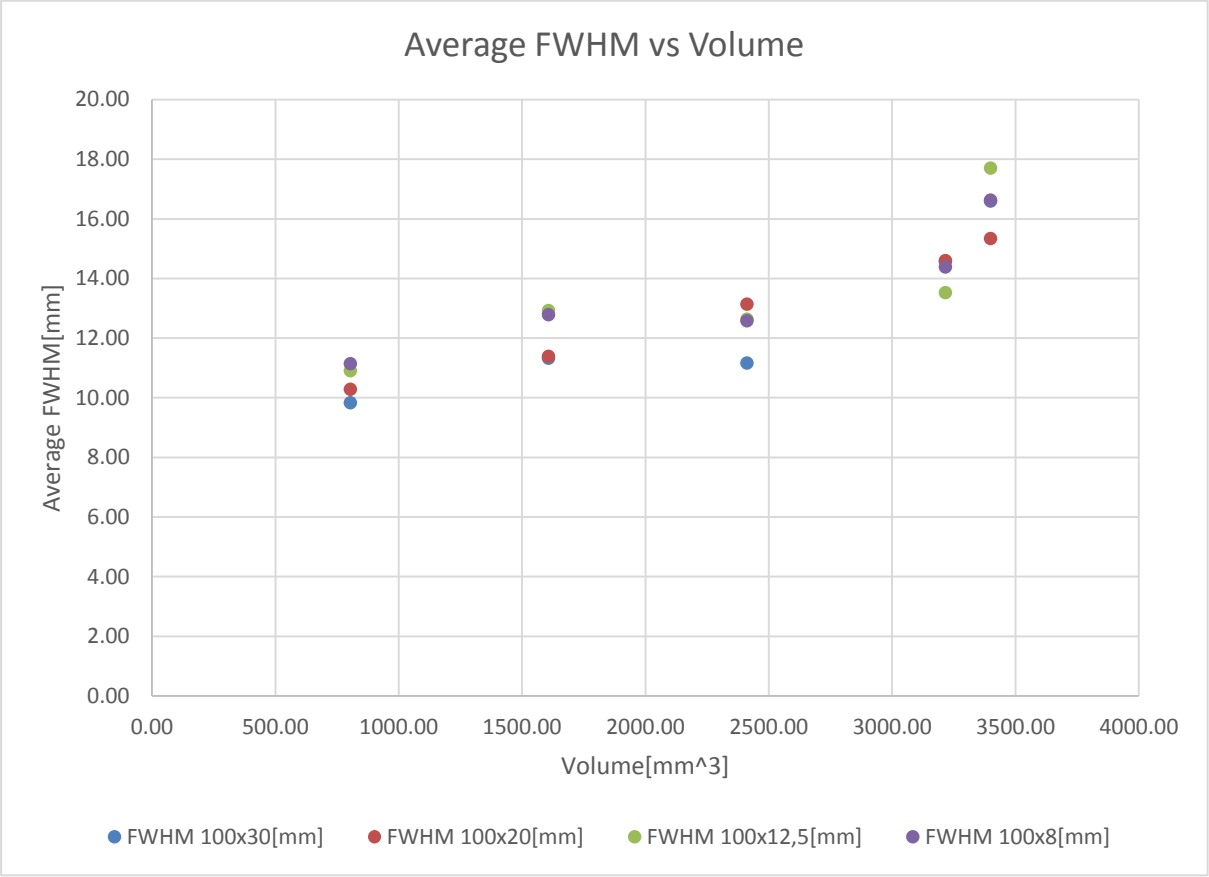


Figure 34: Average FWHM vs. Defect Volume.

The plot shows that the FWHM increases as the defects get bigger but when comparing the same defect in two different bars, however, the FWHM values are really close to each other. That is especially the case at higher magnetization levels where the lines are almost identical. This means that even though the signals might differ in amplitude (signal Strength) the width stays the same.

The reason for that is due to the fact that the signal, no matter the strength, would always start and end at the same point regardless of the sensor position, as this is only dependent on the defect length which is the same for all the defects.

In addition, the signals whether they get stronger or weaker change proportionally, meaning the width will not only stay the same at half of the amplitude (FWHM), but also at any given height ratio.

# 5 Velocity Dependency

So far all the test runs were conducted under low velocity, in order to observe what impact a changing sensor positioning has on the obtained results.

In this chapter, another variable will be introduced into the equation, which is velocity, meaning that in total, three factors will be affecting the quality of the gathered data. Those factors are: sensor positioning, velocity of the tool and magnetization levels.

As mentioned earlier in chapter 3, the 100mmx30mm bar will be left out and will not be part of the tests conducted in this part, as it was seen that the magnetization level was too low to give a clear statement about its results or to observe any specific behaviour patterns, which should become even worse as the velocities get higher. That's why it was decided to focus the work on the three other bars since it is more relevant. Furthermore, the sensor carrier was replaced and four ball-bearings were added to the tall to ensure a stable run over the bars at higher pull velocities.

## 5.1 Offset Comparison

The first thing to be looked at in order to identify the influence of velocity is the offset values from each sensor at each velocity. The offset represents the magnetic field at the non-defected intervals, meaning areas where no flux leakage is present, and it is the basis for measuring the signal's amplitude for a present defect. Offset values for each bar at different velocities were collected, as explained earlier in Figure 16, and put in comparison with one another. The velocities were colour scaled from yellow for the lowest velocity to dark red for the highest velocity. Figure 35-Figure 37 below show the behaviour of the offset for the three metal bars for the seven different velocities.

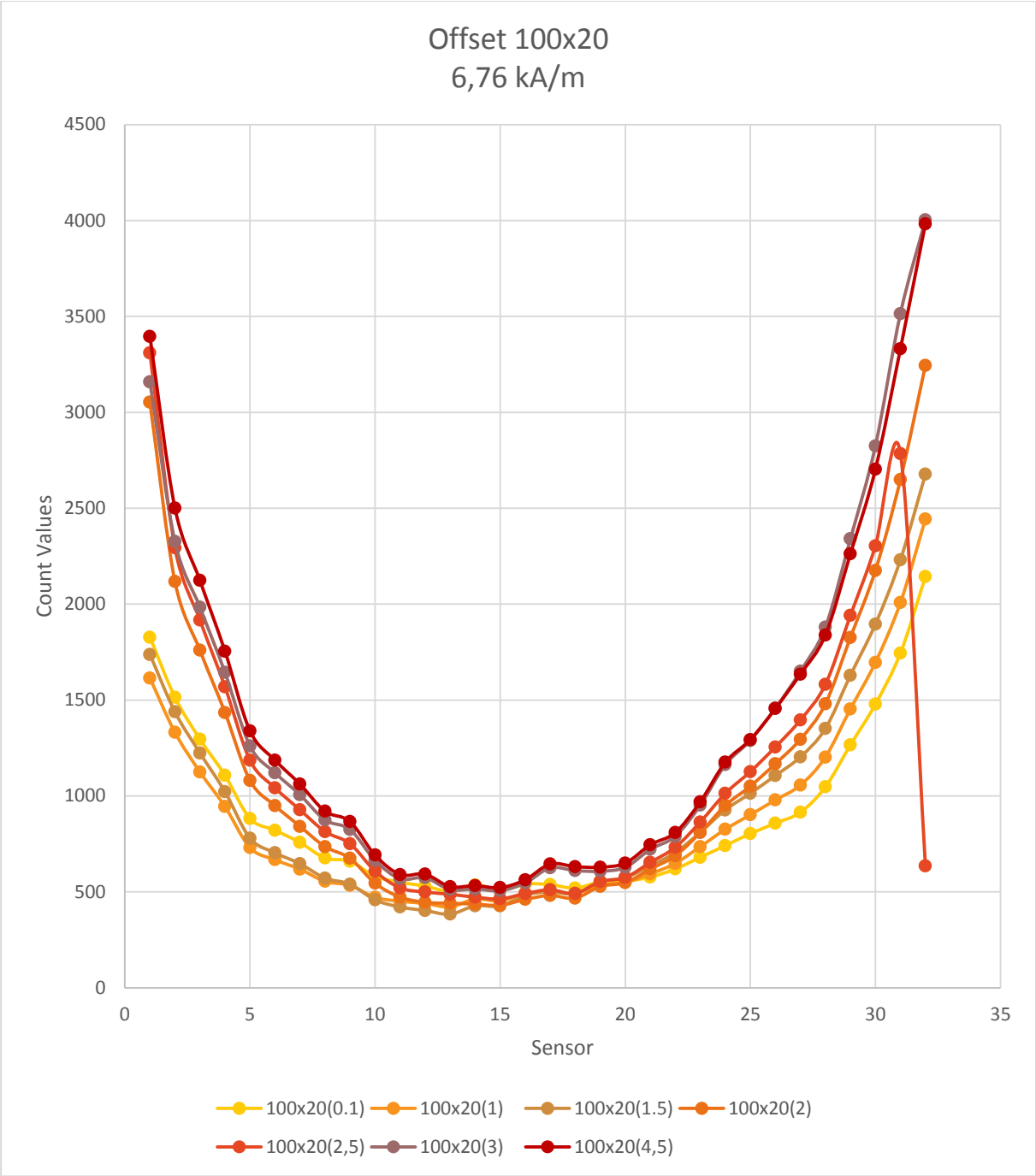


Figure 35: Offset of the 100x20 bar.

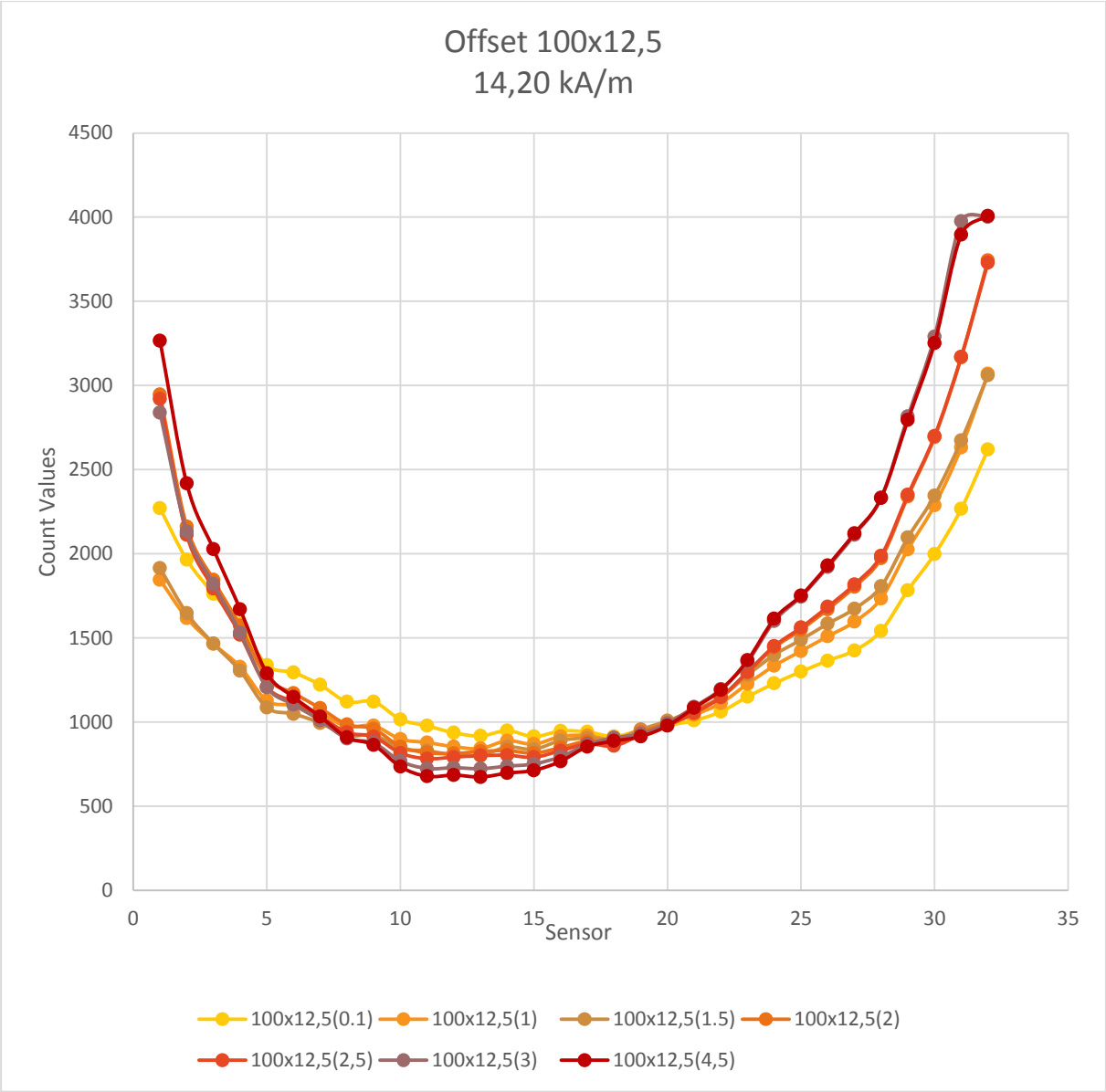


Figure 36: Offset of the 100x12,5 bar.

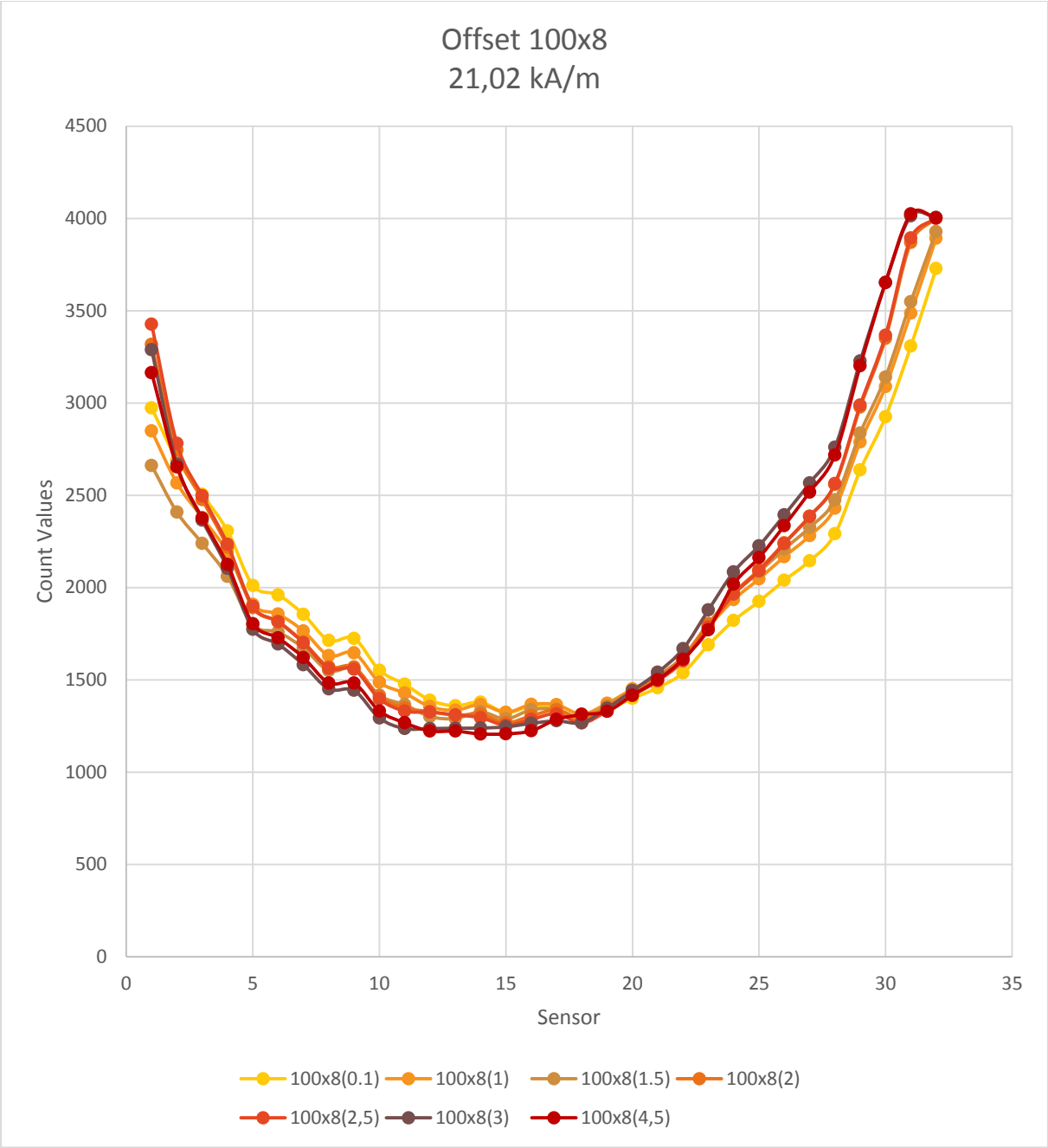


Figure 37: Offset of the 100x8 bar.

It should be noted that 1 is the leading sensor and 32 is the trailing one and that the pulling direction was always the same for all the test runs. Since the sensors are placed in a row between the two magnet poles, it was expected that the offset values would be the highest towards the sides and the lowest close to the middle of the yoke.

When looking at how the offset behaviour changes at different velocities it can be noticed that for a low magnetization level, Figure 35, offsets increases with increasing velocities. As the magnetization level increases, the behaviour tends to change. In Figure 36, only the first 4 sensors at the 4,5 m/s velocity show higher offset values compared to the same sensors at lower velocities. At sensor 5, offset values start to rearrange, and at a certain interval the offset values are such, that lower velocities have the highest values. The offset values then

keep coming together till a certain point is reach, Sensor 20, where they have almost the exact same value. From that point onwards the behaviour is reversed with higher velocities showing higher offset values. To give an example on how the offset changes from one velocity to the other depending on the positioning of the sensor, the 4,5 m/s velocity values were compared to the ones from the 0,1 m/s over 4 different sensors, the results can be seen in Table 5.

Table 5: Offset comparison of the 100x12,5 bar.

| Sensor / Velocity | 1 [counts] | 11 [counts] | 20 [counts] | 32 [counts] |
|---|---|---|---|---|
| 0,1 | 2271 | 971 | 980 | 2620 |
| 4,5 | 3266 | 678 | 978 | 4007 |
| Difference in % | 69,5 | 143,2 | 100,2 | 65,4 |

The table gives the difference in offset between the two velocities as a percentage of the offsets at 4,5 m/s; the values represent the previous explained behaviour perfectly.

To illustrate the behaviour of the offset of the 100x8 bar, the same example will be used, with the same sensors.

Table 6: Offset comparison of the 100x8bar.

| Sensor / Velocity | 1 [counts] | 11 [counts] | 20 [counts] | 32 [counts] |
|---|---|---|---|---|
| 0,1 | 2973,4 | 1475,8 | 1399,6 | 3728,4 |
| 4,5 | 3164,4 | 1267,0 | 1416,8 | 4002,8 |
| Difference in % | 94,0 | 116,5 | 98,8 | 93,1 |

Basically the same behaviour as before, the only difference is that the gap between the offset values is not as big as before, which remains the same when putting the other 5 velocities in perspective. The lines in Figure 37 are more drawn together than in the other 2 figures even at both ends. In general the area in between the two poles can be divided into three parts:

1) Front part: The area from sensor 1 to 10, where the offset values increase with decreasing velocity.
2) Middle part: The area from sensor 11 to 20, where offset values come closer to each other till the point where they have almost the same value.
3) Rear part: The area from sensor 21 to 32, this where the values start separating again, but in a reversed way compared to the front part.

That behaviour is clearer with higher magnetization levels, whereas at low levels like in Figure 35, offset values are always directly proportional to the velocity no matter where the sensors are.

## 5.2 Amplitude Comparison

In chapter4, since the tests were performed at just one velocity, amplitude was simply compared by plotting all the amplitudes for each bar together. In this chapter the amplitude will be compared for each defect separately at each velocity. For this sake only three defects were chosen as the same behaviour can be expected for the other 2 defects as well. Those three defects are:

- Φ16mmx2mm, which will be referred to as defect 1.
- Φ16mmx8mm, which will be referred to as defect 4.
- 16mmx2mm, which is the groove.

### 5.2.1 The Groove

The first defect to be looked at is the groove. Each of the three figures below shows the amplitude of the groove for each of the three bars at the seven different velocities.

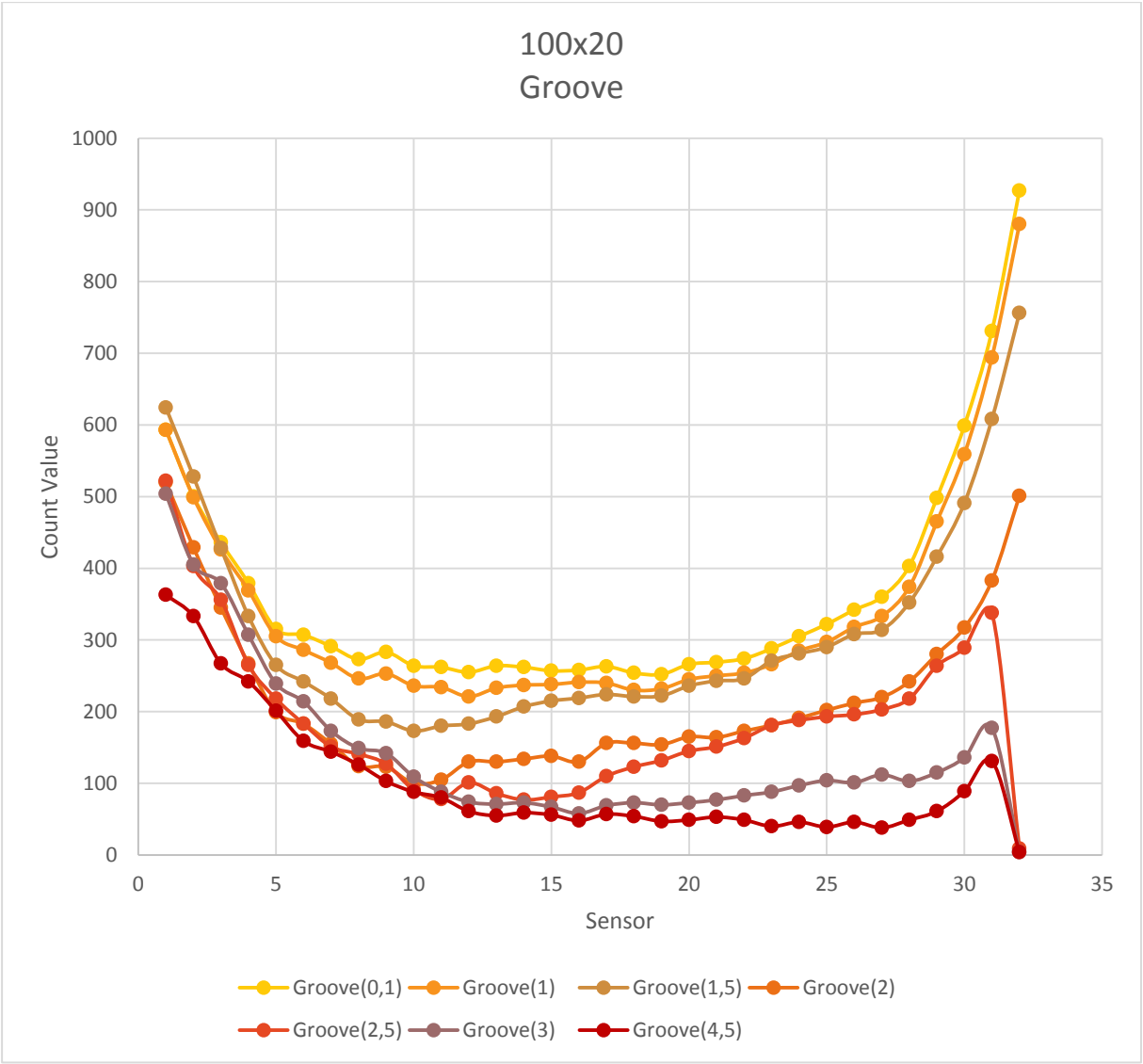


Figure 38: Amplitude at the groove for the 100x20 bar.

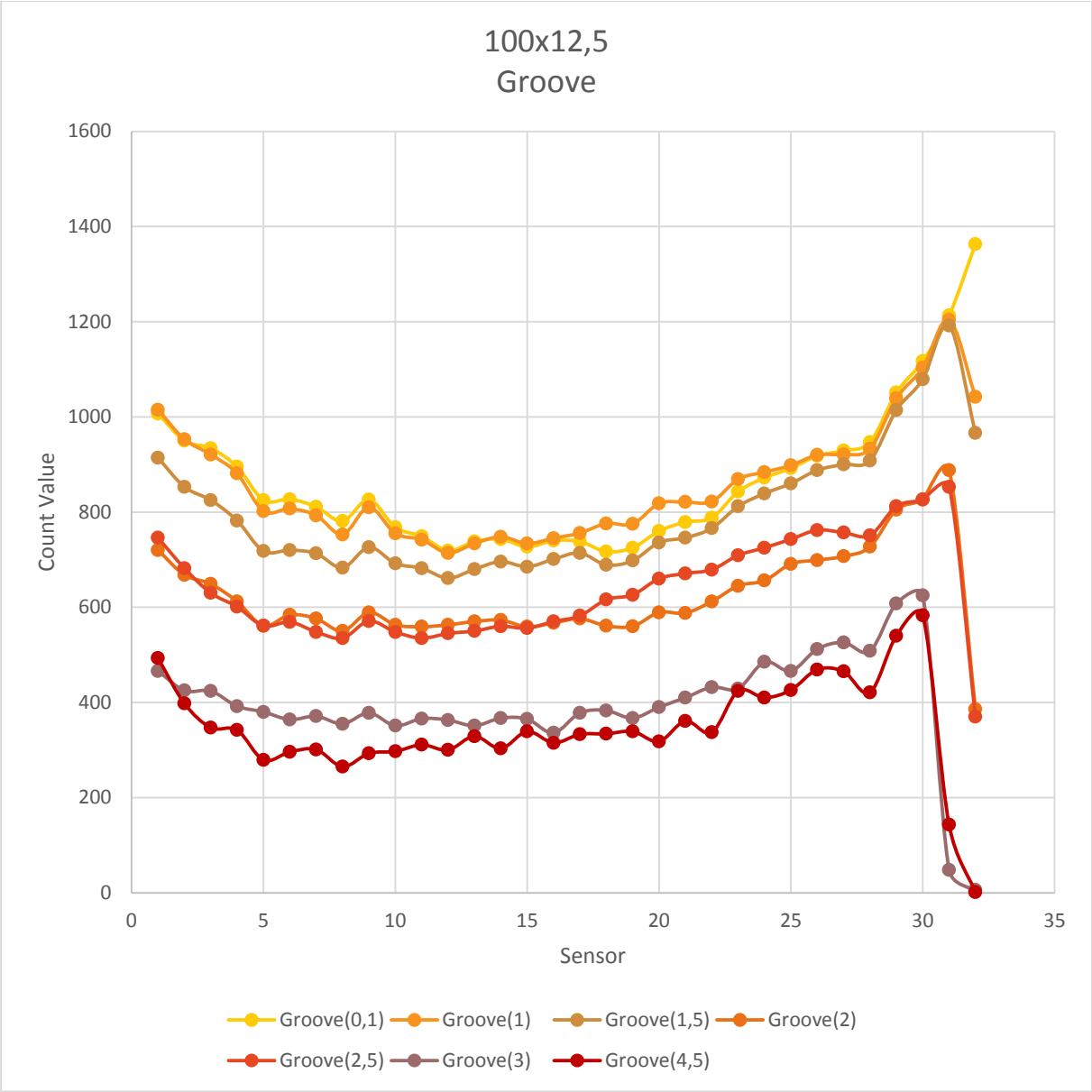


Figure 39: Amplitude at the groove for the 100x12,5 bar.

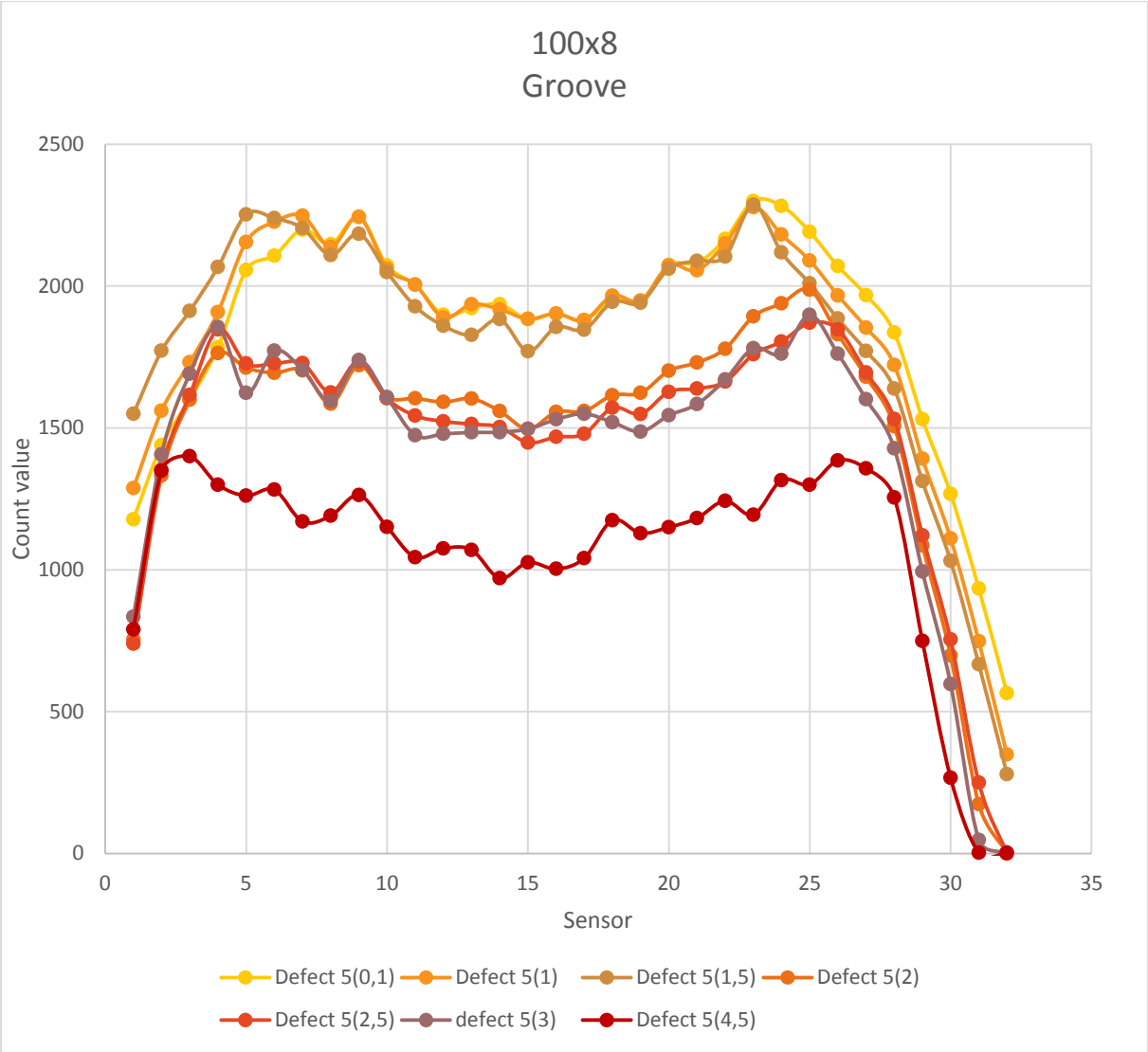


Figure 40: Amplitude at the groove for the 100x8 bar.

As was the case in the previous chapter, thinner wall thickness with higher magnetization in general lead to higher amplitude values when comparing the three bars to each other.

However, the most noticeable feature this time is how the amplitude values drop strongly at the sensors close to the trailing pole in Figure 38 and Figure 39 at higher velocities, and at either pole in Figure 40 at all velocities. In this first part of this chapter it was established that the offset values are the highest on both ends of the sensor array, with the sensors closer to the trailing pole having higher offsets than the leading sensors. Since the amplitude is measured by subtracting the offset counts from the counts at the defect, an extremely high offset will eventually lead to low amplitude when the maximum measurable value of the sensor is reached, leading eventually to such behaviour. This is exactly the case at the sensors where the amplitude drops that strongly. Table 7 below shows the sensors where those drops occurred in all the bars.

Table 7: Sensors where massive amplitude drops occurred.

| Defect | Bar | Sensors |
|---|---|---|
| Groove | 100 x 20 | 31 - 32 |
| | 100 x 12,5 | 30 - 32 |
| | 100 x 8 | 1 - 4 and 24 - 32 |
| Defect 4 | 100 x 20 | 31 - 32 |
| | 100 x 12,5 | 30 - 32 |
| | 100 x 8 | 1 - 3 and 26 - 32 |
| Defect 1 | 100 x 20 | 31 - 32 |
| | 100 x 12,5 | 30 - 32 |
| | 100 x 8 | 29 - 32 |

It can also be seen that an increase in velocity causes the amplitude to drop significantly for any sensor position. This comes as expected and coincides with Lenz's law explained earlier in chapter 2.3.2 on how velocity produces eddy currents that reduce the original magnetic field.

For both defect 1 and defect 4, which can be found in Appendix A, the behaviour was the same, except that for defect 1 those amplitude drops were only limited, since it is a small defect so the maximum flux leakage is really low for all the sensors, causing the drops to occur only at the two trailing sensors where the offset is the highest.

Defect 4 behaved exactly the same as the groove, just with smaller amplitude values corresponding to its lower produced flux leakage.

Furthermore, in order to illustrate the dependency of the amplitude on the sensor positioning as well as the velocity, the amplitude from the 4,5 m/s run was plotted as a percentage of the amplitude at the 0,1 m/s velocity, which represents an ''ideal'' amplitude, this should help identify where the most amplitude losses occur as a result of velocity effects. Each plot represents one defect and its amplitude ratio for each bar.

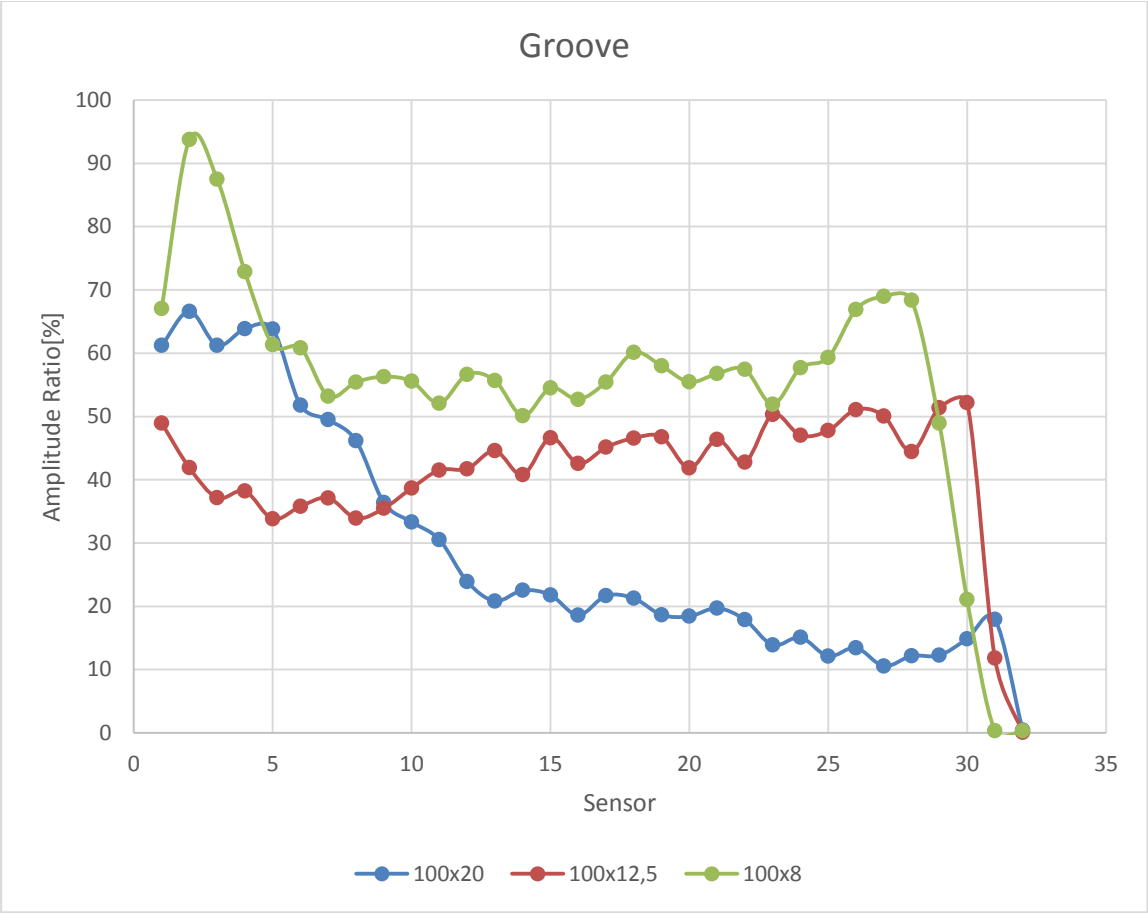


Figure 41: Amplitude ratio groove.


Figure 42: Amplitude ratio defect 4

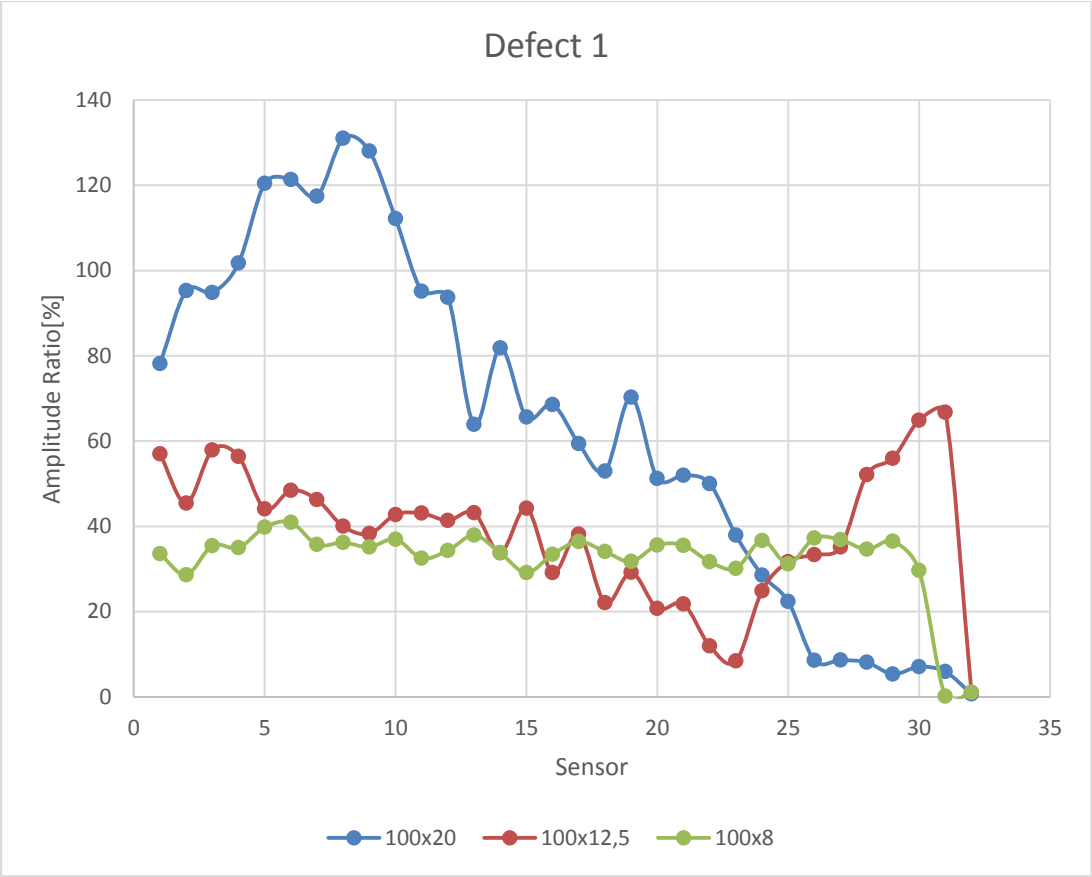


Figure 43: Amplitude ratio defect 1.

It is easy to tell that higher amplitude losses can be expected at lower magnetization levels for bigger defects where sensors are situated around midway between the two poles. Whereas sensors closer to the leading pole showed far better results in comparison. The data shows that amplitude losses at this area are quite small, as a matter of fact at some point it did exceed the 100%. Especially when it comes to the smallest defect 1, at low magnetization level, it is clear that sensors at the leading end of the yoke were not as affected by the velocity as the other sensors.

## 5.3 FWHM Comparison

Like in chapter 4 the FWHM of the defects was to be investigated, as was the case for the amplitude, defects 1, 4 and the groove are of concern. The FWHM will be compared for each defect at each of the tested velocities, starting with the groove.

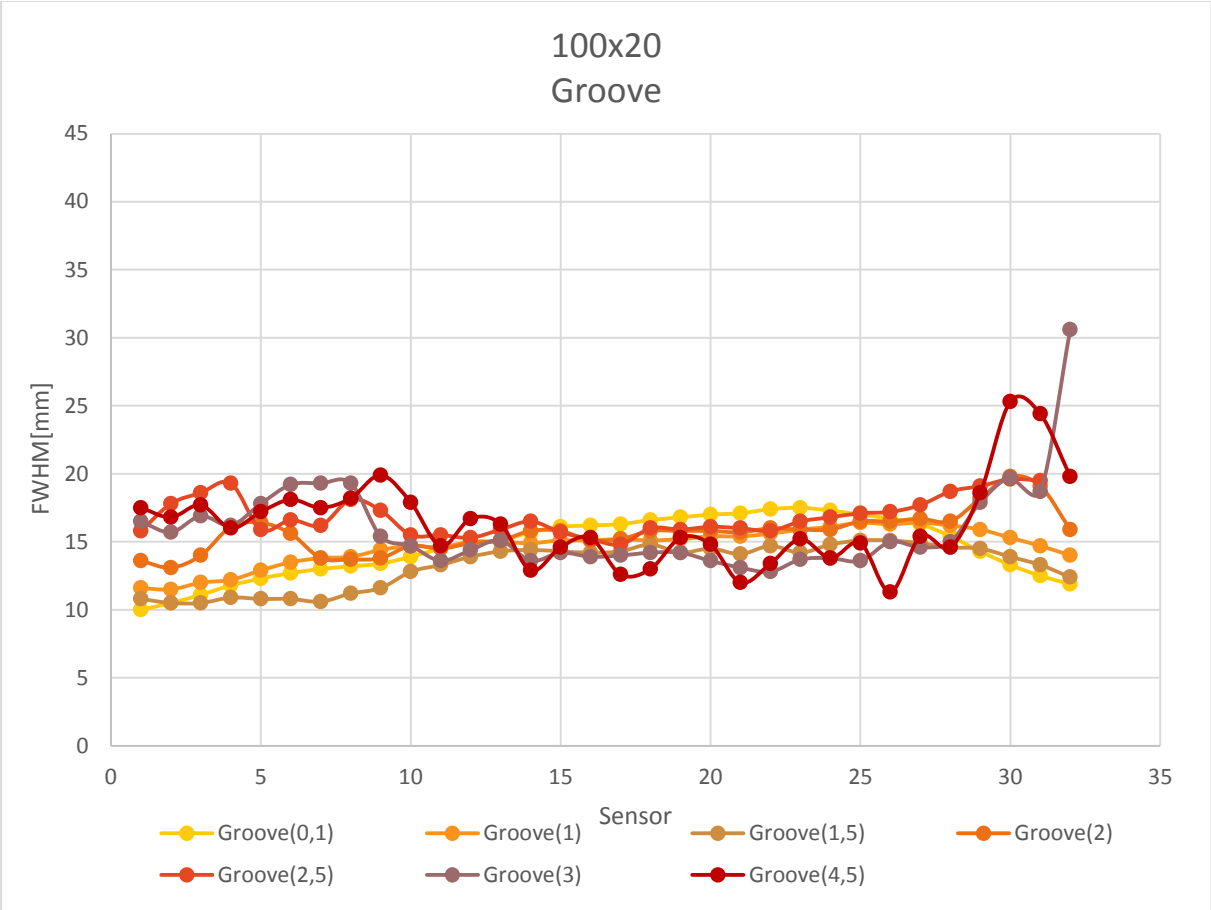


Figure 44: FWHM at the groove for the 100x20 bar

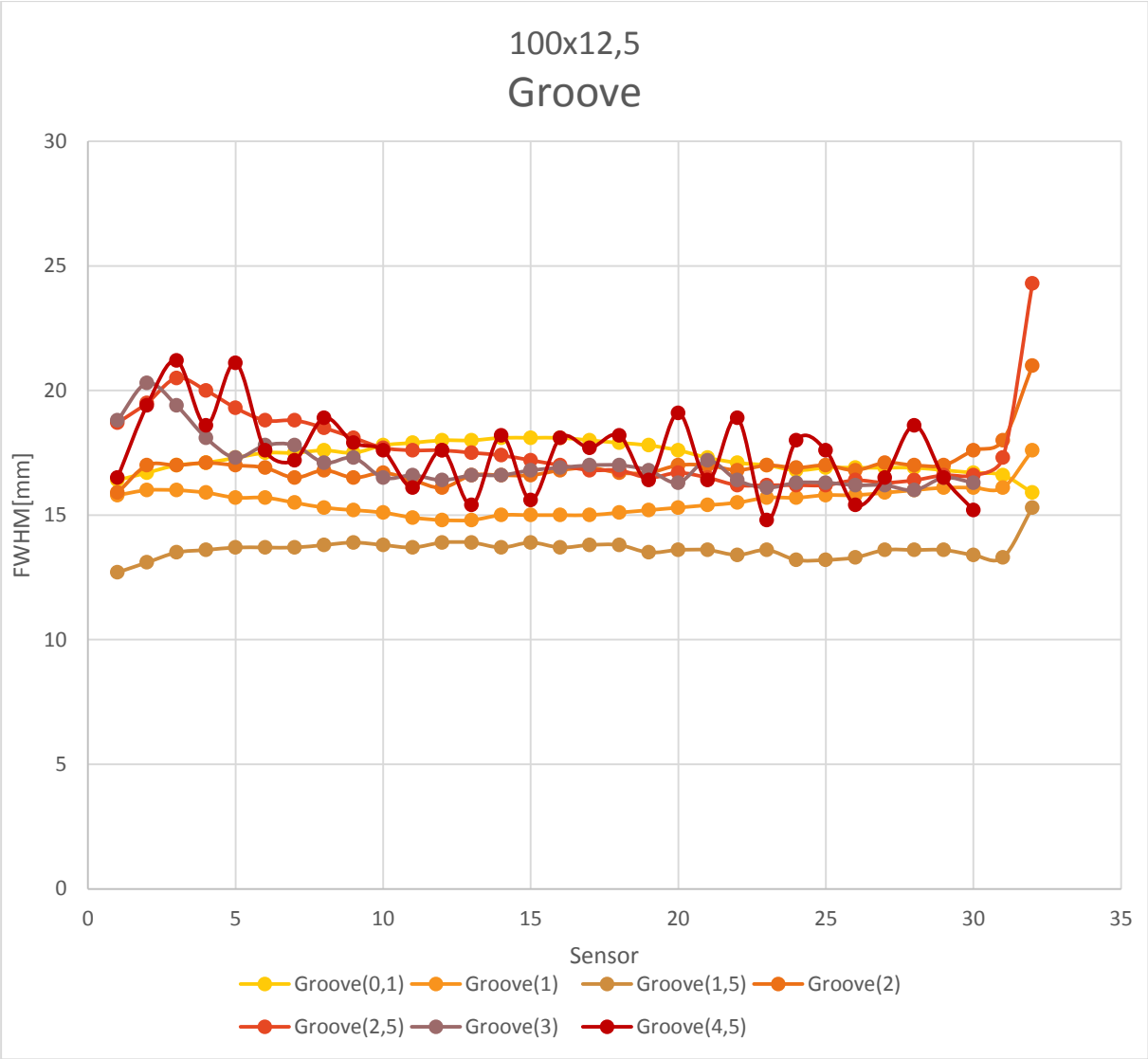


Figure 45: FWHM at the groove for the 100x12,5 bar.

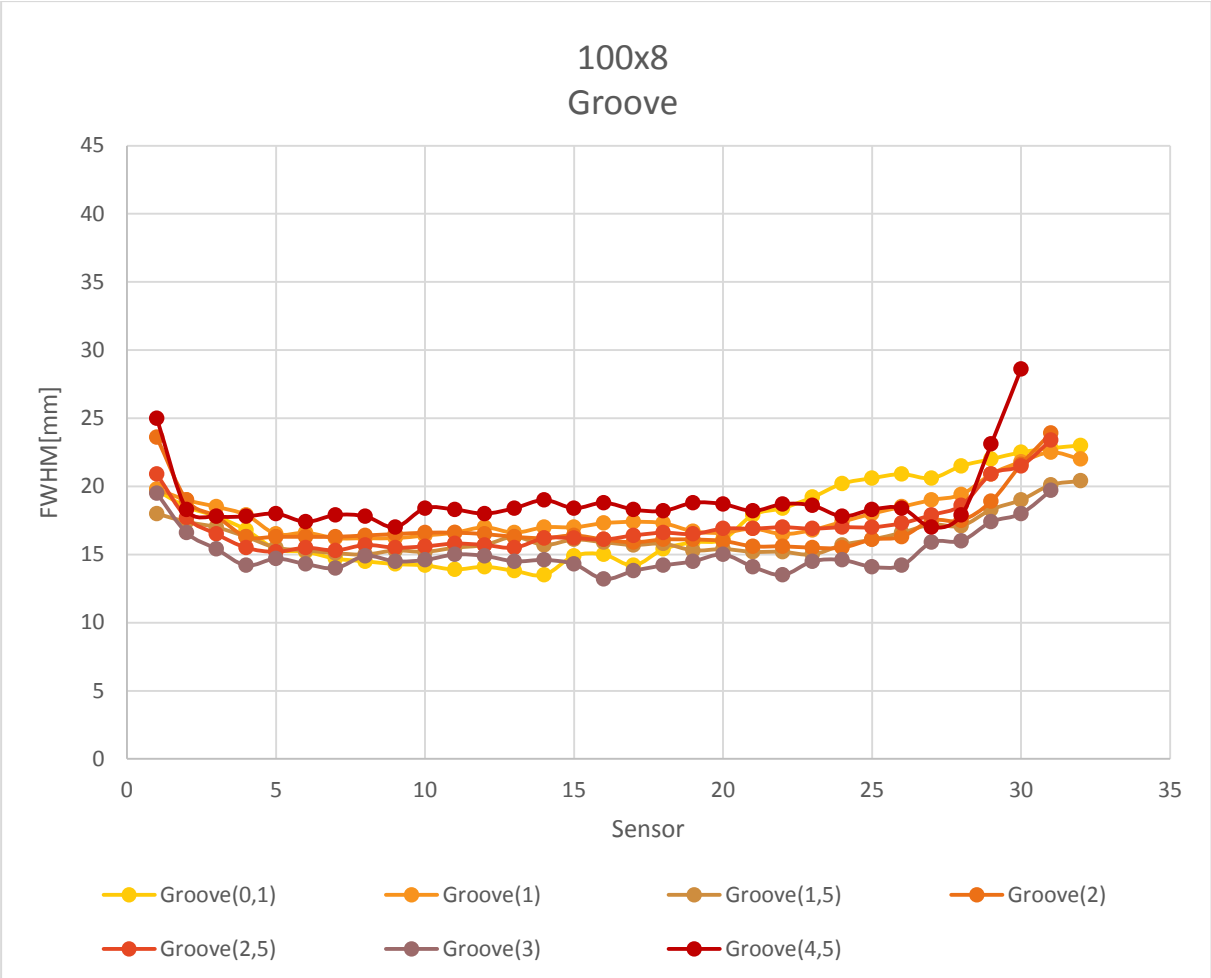


Figure 46: FWHM at the groove for the 100x8 bar.

In chapter 0 it was discovered that the FWHM stayed constant for all the defects regardless of the sensor position. This time the data doesn't only show that the FWHM remains almost the same for any sensor position but also at any of the tested velocities. Even when comparing each of the bars to one another, one can tell that the FWHM of the defect remains the same regardless of the velocity or the magnetization level. For the two other defects the FWHM, which can be seen in Appendix B, behaved exactly the same. Nonetheless, it can be noticed that with the decrease in the flux leakage due to the size of the defects and with increasing velocity, there were more fluctuations in the lines, especially for defect 1. There was however, some deviation at defect 4 at the trailing sensors where the FWHM values rose significantly above the other sensor values. That was also the case for defect 1 but only at the 100x12,5 bar on both the leading and the trailing sides of the sensors. Figure 47 below shows the FWHM of the groove at different magnetization levels but at the same velocity showing clearly that the length of the signal stays the same for the same defect even at different magnetization levels.

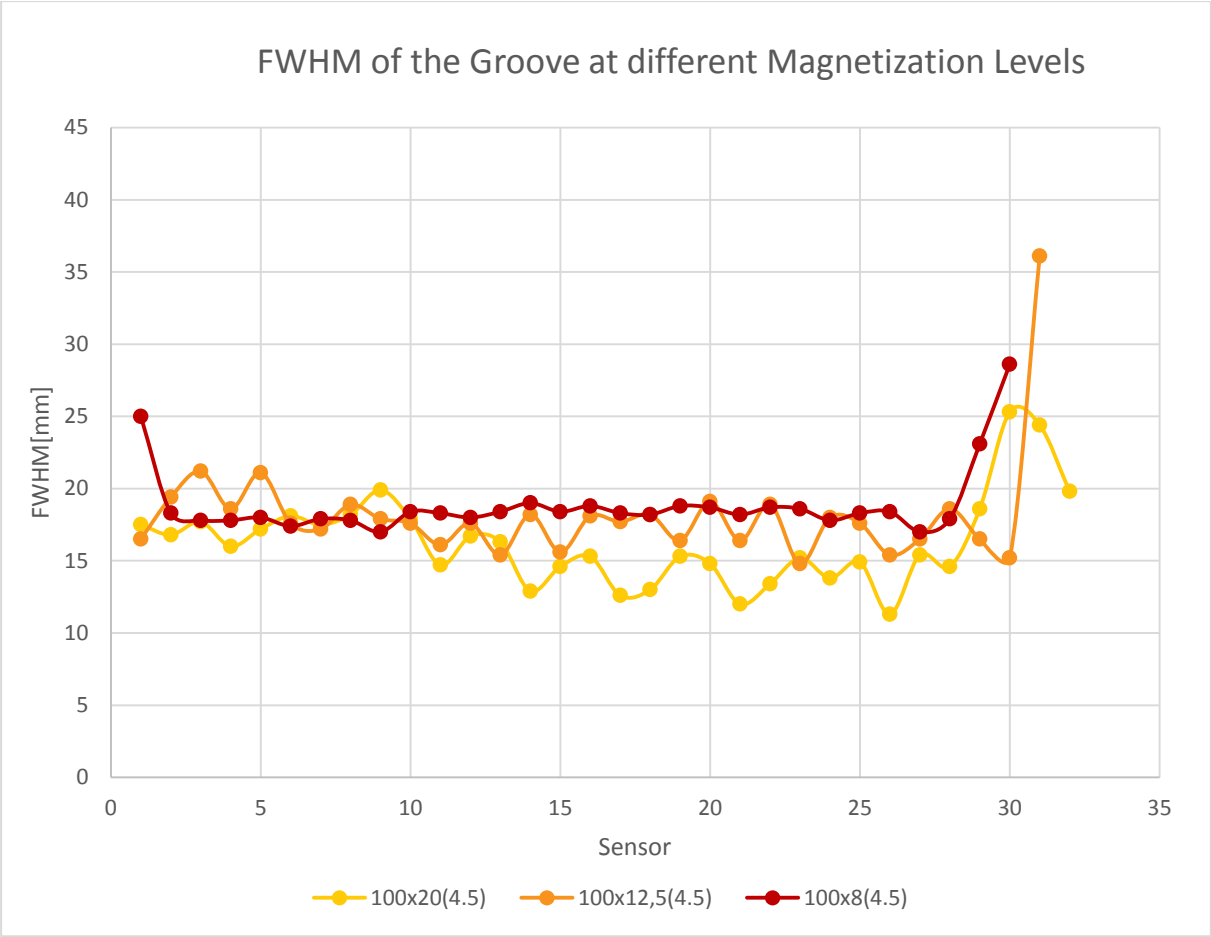


Figure 47: FWHM of Groove at different Magnetization Levels.

# 6 Conclusion

When it comes to implementing the MFL technology in pipeline inspection, it was a common practice to position the sensors exactly in the middle between the two magnet poles of each yoke, as it is believed that this would provide the optimal results when trying to detect the presence of any material losses along a pipeline.

The aim of this work was to prove that this statement is not necessarily true, and that the optimal positioning of the sensor may vary depending on the velocity of the tool as well as the achieved magnetization level at the pipe wall.

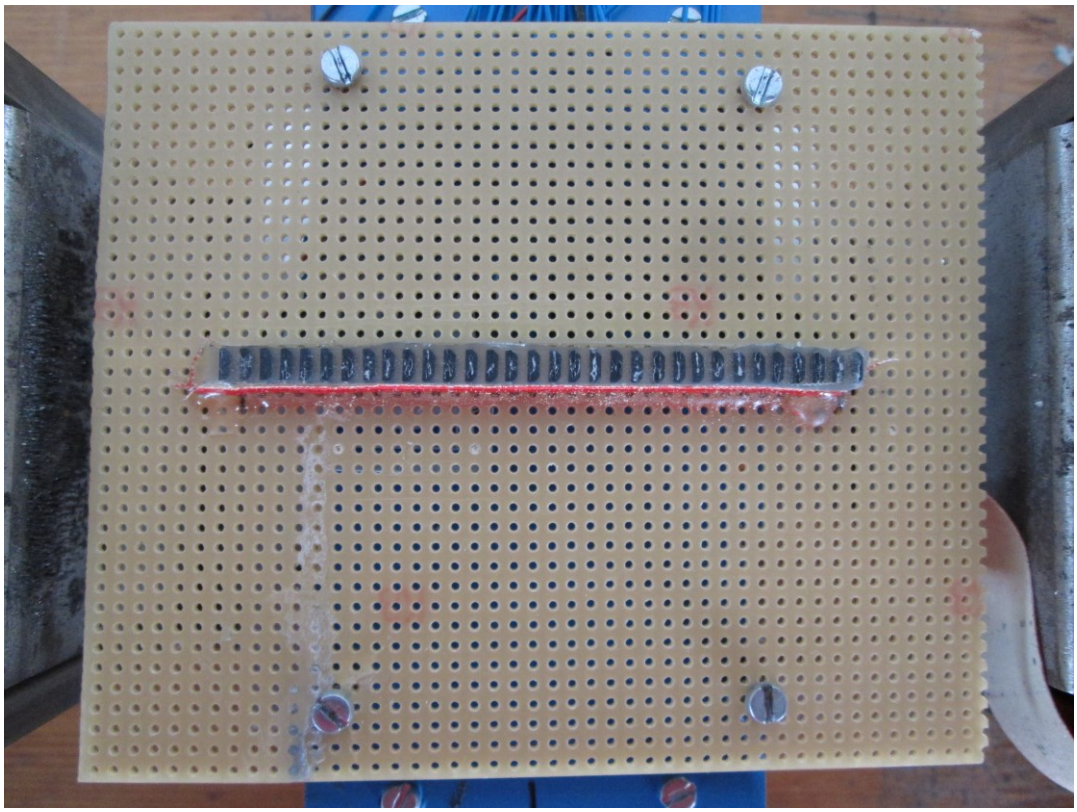

Figure 48: First Sensor Carrier.

By assembling and modifying a yoke piece and mounting a specially designed sensor carrier onto it, several test runs were conducted under different magnetization levels varying from very low (2,94kA/m) to very high(21,02kA/m), and the behaviour of the MFL was thoroughly investigated and analysed.

The work was divided into two major parts:

1. Investigating the sensor positioning dependency.
2. Investigating the velocity dependency.

In the first part the dependency of the MFL signal on the positioning of the sensor between the two magnet poles was investigated by assembling the first sensor carrier, Figure 48, then mounted to the tool, which was run along four different metal bars with different wall

thicknesses and five defected. The pulling was simply performed by pushing the tool slowly by hand over the bar.

The results showed two main features:

1) Sensors lying closer to the magnet poles read higher amplitude than the one suited at the middle of the yoke.
2) The FWHM stayed constant for all the defects along all the bars for each sensor.

The amplitude vs. Sensor plots showed that the more the sensors are closer to the magnet poles, the higher the amplitude values they read, resulting in that curvetted behaviour. That of course is because the magnetic field is strongest at the poles, and as illustrated before, stronger magnetic field results in stronger flux leakage. Contrary to the amplitude, the FWHM didn't behave the same way. The FWHM stayed almost constant for each defect, even when looking at the same defect in two different bars. It can be seen that it always comes down to almost the same values again.

In order to make a better judgement about the behaviour of the signal the sensor carrier was modified, Figure 49, by spreading the sensors further from one another with the outer sensors closer to the magnet poles, the number of sensors however, stayed 32. This allowed for a better coverage of the whole area in between the two poles, allowing for a more accurate investigation of the sensor positioning dependency.

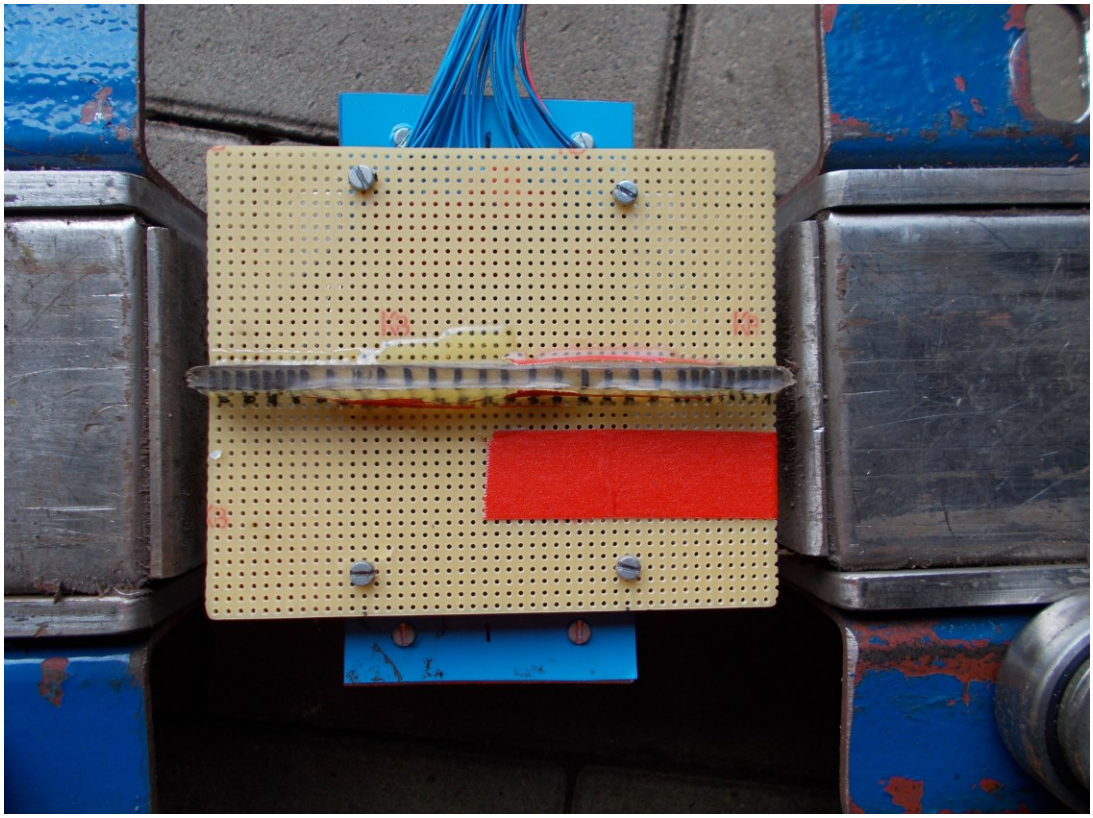

Figure 49: Second Sensor carrier.

Again the amplitude and the FWH for all the defects was investigated, this time at different velocities, and then compared to each other.

As was expected an increase in velocity causes the amplitude to drop significantly for any sensor position coinciding with Lenz's law. Looking at FiguresFigure 41-Figure 42 to see how velocity affected the amplitude, the data showed that higher magnetization leads to less amplitude losses with increasing velocity. But most importantly, it was shown that the least amplitude losses were found at sensors closer to the leading magnet pole, with the losses increasing as the sensors move closer to the trailing pole. That effect was especially evident at smaller defects as the losses were just as low as 10%. That means that for example material losses in a pipeline that are caused by pitting corrosion can be better detected with a tool where the sensors are situated closer to the leading pole and not just in the middle like it is normally done. For the FWHM, the test runs showed that the velocity doesn't affect the length of the defect as all the FWHM plots showed the same values for each defect at different velocities. Even at different magnetization levels the FWHM showed similar values for the same defect.

The results of this work should help optimize the use of the MFL technology when implementing it in the pipeline inspection industry, by knowing the optimal sensor position for the tool, the chances of detecting any types of defects inside a pipe can be increased significantly, which in its turn will assure that the flow and the delivery of the hydrocarbons is consistent and secure, making sure that no safety or environmental hazards could occur.

# References

[1] Bhatia, A., & Westwood, S. (2003, January 1). Developing a Baseline Inline Inspection Program With Design and Operational Decisions on the Use of a High Resolution Magnetic Flux Leakage Tool. NACE International.

[2] Miller, S. (2007, January 1). Prediction of Dent Size using Tri-axial Magnetic Flux Leakage Intelligent Pigs. NACE International.

[3] El Sherbeny, W., Nuic, I., Hasan, G., Abdesslam, A., & Hassane, T. (2015, September 14). Magnetic Flux Leakage (MFL) Technology Provides the Industry's Most Precise Pipe Integrity and Corrosion Evaluation, Accurately Characterizing Casing and Tubing Strength. Technology Overview and Case History. Society of Petroleum Engineers.

[4] Simek, J. (2011, January 1). Oblique Field Magnetic Flux Leakage Survey Complements Axial Field Data. NACE International.

[5] The Gas Research Institute Harvey Haines, "Magnetic Flux Leakage (MFL) Technology For Natural Gas Pipeline Inspection", United States, 1999.

[6] Nestleroth, B., Rust, S. W., Burgoon, D., & Haines, H. (1996, January 1). Determining Corrosion Defect Geometry From Magnetic Flux Leakage Pig Data. NACE International.

[7] P. Gossen, "Evaluierung und Vervollständigung notwendiger Parameter von Molchspezifikationen unter Berücksichtigung verschiedener Sensor- und Molchtypen", BA, Hochschule Osnabrück, 2014.

[8] Sherstan, R., Mcnealy, R., Gao, M., & Katz, D. C. (2005, January 1). Using Cost Effective Magnetic Flux Leakage Inspections As An Scc Screening Tool. NACE International.

[9] Velocity effects and their minimization in MFL inspection of pipelines — a numerical study. (1997). *NDT & E International*, 30(1), pp. 499-505.

[10] I. Mullin, "SECURING THE BEST PERFORMANCE ENTITLEMENT FROM MFL TECHNOLOGY", GE Oil & Gas, PII Pipeline Solutions, Cramlington, UK, p. 2, 2012.

[11] Pan, D., Guo, B., Liu, M., Cao, X., & Xia, L. (2010, January 1). Numerical Simulation of Magnetic Flux Leakage Inspection of Pipelines. International Society of Offshore and Polar Engineers.

[12] Nestleroth, J. Bruce and Davis, Richard J., "The Effects of Magnetizer Velocity on Magnetic Flux Leakage Signals, Boston, MA, 1993, pp. 1891-1898.

[13] Clapham, L., & Atherton, D. L. (2002, January 1). Stress Effects on MFL Signals. NACE International.

[14] Olson, M. (2004, January 1). In-Line Mechanical Damage Detection Using High-Res MFL Technology. NACE International.

# List of Tables

# List of Figures

# Abbreviations

| | |
|---|---|
| MFL | Magnetic Flux Leakage |
| FWHM | Full Width at Half Maximum |
| k | Kilo |
| A | Amber |
| T | Tesla |
| Mm | Millimeter |
| ILI | In-Line-Inspection |

# Appendices

## Appendix A: Amplitude and FWHM Plots

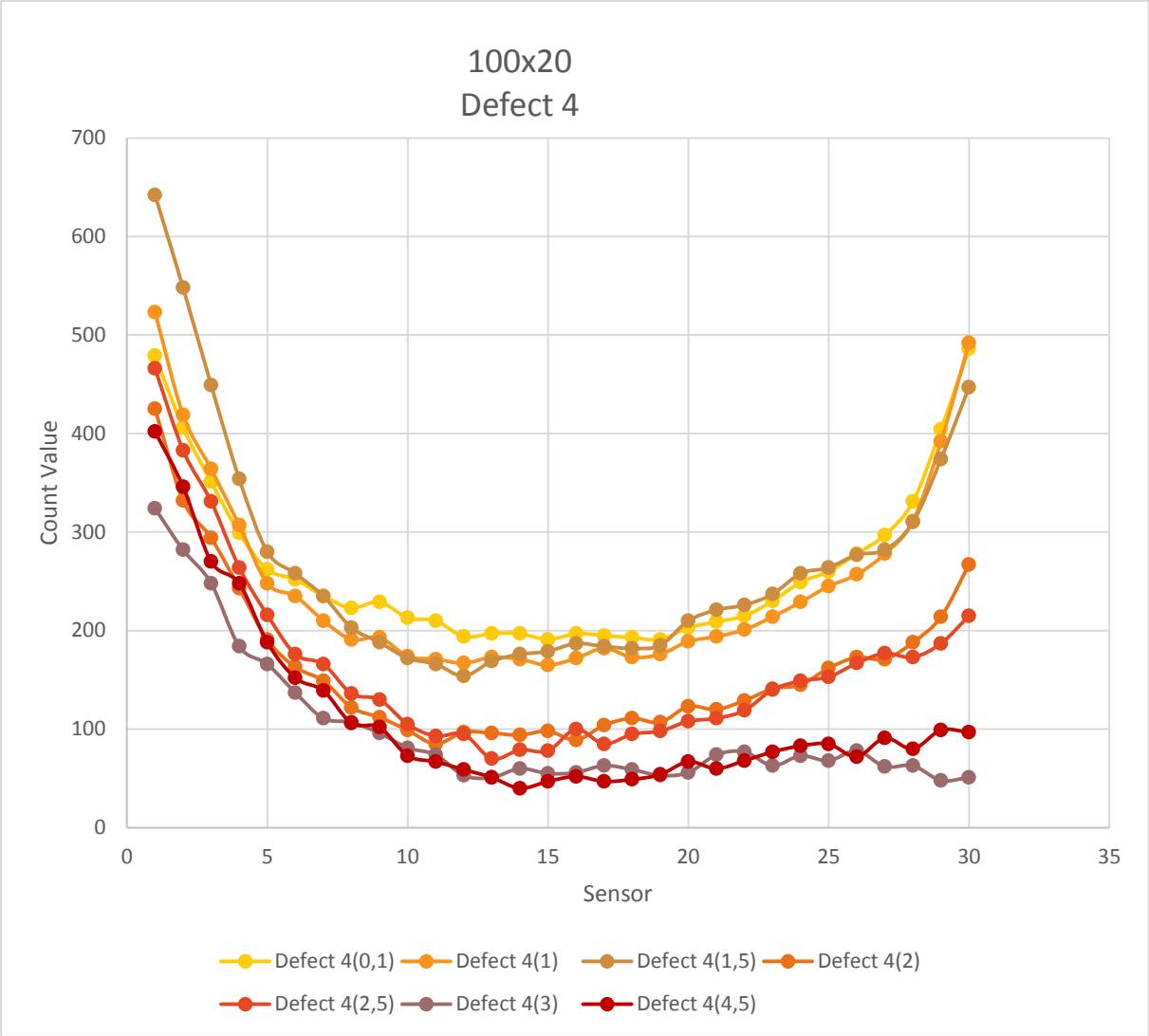

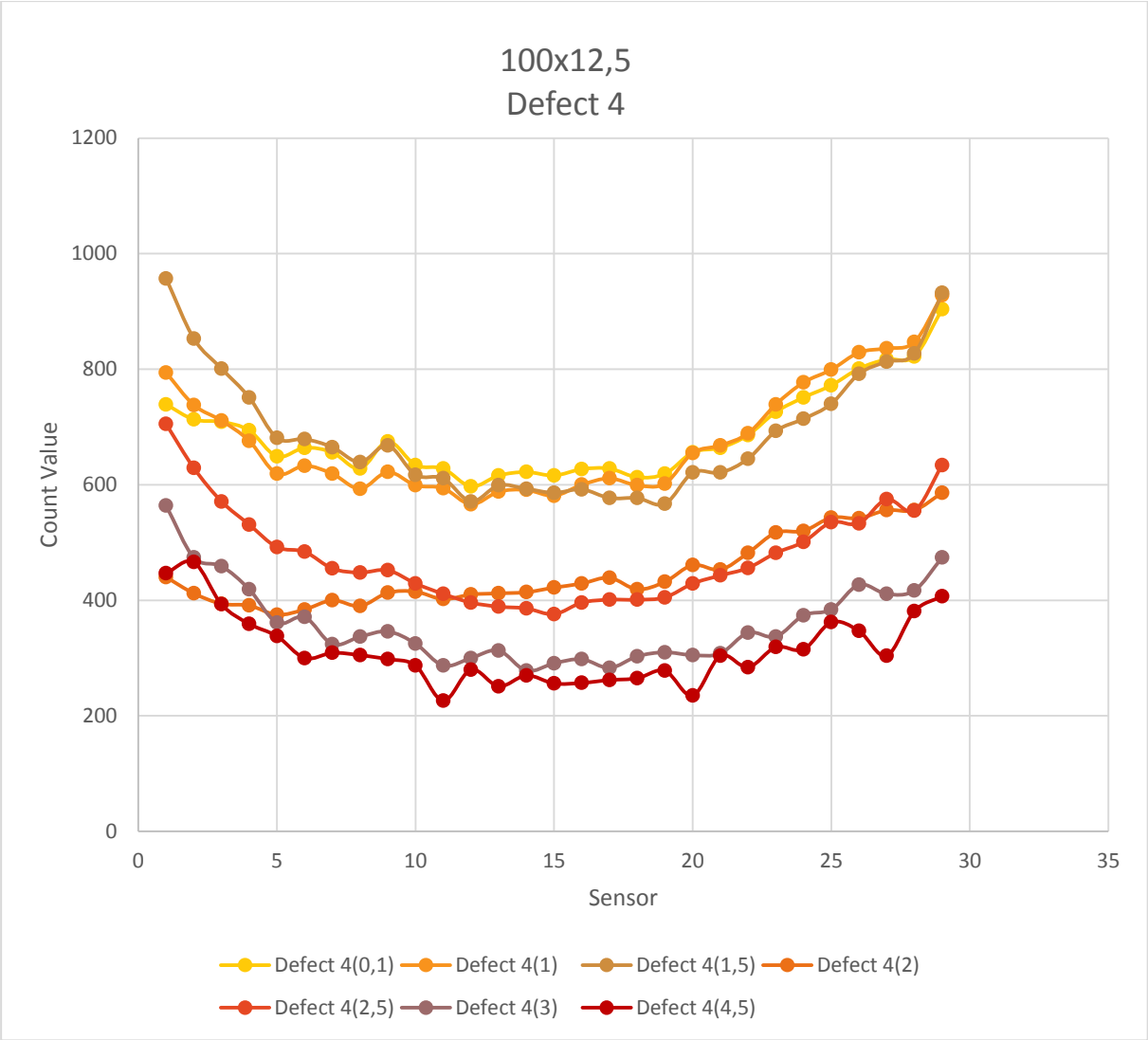
100x12,5
Defect 4
1200
1000
800
600
400
200
0
Count Value
0
5
10
15
20
25
30
35
Sensor
Defect 4(0,1)
Defect 4(1)
Defect 4(1,5)
Defect 4(2)
Defect 4(2,5)
Defect 4(3)
Defect 4(4,5)

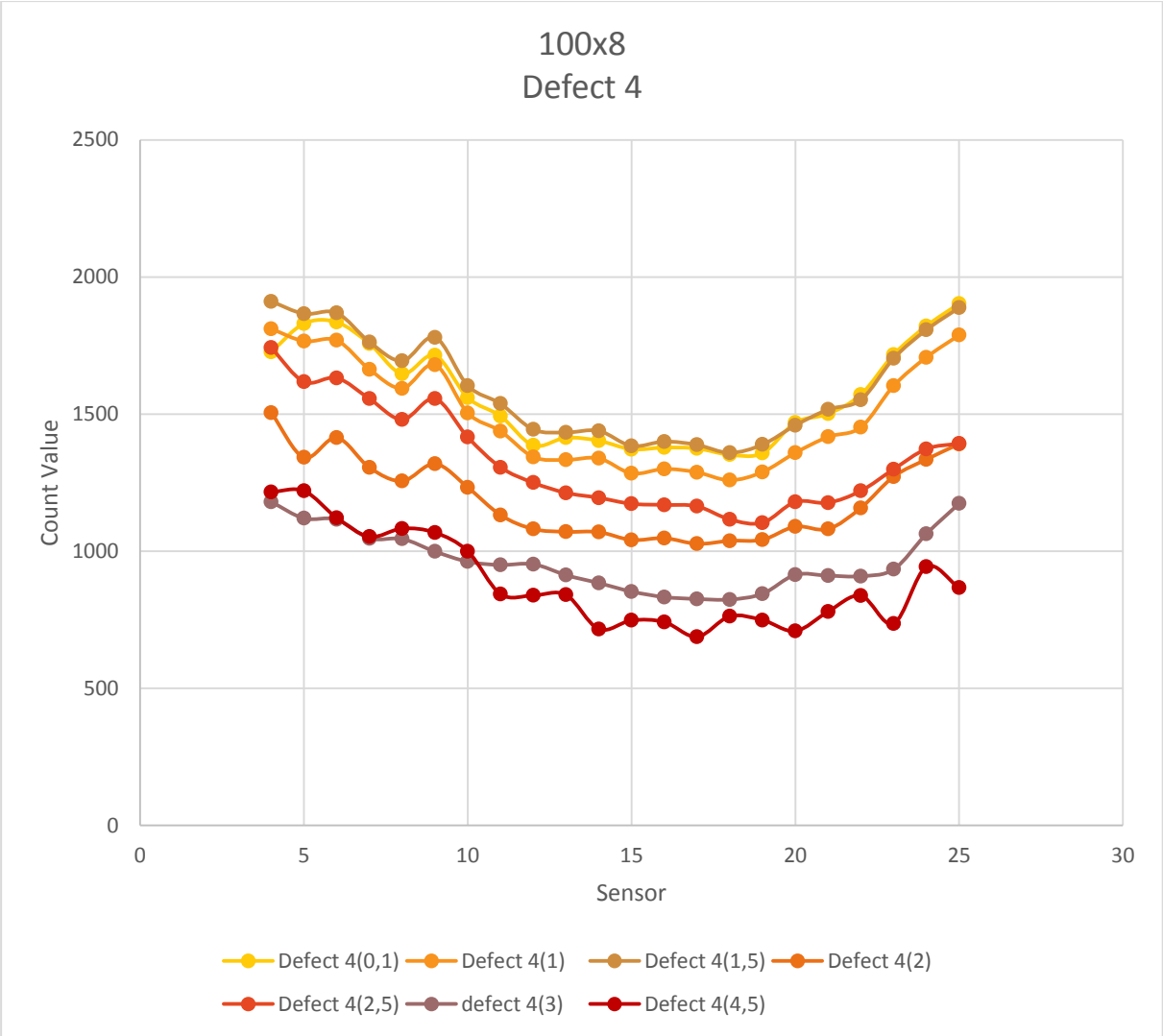
100x8
Defect 4
2500
2000
1500
1000
500
0
Count Value
0
5
10
15
20
25
30
Sensor
Defect 4(0,1)
Defect 4(1)
Defect 4(1,5)
Defect 4(2)
Defect 4(2,5)
defect 4(3)
Defect 4(4,5)

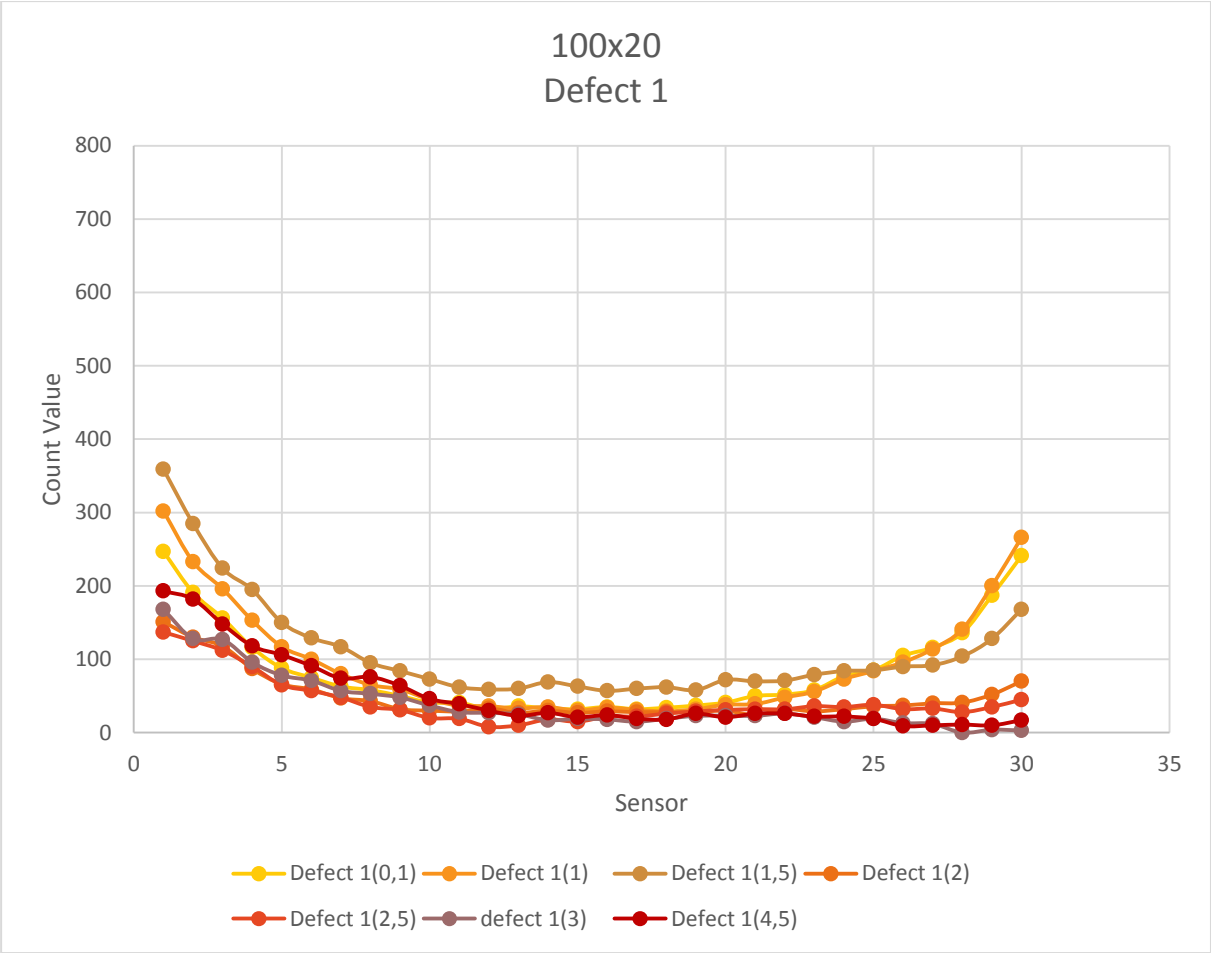
100x20
Defect 1
800
700
600
500
400
300
200
100
0
Count Value
0
5
10
15
20
25
30
35
Sensor
Defect 1(0,1)
Defect 1(1)
Defect 1(1,5)
Defect 1(2)
Defect 1(2,5)
defect 1(3)
Defect 1(4,5)

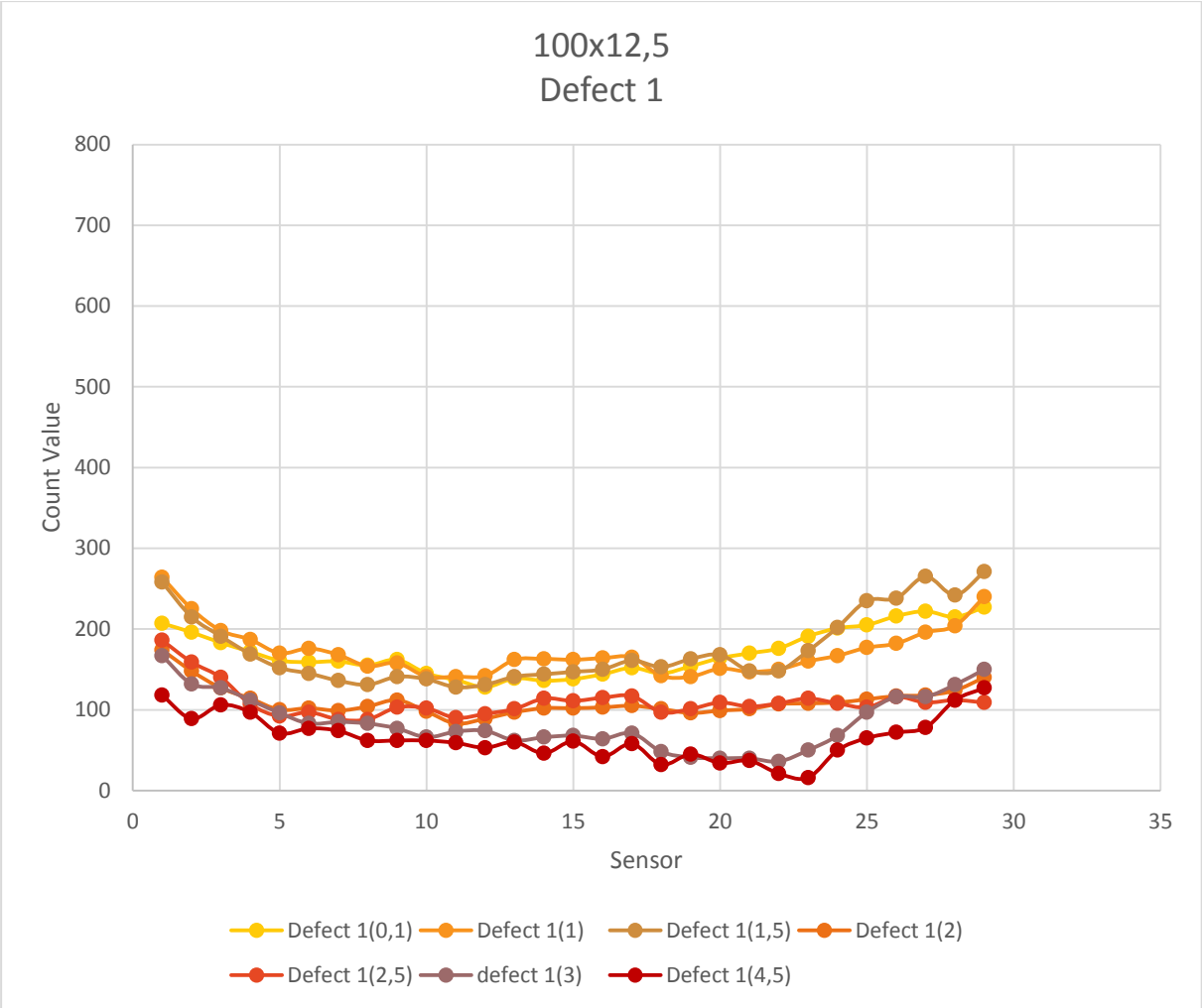
100x12,5
Defect 1
800
700
600
500
400
300
200
100
0
Count Value
0
5
10
15
20
25
30
35
Sensor
Defect 1(0,1)
Defect 1(1)
Defect 1(1,5)
Defect 1(2)
Defect 1(2,5)
defect 1(3)
Defect 1(4,5)

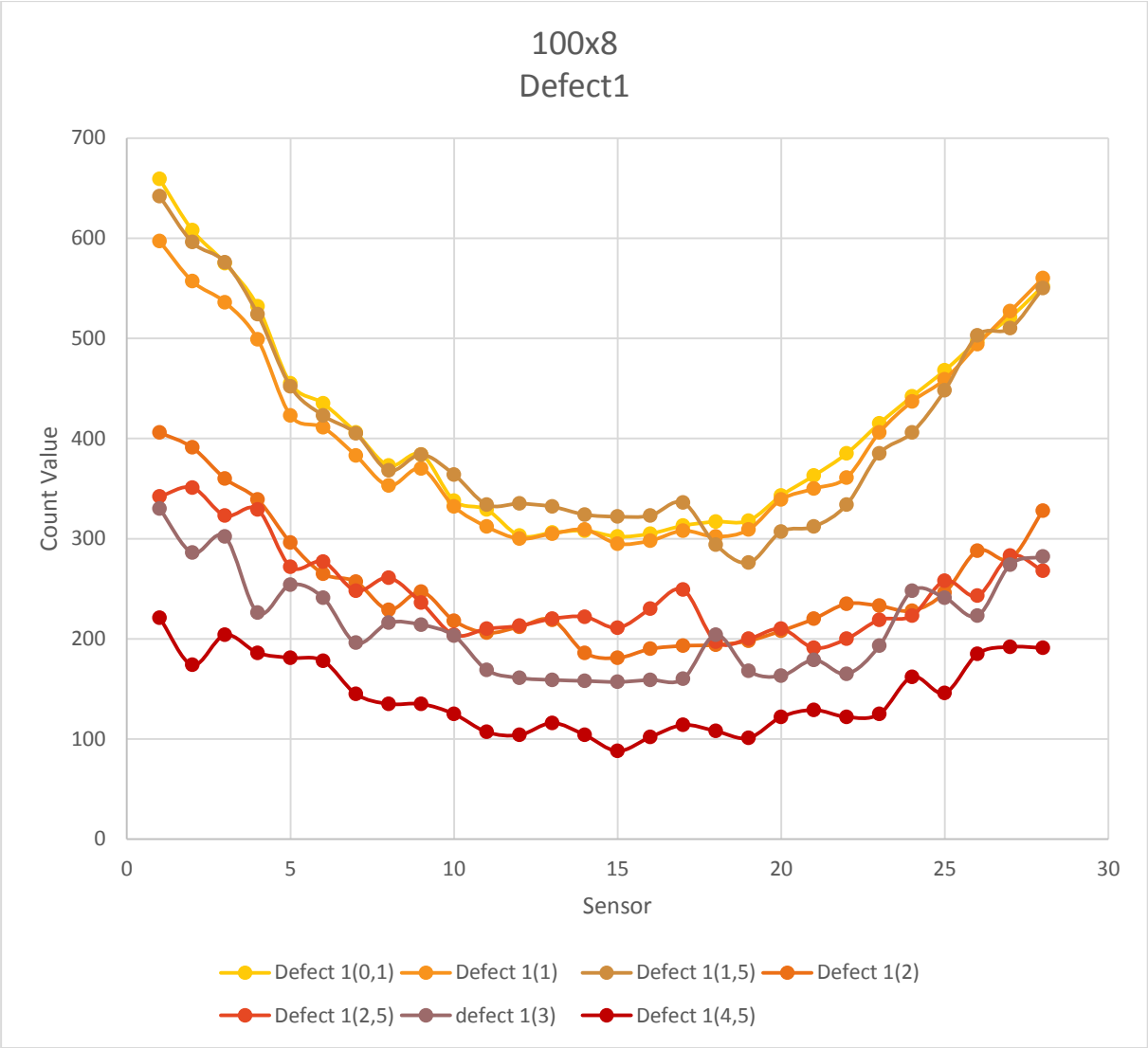
100x8
Defect1
Count Value
700
600
500
400
300
200
100
0
0
5
10
15
20
25
30
Sensor
Defect 1(0,1)
Defect 1(1)
Defect 1(1,5)
Defect 1(2)
Defect 1(2,5)
defect 1(3)
Defect 1(4,5)

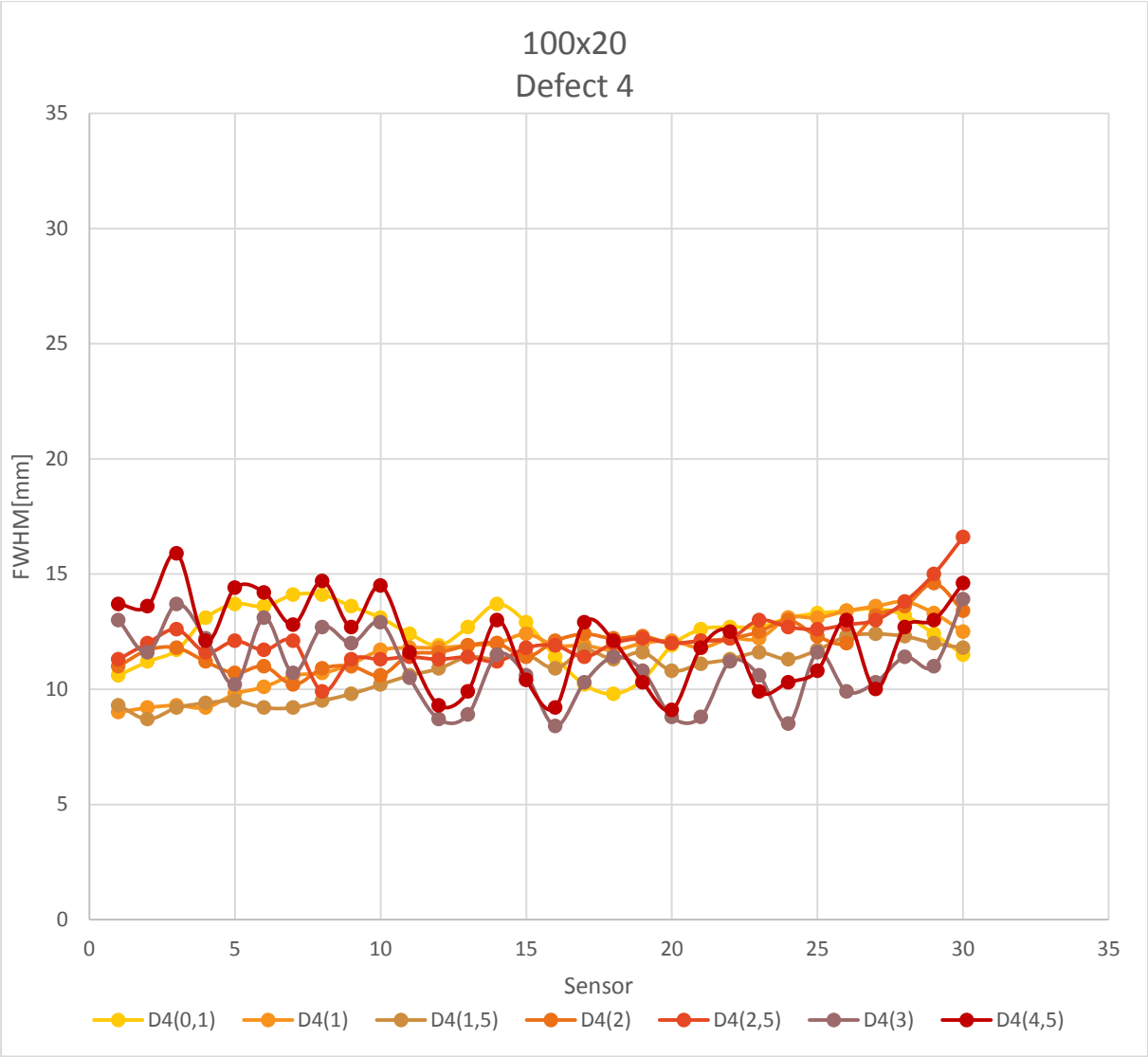
100x20
Defect 4
FWHM[mm]
35
30
25
20
15
10
5
0
0
5
10
15
20
25
30
35
Sensor
D4(0,1)
D4(1)
D4(1,5)
D4(2)
D4(2,5)
D4(3)
D4(4,5)

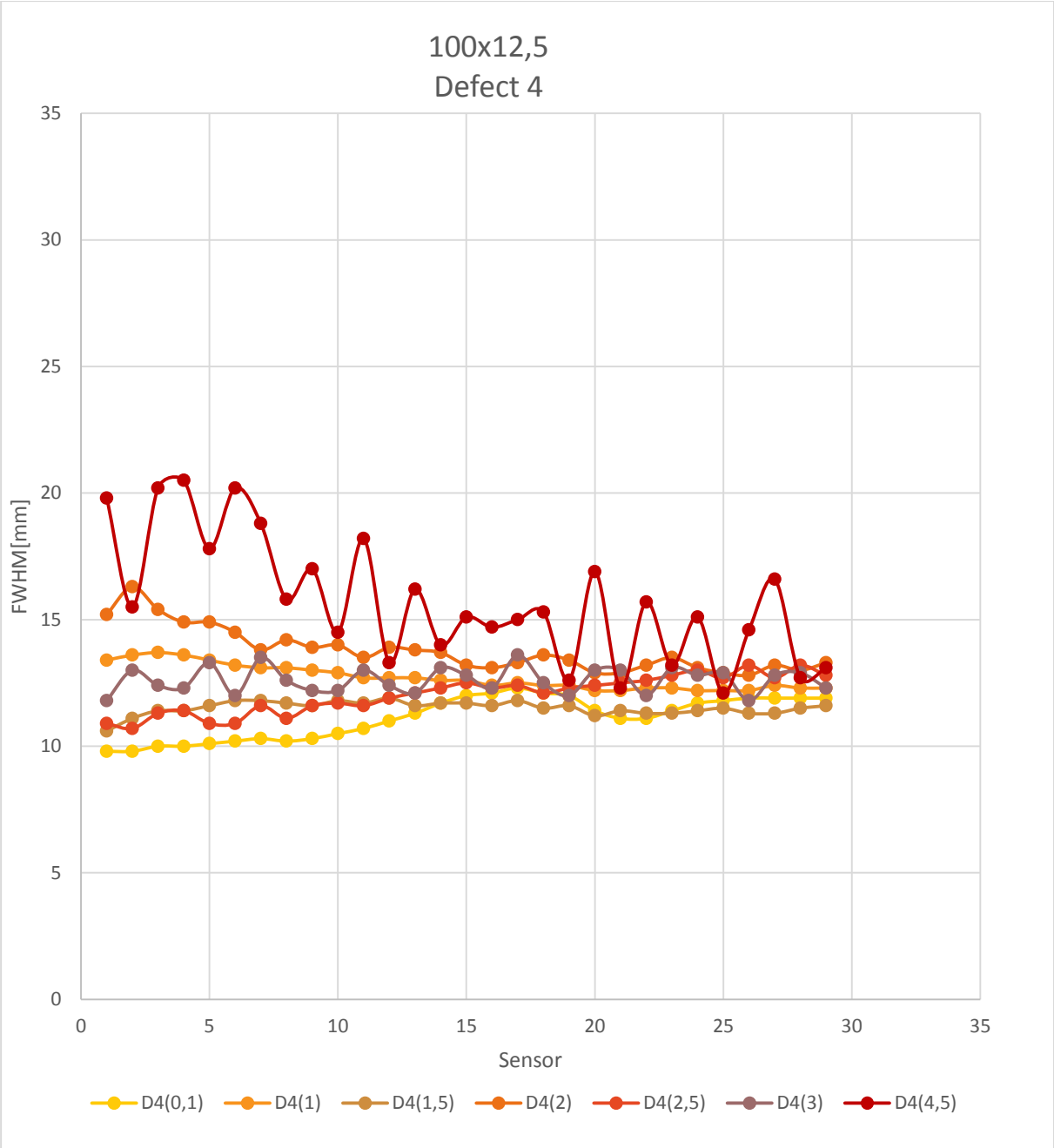
100x12,5
Defect 4
FWHM[mm]
Sensor
0
5
10
15
20
25
30
35
D4(0,1)
D4(1)
D4(1,5)
D4(2)
D4(2,5)
D4(3)
D4(4,5)

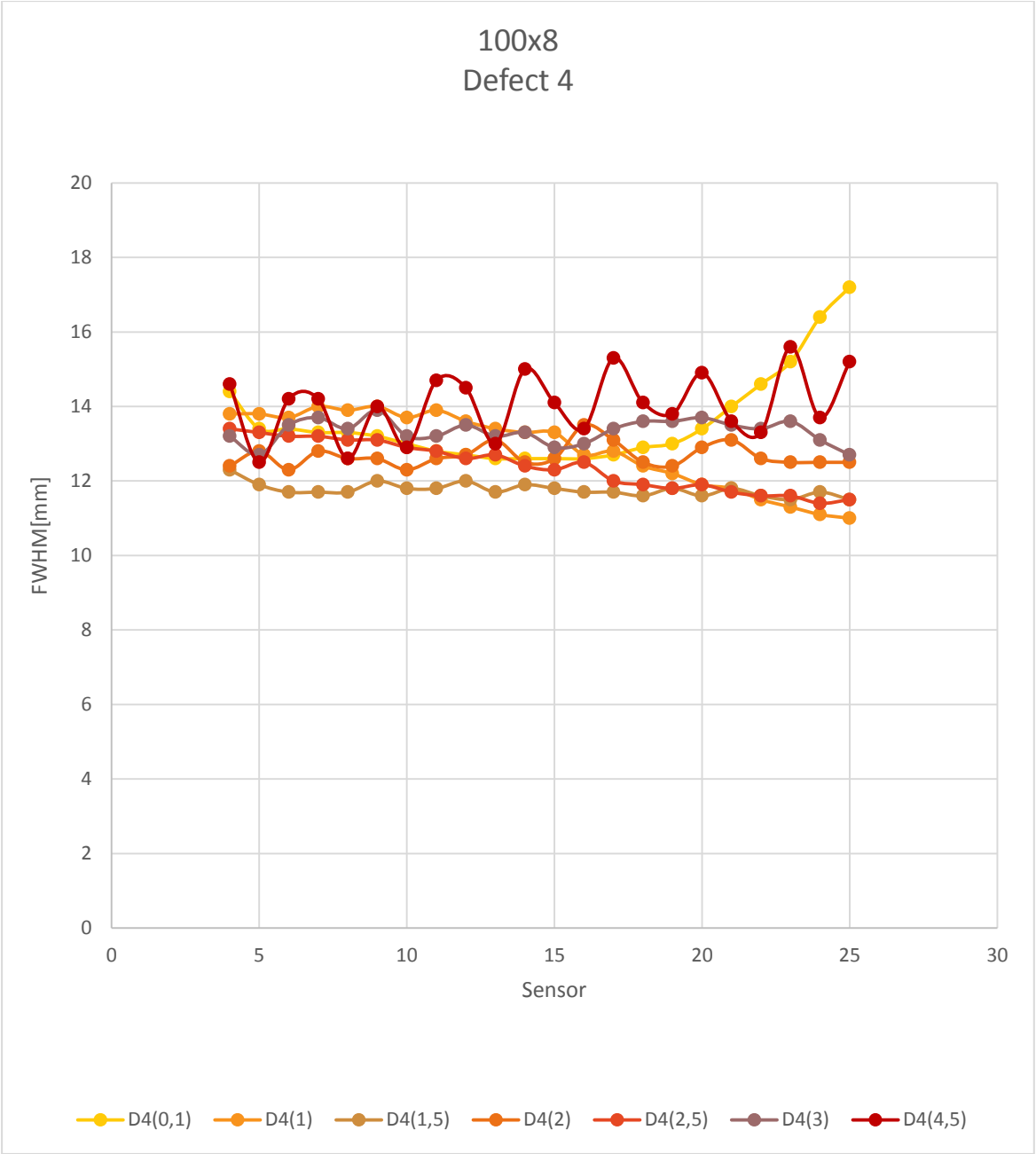
100x8
Defect 4
FWHM[mm]
Sensor
0
2
4
6
8
10
12
14
16
18
20
0
5
10
15
20
25
30
D4(0,1)
D4(1)
D4(1,5)
D4(2)
D4(2,5)
D4(3)
D4(4,5)

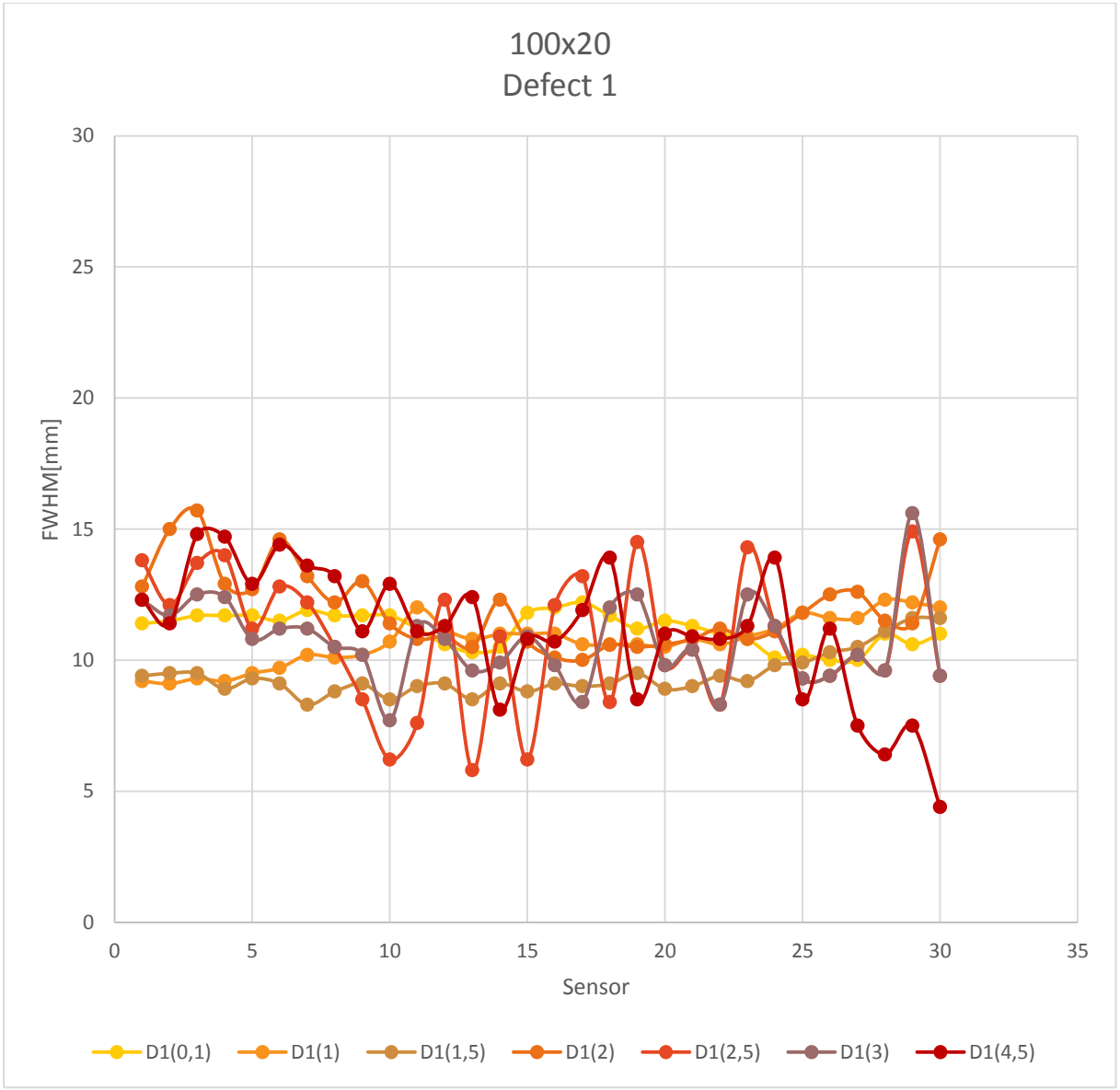
100x20
Defect 1
FWHM[mm]
30
25
20
15
10
5
0
0
5
10
15
20
25
30
35
Sensor
D1(0,1)
D1(1)
D1(1,5)
D1(2)
D1(2,5)
D1(3)
D1(4,5)

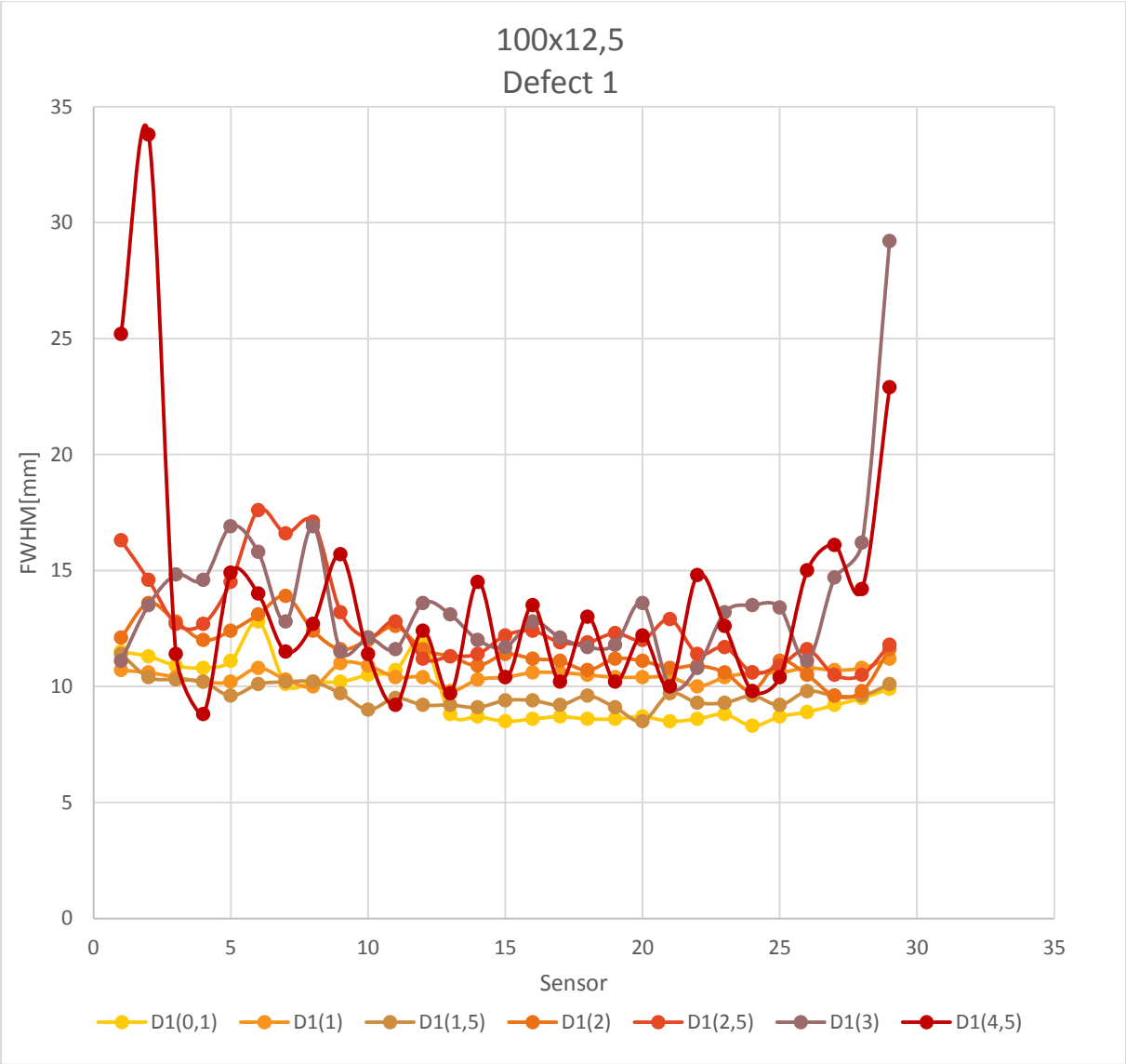
100x12,5
Defect 1
FWHM[mm]
Sensor
0
5
10
15
20
25
30
35
D1(0,1)
D1(1)
D1(1,5)
D1(2)
D1(2,5)
D1(3)
D1(4,5)

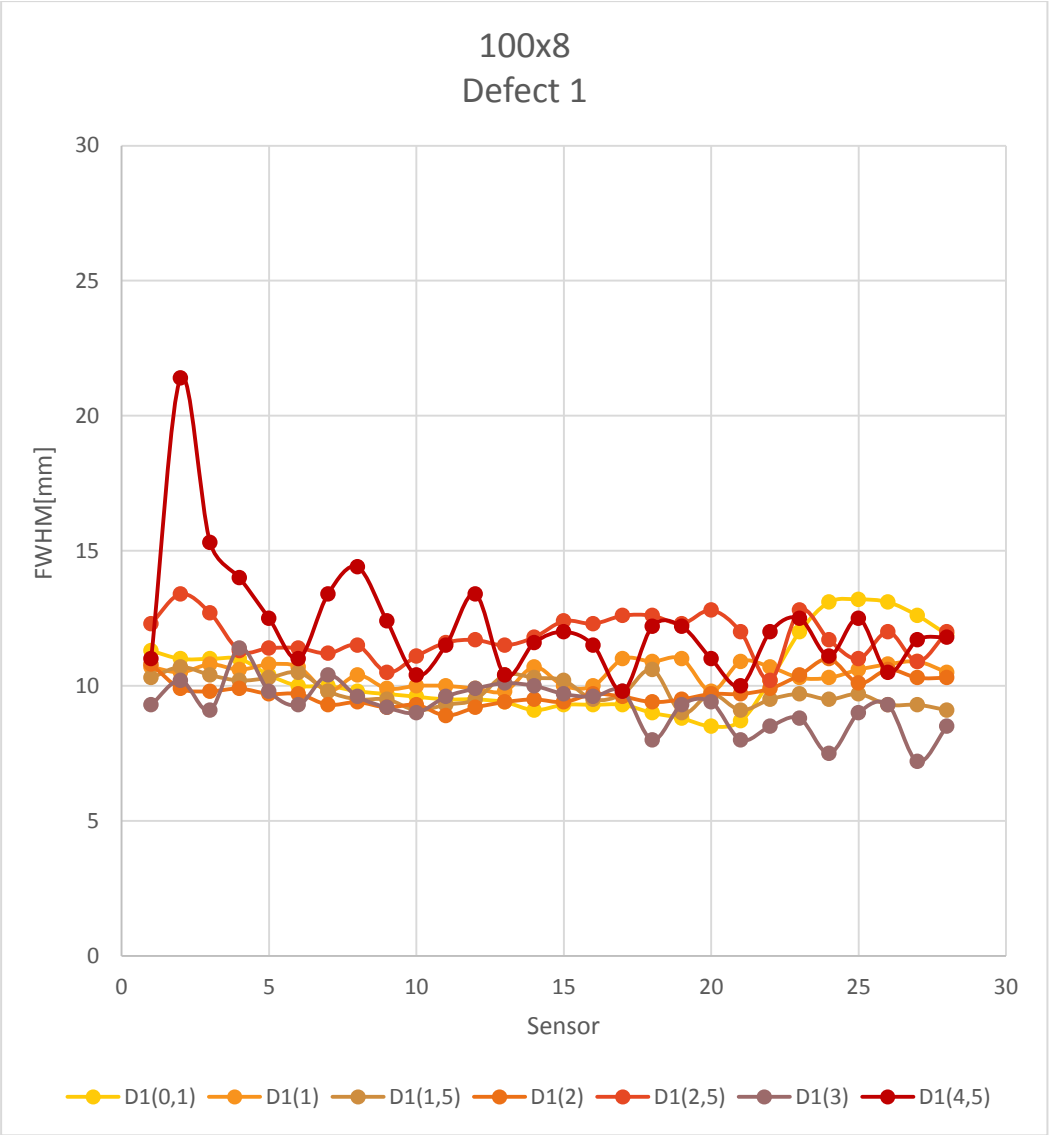
100x8
Defect 1
FWHM[mm]
Sensor
0
5
10
15
20
25
30
D1(0,1)
D1(1)
D1(1,5)
D1(2)
D1(2,5)
D1(3)
D1(4,5)